OUKA
Osaka University Knowledge Archive

Title	A Study on Inter-Cell Interference Control for Cellular Mobile Communications
Author(s)	長手, 厚史
Citation	大阪大学, 2016, 博士論文
Version Type	VoR
URL	https://doi.org/10.18910/55862
rights	
Note	

Osaka University Knowledge Archive : OUKA

https://ir.library.osaka-u.ac.jp/

Osaka University

A Study on Inter-Cell Interference Control for Cellular Mobile Communications

Atsushi Nagate

Graduate School of Information Science and Technology
Osaka University

January 2016

List of publications

Journal Papers

1. Atsushi Nagate, Masashi Sugano, Masayuki Murata, Hideo Miyahara, "Impact of Limited Number of Wired Channels on Soft Handoff in CDMA Cellular Systems," IEICE Transactions on Communications, vol.E84-B, no.3, pp.520-526, March, 2001.
2. Atsushi Nagate, Teruya Fujii, "A Study on Channel Estimation Methods for Time-Domain Spreading MC-CDMA Systems," IEEE Transactions on Wireless Communications, vol.7, no.12, pp.5233-5237, December, 2008.
3. Atsushi Nagate, Teruya Fujii, "A Study on Channel Estimation Methods for Time-Domain Spreading MC-CDMA Systems," IEICE Transactions on Communications, vol.E92-B, no.3, pp.980-991, March, 2009.
4. Atsushi Nagate, Kenji Hoshino, Teruya Fujii, "Frequency Offset Interference Canceller for Multi-Link Transmission in OFDM Systems," IEICE Transactions on Communications, vol.E93-B, no.3, pp.620-628, March, 2010.

Refereed Conference Papers

1. Atsushi Nagate, Masayuki Murata, Hideo Miyahara, Masashi Sugano, "An Integrated Approach for Performance Modeling and Evaluation of Soft Handoff in CDMA Mobile Cellular Systems," in Proceedings of the 52nd IEEE Vehicular Technology Conference (VTC2000 Fall), September, 2000.
2. Atsushi Nagate, Hiroyoshi Masui, Teruya Fujii, "A Study on Channel Estimation Methods for MC-CDMA Systems," in Proceedings of the 57th IEEE Vehicular Technology Conference (VTC2003 Spring), April, 2003.
3. Atsushi Nagate, Kenji Hoshino, Teruya Fujii, "A Study on Frequency Offset Interference Canceller for Multi-Link Transmission in OFDM Systems," in Proceedings of the 67th IEEE Vehicular Technology Conference (VTC2008 Spring), May, 2008.
4. Atsushi Nagate, Kenji Hoshino, Manabu Mikami, Teruya Fujii, "A Field Trial of

Multi-Cell Cooperative Transmission over LTE System," in Proceedings of IEEE International Conference on Communications (ICC2011), June, 2011.

5. Atsushi Nagate, Daigo Ogata, Teruya Fujii, "Cell Edge Throughput Improvement by Base Station Cooperative Transmission Control with Reference Signal Interference Canceller in LTE System," in Proceedings of the 75th IEEE Vehicular Technology Conference (VTC2012 Spring), May, 2012.
6. Atsushi Nagate, Daigo Ogata, Teruya Fujii, "Experimental Evaluation of Reference Signal Interference Canceller for Multi-BS Cooperative Transmission Control in LTE," in Proceedings of the 76th IEEE Vehicular Technology Conference (VTC2012 Fall), September, 2012.
7. Atsushi Nagate, Sho Nabatame, Daigo Ogata, Kenji Hoshino, Teruya Fujii, "Field Experiment of CoMP Joint Transmission over X2 Interface for LTE-Advanced," in Proceedings of the 77th IEEE Vehicular Technology Conference (VTC2013 Spring), June, 2013.
8. Atsushi Nagate, Sho Nabatame, Kenji Hoshino, Teruya Fujii, "Experimental Evaluations of Coordinated Interference Control for Co-channel Overlaid Cell Structure," in Proceedings of the 81st IEEE Vehicular Technology Conference (VTC2015 Spring), May, 2015.

Preface

Cellular mobile communications systems first launched in 1979 have evolved drastically and are now essential for our daily lives. They started as 1st generation narrow-band analog systems and then evolved to narrow-band digital systems as 2nd generation systems in 1990s. They further enhanced to wide-band digital systems as 3rd generation systems in 2000s, which employed CDMA (Code Division Multiple Access) as multiple access system. In 2010s, 4th generation systems targeting further mobile broadband communications with OFDM (Orthogonal Frequency Division Multiplexing), MIMO (Multiple Input Multiple Output) etc. are spreading rapidly all over the world. On the other hand, 5th generation mobile communications systems targeting 2020s are now attracting much attention and intensively studied in order to achieve further mobile broadband, highly-reliable and low-latency communications targeting self-driving car, remote surgery and so on, and connection of massive number of devices for the spread of IoT (Internet of Things).

As the generations of mobile communications systems went by, network capacity has drastically increased by the improvement of radio transmission efficiency and more allocation of frequency band. However, in recent years, mobile data traffic is doubling every year and increasing more rapidly than the growth of network capacity by the wide spread of advanced mobile devices such as smartphone and tablet devices, so further network capacity improvement is the top priority of mobile network operators.

The network capacity of cellular mobile communications can be denoted as the product of "radio transmission capability per Hz achieved by radio transmission technology", "allocated spectrum bandwidth", and "geographical reuse of the same frequency". Accordingly, the introduction of a new radio transmission system with higher radio transmission efficiency or the allocation of new spectrum is effective to improve network capacity. However, the radio transmission efficiency has already become close to its theoretical upper bound, Shannon limit, and the spectrum resources allocated for mobile communications has already been congested. This means that it is difficult to cope with the rapid growth of mobile data traffic, which is doubling every year and increases 1000 times in 10 years, only with these countermeasures.

Therefore, "cell configuration technology", in which we increase the number of Base Stations (BSs) and reuse the same frequency in shorter distance, is essential to cope with the rapid increase of mobile data traffic. I first explain cell configuration technology. In mobile communications systems, cellular system has been used since its 1st generation. In cellular system, communication service is provided by placing BSs in a service area, which covers a certain area called "cell". The system can use frequency effectively by reusing frequency in the cells. We can increase capacity per service area by placing more BSs and reusing frequency more. Cell radius has been shrinking since the start of mobile communications services in 1979 with 5 to 10 km, and it becomes around 100m recently in dense urban area. In cellular system, as a BS has its service area in a concentric fashion, the communication quality of Mobile Stations (MSs) is high when they are close to BS. On the other hand, it is low when MSs are located at the border of cover areas (cell edge) because they receive lower signal power from BS and higher interference power from neighbor BSs. However, the users of mobile communication service are unaware of their location, so mobile network operators are required to provide high communication quality to users regardless of their locations. Therefore, it is also important to improve cell-edge communication quality on top of capacity increase by placing more BSs.

Against the backdrop described above, technologies improving cell-edge communication quality are studied in this thesis. The downlink transmission from BS to MS is targeted because its traffic volume is huge by web browsing and video streaming. It is most important to control the interference from neighbor BSs in order to improve cell-edge throughput, so I first study on multi-BS cooperative transmission control. Multi-BS cooperative transmission control is categorized into two technologies: (i) multi-BS cooperative muting control and (ii) multi-BS cooperative signal transmission. In multi-BS cooperative muting control, neighbor BS stops signal transmission to decrease interference to cell-edge MSs and around 40% of cell edge throughput improvement is possible. However, in most of mobile communications systems such as Long Term Evolution (LTE), even when signal transmission is stopped, common reference signal used for handover measurement etc. cannot be stopped, which prevents the performance improvement. Then, I propose a reference signal interference canceller, which removes the residual reference signal interference and clarify that almost the same throughput at cell edge can be achieved as the case without reference signal by computer simulations and experiments

with a prototype. Multi-BS cooperative signal transmission is another approach having a potential to achieve the similar cell-edge performance gain by jointly transmitting signals from neighboring BSs in a coordinated manner. In this transmission, multiple BSs need to transmit signal simultaneously within a microsecond, and its feasibility needs to be clarified towards the introduction to commercial network. In this thesis, I develop a prototype and demonstrate the feasibility through laboratory and field experiments.

I also study on multi-link signal transmission for the environment such as rural area where the received signal power of cell-edge MSs is weak, so the influence of thermal noise as well as interference from neighbor BS is severe. In multi-link signal transmission, each BS first concentrate transmit power in a part of its system bandwidth in order to improve the tolerance to thermal noise. On top of this power concentration, neighboring BSs transmit their signal in different frequency to cell-edge MSs in a coordinated fashion, which increases the throughput at cell edge. The signal reception at cell-edge MSs can be achieved simpler compared to multi-BS cooperative signal transmission because the signal from both neighboring BSs are received in a simple frequency-division fashion. However, when neighboring BSs have different frequency offset, the signals from both BSs interfere with each other in the frequency domain, which results in lower communication quality. In order to resolve this issue, I propose an interference canceller, which cancels the interference in the frequency domain. I evaluated the proposed method by mathematical analysis and computer simulations and clarified that the same communication quality as that without frequency offset is achieved.

Radio transmission technologies such as modulation, error correction coding, and channel estimation are not cell-edge specific technologies but effective to all MSs, so it also contributes to cell-edge performance improvement. In this thesis, I focus on channel estimation, which is necessary to compensate fading fluctuation in mobile communications. I propose a channel estimation method, in which the averaging of channel estimate is conducted in both time and frequency domains by taking into account the fading fluctuation in both domains. I also combine a channel estimation method based on impulse response. I evaluated the proposed method by computer simulations and clarified that the channel estimation accuracy could be improved compared with conventional methods.

I also investigate the impact of the limitation in wired channel capacity. When Multi-BS

cooperative signal transmission is used, the wireless channel quality of a cell-edge MS becomes better by the cooperative signal transmission from both BSs, while each of the both BSs needs to secure the wired channel for the cell-edge MS. Accordingly, excessive use of Multi-BS cooperative signal transmission may result in the exhaustion of wired channel in a BS. This exhaustion of wired channel causes blocking of newly generated calls and forced termination of handover. Therefore, the region where multi-BS cooperation is conducted should be controlled based on handover threshold control by taking into account both wireless and wired channels. However, such a research has not been conducted, and I propose a handover threshold control method taking both wireless and wired channels into account and clarifies the tradeoff relationship by mathematical analysis and computer simulations.

Finally, I study on newly-emerged cell-edge issue caused by the introduction of layered cell configuration, which is attracting much attention in recent years. The layered cell configuration puts a large number of small cells in a macro-cell coverage area; capacity is drastically improved by the small cells while mobility and coverage is secured by macro cell. However, when the layered cell configuration is realized within the same frequency, there exists interference between macro and small cells, which generates new cell edge. Inter-cell interference coordination based on muting is effective in order to solve the interference. In this interference coordination, it is important to optimize the interference control by taking into account user distribution to improve spectral efficiency. In this thesis, I develop a prototype to realize the interference control based on network coordination among macro and small cells and clarify the performance through field experiment. I also study on radio resource allocation control for the layered cell configuration. Even with the layered cell configuration, because of the distribution of users, there may be some congested cells, in which MS throughput becomes quite low especially at cell edge. In order to resolve this issue, I propose a resource allocation priority control method, which is conducted individually per cell. It was clarified that the cell edge performance was improved without degrading cell overall throughput by computer simulations.

Acknowledgements

I have been engaged in research activities since I entered the graduate school of Osaka University in 1999 and have the privilege of writing a doctoral thesis this time. This work could not have been done without the support from many people, and I would like to show my appreciation to all of them.

First of all, I would like to express my great gratitude to my supervisor, Professor Masayuki Murata, for his generous guidance, insightful comments, and meaningful discussion. I was able to complete my thesis owing to his kind guidance, timely encouragement, and valuable advice.

I am heartily thankful to the members of my thesis committee, Professor Takashi Watanabe, Professor Toru Hasegawa, Professor Teruo Higashino, and Professor Morito Matsuoka of the Graduate School of Information Science and Technology, Osaka University, for their multilateral reviews and perceptive comments.

Furthermore, I would like to express my great gratitude to Teruya Fujii, the head of R&D division, SoftBank Corporation, who has taught me mobile communications from the basics and raised me as a researcher since I started to work in 2001.

I am also grateful to all of the members in R&D division, SoftBank Corporation, for their support and encouragement during the course of this study. A lot of discussion with them greatly helped and encouraged me.

Finally, I deeply thank my parents, my wife, and my son for their understanding and hearty support and encouragement. This work would not have been achieved without them.

Contents

List of Figures

List of Tables

Chapter 1

Introduction

1.1 Background

Cellular mobile communications systems first launched in 1979 have evolved drastically and are now essential for our daily lives [1.1]. They started as 1st generation narrow-band analog systems and then evolved to narrow-band digital systems as 2nd generation systems in 1990s, with which we could enjoy e-mail and the Internet connection. It further enhanced to wide-band digital systems employing CDMA (Code Division Multiple Access) as multiple access system as 3rd generation systems in 2000s, which enabled multi-media service such as TV phone and high-speed data communications. Recently, 4th generation systems targeting further mobile broadband communications with OFDM (Orthogonal Frequency Division Multiplexing), MIMO (Multiple Input Multiple Output) and so on are becoming popular. On top of this, 5th generation mobile communications systems are attracting much attention with the goal of further mobile broadband, highly-reliable and low-latency communications targeting self-driving car and remote surgery, and accommodation of massive number of IoT (Internet-of-Things) devices. Against the backdrop of this drastic evolution of mobile communications systems, the number of subscribers has increased rapidly and reached 150 million in Japan and 7 billion in the world. Besides, advanced mobile terminals such as smart phones and tablet devices have spread widely in recent years, and mobile communications data traffic is doubling every year, i.e. 1000 times every ten years [1.2] .

As the generations of mobile communications systems went by, capacity has drastically increased by the improvement of radio transmission efficiency and more allocation of frequency band. However, in recent years, mobile data traffic has increased more rapidly by the wide spread of advanced mobile devices such as smartphone and tablet devices, so further capacity improvement is the top priority for mobile network operators. In mobile communications

systems, cellular system has been used since its 1st generation. In cellular system, communication service is provided by placing Base Stations (BSs) in a service area, which covers a certain area called "cell". The system can use frequency effectively by reusing frequency in the cells. We can increase capacity per service area by placing more BSs and reusing frequency more. Cell radius has been shrinking since the start of mobile communications services in 1979 with 5 to 10 km, and it becomes around 100m recently in dense urban area.

In cellular system, as a BS has its service area in a concentric fashion, the communication quality of Mobile Stations (MSs) is high when they are close to BS. On the other hand, it is low when MSs are located at the border of cover areas (cell edge) because they receive lower signal power from BS and higher interference power from neighbor BSs. However, the users of mobile communication service are unaware of their location, so mobile network operators are required to provide high communication quality to users regardless of their locations. Therefore, it is also important to improve cell-edge communication quality on top of capacity increase by placing more BSs.

Against the backdrop described above, technologies to improve cell-edge communication quality are studied in this thesis. The downlink transmission from BS to MS is targeted because its traffic volume is huge by web browsing and video streaming.

1.2 Overview and issues of conventional technologies to improve cell-edge communication quality

In wireless communications, it is widely known that the theoretical upper bound of the capacity of a communication channel, C, is denoted by Shannon-Hartley theorem and shown as follows [1.3].

$$C = B\log_2\left(1+\frac{S}{N}\right). \tag{1.1}$$

Here, B is the bandwidth of the channel, S is the received signal power, and N is noise power. Unlike stand-alone cell system, in cellular mobile communications systems, the interference from neighbor cells also affects the channel capacity. The theoretical upper bound of the channel

capacity in cellular mobile communications can be rewritten as follows.

$$C = B\log_2\left(1+\frac{S}{I+N}\right). \tag{1.2}$$

Here, I is the interference power from neighbor BSs. In cellular mobile communications, as an MS approaches cell edge, the interference power from neighbor BSs becomes stronger and degrades the MS's channel capacity, in other words user throughput. Therefore, it is most important to control the interference from neighbor BSs in order to improve cell-edge throughput.

The cooperation of neighboring multiple BSs in signal transmission is essential in order to control interference power. This multi-BS cooperative transmission control technologies have been studied intensively and they are well summarized in [1.4]. Multi-BS cooperative transmission control can be mainly categorized into two technologies: (i) Multi-BS cooperative muting control and (ii) Multi-BS cooperative signal transmission. In Multi-BS cooperative muting control, when an MS is located at cell edge, one or multiple neighbor BSs stop (mute) their signal transmission in radio resources where the cell-edge MS receives its desired signal from its connecting BS. The stop of signal transmission is beneficial not only for the cell-edge MS but also for other MSs belonging to the surrounding cells. We have clarified that cell-edge user throughput is improved by around 40% without degrading overall network capacity by applying Multi-BS cooperative muting control compared with the case without any cooperation [1.5]. In the throughput evaluation in [1.5], we assumed that there was no interference at all in the radio resource where a neighbor-cell BS stopped its signal transmission. However, in actual mobile communications systems such as LTE, a common signal called reference signal continues to be transmitted even when the stop of signal transmission is applied. This is because reference signal is a signal commonly used for all MSs in order to conduct channel estimation or handover measurement. Accordingly, the residual interference by reference signal prevents achieving the improvement in cell-edge user throughput shown in [1.5]. In this thesis, I propose an interference canceller, which reduces the residual interference from reference signal and clarify the performance by computer simulations in Chapter 2 [1.6]. Moreover, I develop a prototype system of the proposed interference canceller and demonstrate the feasibility through laboratory and field experiments also in Chapter 2 [1.7].

Multi-BS cooperative signal transmission is another approach to achieve the improvement in cell-edge user throughput. When multiple BSs transmit signals to an MS in the same radio resource in a coordinated fashion, it is called Joint transmission [1.4]. There is another simplified form of Multi-BS cooperative signal transmission, in which each cooperating BS transmits its signal in different frequency from other cooperating BSs. This is called Multi-link signal transmission and is described in detail later. In Joint transmission, neighboring BSs transmit signal to a cell-edge MS in a coordinated fashion, so the cell-edge MS can utilize the transmit power and antennas of both BSs unlike Multi-BS cooperative muting control, in which the signal transmission of neighbor BS is stopped. Therefore, the total received signal power of cell-edge MS can be improved. On the other hand, unlike Multi-BS cooperative muting control, the effect of the stop of signal transmission to all of the surrounding cells cannot be obtained in Multi-BS cooperative signal transmission, and it has been reported that almost the same throughput characteristics are obtained especially in a congested service area [1.4]. However, certain performance gain is observed when the traffic in a service area is not so busy in exchange for the increase in signal processing cost in MS and traffic volume in backhaul network, which is caused by the nature of the joint transmission from both neighboring BSs. Therefore, it is the best strategy to use both Multi-BS cooperative muting control and Joint transmission depending on the congestion degree of the traffic in a service area and backhaul network. Towards the introduction of these technologies into commercial networks, it is essential to demonstrate the feasibility of the technologies in a real field environment. In order to realize the simultaneous transmission from both BSs, it is required to synchronize the transmission timing of the signals from both BSs by taking into account signal processing delay and backhaul-network latency. In this thesis, I conduct field experiments of Joint transmission and demonstrate the feasibility of the technology in a real field environment in the latter part of Chapter 2 [1.8, 1.9].

Multi-link signal transmission is a form of Multi-BS cooperative signal transmission and effective to increase the cell-edge user throughput especially in large cells, which are typically deployed in a rural area [1.10]. In a service area with normal size of cells from a few hundreds of meters to a few kilometers, the effect of the interference from neighbor cells is dominant compared to noise power because the received signal power is usually much higher than noise

power. On the other hand, in a service area with large cells, cell-edge user throughput is affected not only by neighbor-cell interference described in the previous paragraphs but also noise because the received signal power at cell edge becomes quite low by large propagation loss. In order to solve this issue, it is effective to concentrate the transmit power of a BS on a part of its total bandwidth and increase resistance to noise [1.11]. Although the received signal quality, in other words signal-to-interference plus noise ratio (SINR) as in Eqn. 1.2, can be improved by the power concentration, the allocated bandwidth, B in Eqn. 1.2, is decreased because only a part of total bandwidth can be allocated to the cell-edge MSs by the power concentration. Multi-link signal transmission solves this issue by having multiple BSs cooperate each other. When a BS transmits signal to a cell-edge MS in a part of total bandwidth, another cooperating BS transmits signal to the cell-edge MS in other part of total bandwidth in a coordinated fashion. Because the multiplexing of the signals from both BSs is conducted in the frequency domain, the signal processing of MSs is the same as normal single-cell transmission and much simpler than that of Joint transmission. However, when the frequencies of the cooperating BSs are different by frequency error, the signals received from both BSs interfere with each other and causes the degradation in communication quality. In this thesis, I propose an interference canceller to solve this issue in Chapter 3 and clarify the effect of the proposed method by mathematical analysis and computer simulations [1.12, 1.13].

Radio transmission technology is the technology to increase radio transmission efficiency of a communication channel and consists of modulation and demodulation, error correction coding and decoding, antenna technology, channel estimation, synchronization and so on [1.3, 1.14]. These technologies are not cell-edge specific but effective for all MSs, and it is possible to use these technologies in combination with Multi-BS cooperative transmission control in order to further improve cell-edge user throughput. Among these radio transmission technologies I focus on channel estimation in this thesis. In mobile communications, data signal is transmitted from a BS to an MS through radio communication channel, in which the amplitude and phase of the transmitted signal change dynamically by fading fluctuation caused by the mobility of the MS and propagation environment [1.14]. Therefore, MSs need to estimate the change in amplitude and phase accurately and compensate the fading fluctuation in order to receive the signal correctly. The estimation of the fading fluctuation is called channel estimation,

and the improvement in channel estimation accuracy results in the increase in throughput performance. It is noteworthy that the improvement in channel estimation accuracy is apart from the improvement in received signal quality, in other words SINR, shown in Eqn. 1.2. However, if channel estimation accuracy is low, effective received signal quality is degraded because of the fading compensation error in amplitude and phase. For example, if the simplest channel estimation without averaging is used, the necessary received signal quality to achieve the same throughput is degraded by 3dB [1.15]. This means 1bps/Hz loss in spectral efficiency from Eqn. 1.2, i.e. throughput loss of 10Mbps in a system with 10MHz bandwidth. Therefore, the improvement in channel estimation accuracy should be applied in combination with Multi-BS cooperative transmission control in order to improve cell-edge throughput. In channel estimation, a pilot signal is usually used, which is a known signal for both BS and MS. We can estimate fading fluctuation by dividing the received pilot signal by the known transmitted pilot signal, which is the change of amplitude and phase in radio channel. In most of mobile communications systems based on OFDM such as LTE, it is common to transmit pilot signals at regular intervals in both time and frequency domains. Therefore, it is effective to coherently average the channel estimates obtained by each pilot signal in both time and frequency domains [1.16, 1.17]. Moreover, another type of channel estimation method has been proposed; this is called "impulse-response based channel estimation" and does not rely on the averaging in the time or frequency domain [1.18]. However, the both works have been conducted independently, and I propose an integrated channel estimation approach and also conduct a dynamic optimization of channel estimation parameters by taking into account dynamically-changing fading environment [1.19-1.21].

Up until now, I described cell-edge communication quality from the view point of wireless channel. Although wireless channel quality usually affects communication quality the most, the impact of wired channel allocation should also be taken into account [1.22]. When Multi-BS cooperative signal transmission is used, the wireless channel quality of a cell-edge MS becomes better by the cooperative signal transmission from both BSs, while each of the both BSs needs to secure the wired channel for the cell-edge MS. Accordingly, excessive use of Multi-BS cooperative signal transmission may result in the exhaustion of wired channel in a BS. It is noteworthy that the limitation of wired channel means not only the shortage in wired access

channel capacity but also the number of simultaneous connections by the limitation of user management in BS. This exhaustion of wired channel causes blocking of newly generated calls and forced termination of handover. Therefore, the region where multi-BS cooperation is conducted should be controlled based on handover threshold control by taking into account both wireless and wired channels. However, such a research has not been conducted, and I propose a handover threshold control method taking both wireless and wired channels into account and also conduct a numerical analysis of the approach in Chapter 5 [1.23, 1.24].

In mobile communications, homogeneous network configuration has been widely used, in which almost the same size of cells are placed in a service area. However, in recent years, a new type of network configuration, which is called heterogeneous network configuration, is attracting much attention [1.25, 1.26]. In the heterogeneous network configuration, a large number of small cells are placed over macro-cell coverage area in order to increase network capacity drastically. When compared with homogeneous network configuration with small cells, heterogeneous network configuration does not degrade handover stability because MSs with high terminal speed such as vehicles can be connected to large macro cells even when a small cell is close to the MSs [1.26]. Moreover, heterogeneous network configuration is characterized by its flexibility in network capacity increase; it can increase its capacity by placing small-cell BSs in traffic hotspots while securing its coverage area by relatively large macro cells. One thing needed to be considered in heterogeneous network configuration is co-channel interference between macro and small cells. In LTE-Advanced, an interference control method called enhanced Inter-Cell Interference Coordination (eICIC) has been standardized [1.27]. eICIC avoids the interference between macro and small cells by setting some time slots, in which signal transmission is stopped. Here, it is important to decide the number of time slots dynamically depending on the distribution of MSs in the service area. I propose a centralized control system dynamically deciding the time-slot allocation based on network coordination in Chapter 6 [1.28]. Here, it is noteworthy that Multi-BS cooperative transmission control is still important even in heterogeneous network because the interference in the same layer, i.e. the interference among macro cells or among small cells, continues to exist. I also propose a control method of radio resource allocation for heterogeneous network configuration. In heterogeneous network configuration, the degree of congestion differs substantially per cell because of the

various sizes of cells. The user throughput of the MSs at cell edge in a congested cell tends to be extremely low because of few resource allocation as well as low received signal quality. Considering this, I propose a method giving cell-edge MSs a priority in resource allocation in order to avoid excessively low throughput of the MSs [1.29].

1.3 Outline of thesis

Multi-BS cooperative transmission control [1.6-1.9]

In Chapter 2, I study on Multi-BS cooperative transmission control, which consists of two technologies: (i) multi-BS cooperative muting control and (ii) multi-BS cooperative signal transmission. First, multi-BS cooperative muting control is investigated. As described in the previous section, the residual interference from reference signal prevents the throughput improvement in Multi-BS cooperative transmission. In order to solve this issue, I propose a reference signal interference canceller, in which MSs autonomously remove the residual reference signal interference. The proposed canceller utilizes the fact that reference signal is a known signal also for MSs, so MSs can make the replica signal of reference signal autonomously and remove the interference from the received signal, which results in throughput improvement. The control algorithm of the proposed canceller is also proposed, which decides whether the canceller should be turned on or off depending on the received signal quality implicating the effect of the canceller. I evaluate the effects of the proposed reference signal interference canceller by computer simulations and clarify its performance gain. I also develop a prototype system of the proposed canceller and demonstrate its feasibility through laboratory and field experiments.

In multi-BS cooperative signal transmission, both neighboring BSs transmit signal to cell-edge MSs in a coordinated manner. As described in the previous section, it is necessary to demonstrate its feasibility for the smooth introduction of the technology to commercial networks. From the view point of network configuration, there are two types: (i) centralized configuration and (ii) distributed configuration. In multi-BS cooperative signal transmission, the transmission timing of the signals from both BSs should be synchronized accurately. Centralized approach is relatively easier to realize the synchronization because the control is

conducted in the same centralized unit. However, depending on the signal processing capability of the centralized unit, cluster border is generated and the application of multi-BS cooperative signal transmission is impossible between the clusters. On the other hand, distributed configuration enables flexible cooperation among BSs because it does not rely on a centralized unit and realize Multi-BS cooperative signal transmission by using the network interface among BSs. However, the difficulties to achieve the synchronization control become higher. In the latter half of Chapter 2, I develop a prototype system of Multi-BS cooperative signal transmission with both centralized and distributed network configuration and demonstrate their feasibilities through laboratory and field experiments.

Multi-link signal transmission [1.12, 1.13]

Multi-link signal transmission is a form of Multi-BS cooperative signal transmission and effective to increase the cell-edge user throughput especially in large cells. As described in the previous section, in Multi-link signal transmission based on OFDM systems, the difference in frequency error between BSs collapses the orthogonality among signals and causes adjacent-channel interference, which degrades throughput. To solve this problem, I propose an interference canceller that mitigates the adjacent-channel interference caused by the frequency-offset differences in Chapter 3. This is achieved by the generation of the replica signal of the adjacent channel. In the proposed canceller, we first demodulate the signal from one BS and then generate the replica signal by taking into account the difference in frequency offset between the BSs. Finally, by subtracting the replica signal from the original received signal, we can mitigate the adjacent-channel interference from one BS when we demodulate the signal from the other BS. I also propose an extension method, which incorporate forward error correction decoding after demodulation in order to further improve the performance. I evaluate the effect of the proposed canceller by both numerical analysis and computer simulations.

Channel estimation [1.19-1.21]

As described in the previous section, accurate channel estimation is essential to prevent throughput degradation caused by fading compensation error. For OFDM-based systems, two types of channel estimation methods have been proposed: (i) averaging in the time and

frequency domains and (ii) impulse-response based method. In Chapter 4, I first propose a two-dimensional adaptive channel estimation method for time-domain spreading MC-CDMA systems, which is a combination of CDMA and OFDMA. Because fading fluctuates dynamically in both time and frequency domains caused by user mobility and multi-paths, I propose a method averaging channel estimates in both time and frequency domains with independent weight coefficient by taking into account channel conditions. The optimization of the weight coefficients depending on channel conditions is also conducted through computer simulations. I also extend this two-dimensional adaptive channel estimation method by combining impulse-response based channel estimation method in order to further improve channel estimation accuracy. I re-optimize the weight coefficient of the two-dimensional channel estimation methods by considering the additional gain from impulse-response based channel estimation and then evaluate channel estimation accuracy by computer simulations.

Handover [1.23, 1.24]

As described in the previous section, the impact of wired channel should also be taken into account when applying Multi-BS cooperative signal transmission when there is a limitation in wired channel capacity. In Chapter 5, I investigate the relations between wireless-channel quality and wired-channel capacity for CDMA mobile communications systems with soft handover as a simple form of Multi-BS cooperative transmission. In CDMA mobile cellular systems, MSs can simultaneously connect with multiple BSs by a soft handover technique. Soft handover has following advantages over conventional hard handover: (i) improving the radio channel quality by virtue of the decrease of total interference power, (ii) avoiding the interruption resulting from the connection switching and frequent connection changes (known as “ping-pong effect”). Its drawback is apparent; each MS in the soft handover state occupies wired channels at multiple BSs. Therefore, we need to identify the influence of such a redundancy on the wired channels. If all of wired channels of one BS have already been occupied, some MSs cannot enjoy soft handover because of lack of wired channels. The existence of such MSs must affect wireless channel quality. In Chapter 5, I evaluate the effect of the size of soft handover region on qualities of both wired and wireless channels comprehensively. I adopt blocking probability for newly arriving calls and forced termination

probability of handover calls as performance measures of wired channels, and outage probability for wireless channel quality. I derive these performance measures by an approximate analytical method. Through numerical examples, I show the effect of the size of soft handover region on the system performance.

Layered cell configuration [1.28, 1.29]

As described in the previous section, the adaptive interference control between macro and small cells based on eICIC is the key to improve the spectral efficiency of Layered cell configuration. In eICIC, the interference is reduced by stopping some parts of the downlink signal transmission of a BS. Therefore, it is important to decide the amount and the position of the muting effectively in order to increase system capacity. This decision is basically conducted in a distributed fashion at each BS, so that it becomes more difficult to control the co-channel interference effectively as the interference among cells becomes more complicated. In Chapter 6, I propose a network-based coordinated interference control system, in which all macro-cell and small-cell eNBs are connected to an IP backhaul network and the co-channel interference control is conducted in a centralized fashion. I also develop a prototype system of the network-based coordinated interference control system. In the prototype system, three types of interference avoidance schemes such as Non Multicast Broadcast Single Frequency Network Almost Blank Subfarme (Non-MBSFN ABS), MBSFN ABS and Blank subframe are implemented and I clarify the difference of the three types of ABSs through laboratory experiments. Moreover, I conduct field experiments in order to demonstrate the feasibility and clarify the throughput performance of the network-based coordinated interference control system.

In Chapter 6, radio resource allocation for layered cell configuration is also studied. This cell configuration yields a mixture of variously sized cells, from macro to small, and the MS and traffic distribution of each cell are quite different. Therefore, the distribution of the number and the received signal quality of the MSs is much wider than the conventional macro-cell homogeneous networks. This means that the cell-edge user throughput in a cell with large number of MSs is still expected to be low even in layered cell configuration.

The proposed scheme controls the scheduling priority individually per cell by taking into

account its cell-edge throughput performance. This is conducted based on the Generalized Proportional Fair (GPF) scheduling algorithm, which is an extension of the widely-used Proportional Fair (PF) scheduling algorithm. Because implementing the proposed scheme changes only the control algorithm of GPF, it is quite simple and can be applied simultaneously with Multi-BS cooperative signal transmission. We also propose a dynamic control algorithm in order to adaptively follow changes in the distribution over time. The performance of the proposed method is confirmed by computer simulations.

Chapter 2

Multi-BS Cooperative Transmission Control

2.1 Issues and Approaches for Multi-BS Cooperative Transmission Control

Many technologies such as OFDMA, MIMO, time/frequency-domain packet scheduler have been proposed and standardized in 3GPP LTE and LTE-Advanced to mainly improve capacity [2.1]. In cellular mobile communications, it is also important aspect to improve cell-edge throughput in order to improve user experience regardless of their place. The multi-BS cooperative transmission control, which is referred to as Coordinated Multi-Point (CoMP) transmission and reception in LTE-Advanced, is attracting attention recently as a promising way to improve cell-edge throughput [2.2]. The multi-BS cooperative transmission control can be mainly classified as multi-BS cooperative muting control and multi-BS cooperative signal transmission. The former mitigates neighbor-cell interference by muting its transmission, while the latter is more aggressive and transmits desired signal from both serving and neighbor BSs to cell-edge UEs [2.12, 2.15].

In this chapter, we first tackle multi-BS cooperative muting control in Section 2.2. Then, we also study on multi-BS cooperative signal transmission in Section 2.3 and 2.4. Finally, I summarize this chapter in Section 2.5.

2.2 Multi-BS Cooperative Muting Control

In ICIC, only scheduling and control information exchange is conducted, so that it is easier to implement compared to multi-BS cooperative signal transmission. This approach also eliminates the burden of signal processing for the simultaneous transmission from multiple BSs

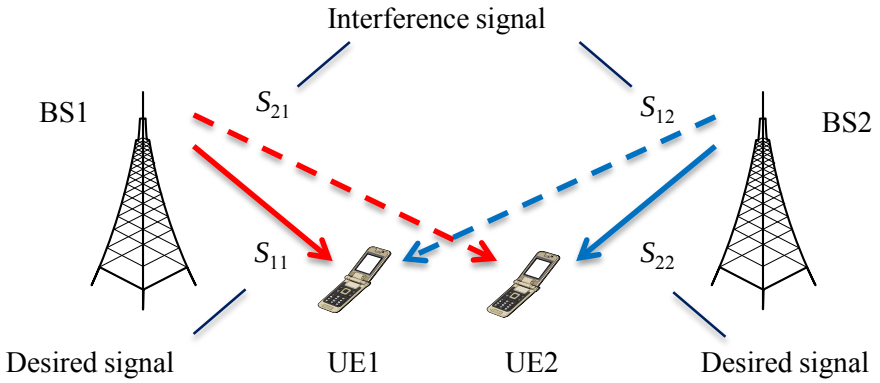

Figure 2. 1: Two-cell model

because the signal for a UE is transmitted from only one BS at any instant. In ICIC, the cell-edge throughput is improved by adaptively preventing BSs from transmitting signals that would otherwise impose strong interference on the cell-edge UEs in the neighboring cells. On the other hand, the cell overall throughput may degrade because no radio resource is allocated to UEs belonging to the muted BS. To resolve this issue, we propose a scheduling method, in which a neighbor BS is muted only when the improved throughput of a UE obtained by muting is superior to the total throughput possible without muting [2.13] . The proposed method makes it possible to increase cell edge throughput without degrading overall cell performance.

However, to apply this ICIC technique for current commercial systems such as LTE, one thing should be noted that reference signals (RSs) are always transmitted from each BS regardless of muting. RSs are generally known as pilot signals and used for channel estimation or received power estimation for handover. Therefore, even when muting is conducted, the muted BS still transmits RS and limits the performance improvement possible with the muting.

To solve this issue, we also propose an RS interference canceller for ICIC. In the proposed canceller, the RS received from the neighbor BS is cancelled by the UE; this is easily achieved because the RS is a common signal and can be detected by any UE. We also propose a control algorithm for the proposed canceller. When the received desired signal power is much larger than the received interference RS signal power, it becomes difficult to detect the neighbor RS accurately, which results in poor quality replica signal generation, which makes use of the canceller counterproductive. To prevent this, the proposed control algorithm activates the RS

interference canceller according to the reception environment of UE. We also conduct a basic lab experiment with 3GPP Rel. 8 LTE-compliant equipment to confirm the effect of the proposed RS interference canceller.

2.2.1 Inter-Cell Interference Coordination

Fig. 2.1 shows a two-cell model, in which two BSs exist, each with one UE. The following uses this two-cell model to explain the basic concept of ICIC. The received desired signal power of UE1 belonging to BS1 is defined as S_{11}; the received interference signal power from BS2 is S_{12}. The received desired and interference signal power for UE2 is denoted as S_{22} and S_{21}, respectively. We denote the received noise power of both UEs as N_0. The signal-to-interference plus noise ratio (SINR) of both UEs, γ_1 and γ_2, can be written as $\gamma_1=S_{11}/(S_{12}+N_0)$ and $\gamma_2=S_{22}/(S_{21}+N_0)$, respectively.

When we assume that both UEs are located at the cell border of BS1 and BS2 and all the received desired and interference signal powers are the same as S, i.e. $S_{11}=S_{12}=S_{22}=S_{21}=S$, and the S is sufficiently higher than the noise level, N_0, the SINRs, γ_1 and γ_2, are given as $\gamma_1=\gamma_2=S/(S+N_0)\approx 1$. In ICIC, when a BS is muted, the performance of the UE in the neighbor cell is improved because its major interference source is eliminated. The improved SINRs of UE1 and UE2, γ_1', γ_2', can be written as $\gamma_1'=S_{11}/N_0$ and $\gamma_2'=S_{22}/N_0$, respectively.

Although the SINR of the UE in the neighbor cell is improved, no radio resource is assigned to the UE in the muted BS, which may degrade overall cell throughput. To prevent this issue, we propose a criterion to trigger muting appropriately; BS muting is set only when it provides a gain in overall cell throughput [2.13] . This criterion is expressed as $\log_2(\gamma_1'+1)>\log_2(\gamma_1+1)+\log_2(\gamma_2+1)$.

When this criterion is satisfied, BS2 is muted. If UE2's throughput with muting is higher than that of UE1, BS1 is muted. In this example, the SINRs for UE1 and UE2 without muting are assumed to be 1, each capacity (spectral efficiency) can be 1 from the Shannon limit, so that muting is triggered if the capacity of UE1 or UE2 with muting becomes higher than 2. If we assume S/N_0 is 20 [dB], the capacity with muting is around 6.6 and so muting should be triggered.

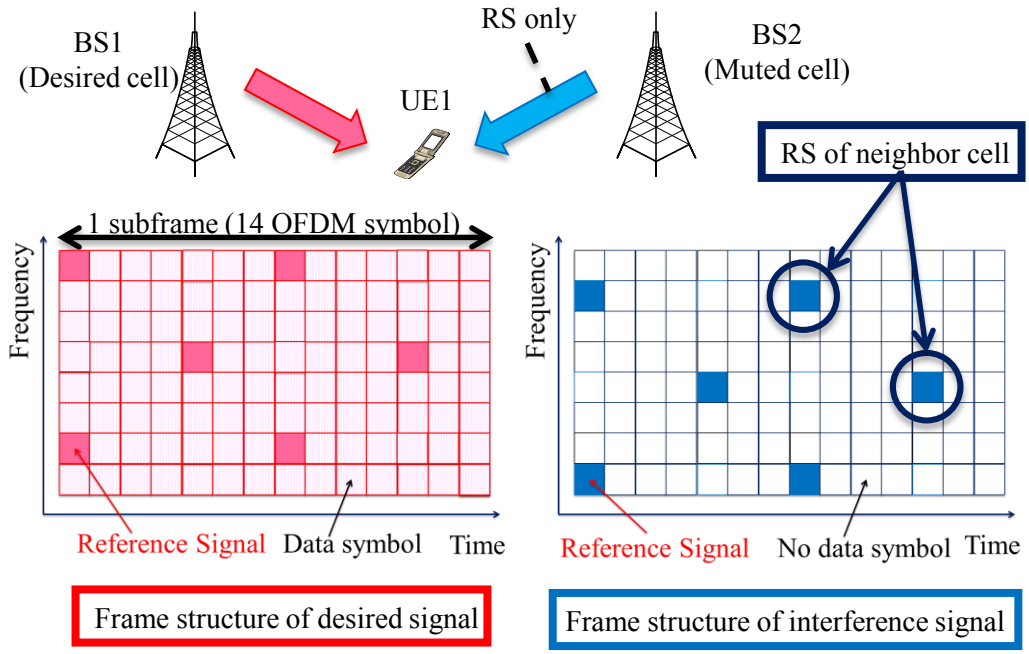

Figure 2. 2: Frame structure

2.2.2 RS Interference Canceller

2.2.2.1 Interference Cancellation

We assume the frame structure shown in Fig. 2.2. One subframe consists of 14 OFDM symbols, and the RSs are inserted every six subcarrier in the frequency domain and transmitted in the 1st, 5th, 8th, and 12th OFDM symbols in the time domain. We also assume that the received subframe and symbol timing for the UE are the same for BS1 and BS2, and that the RSs of each BS are offset by one-subcarrier in the frequency domain so as not to interfere with each other. Here, UE1 belongs to BS1 and receives its desired signal, and BS2 is muted by ICIC, which means that only RS is transmitted from BS2.

Because RS is transmitted every six subcarrier in the frequency domain and on four OFDM symbols out of the 14 OFDM symbols in a subframe, 4/84 of the total transmit power from the neighbor BS is still transmitted even when BS2 data signal transmission is muted. This remaining interference suppresses the performance gain possible with ICIC.

Therefore, we propose an RS interference canceller for ICIC, in which the RSs of neighbor cells are cancelled at UE. RS is a common signal used by all UEs to conduct channel estimation or measure received signal power from neighbor BSs for handover decision. Therefore, any UE can detect and cancel the RSs of neighbor cells with the following procedure. In the following, we assume that the first OFDM symbol in the subframe shown in Fig. 2.2 is transmitted, in which RSs are included for both BSs. The cancellation procedure is summarized by the following three steps.

(i) Conduct channel estimation for neighbor BS2
(ii) Generate replica signal from the channel estimate and cancel it from the original received signal
(iii) Conduct desired signal demodulation with the received signal after cancellation

Accordingly, first, channel estimation for BS2 is conducted. The received RS from BS2 experiences severe interference from the data signal from BS1, so an accurate channel estimation technique should be applied. There are many channel estimation techniques and any one of them can be used here as long as it offers sufficient channel estimation accuracy. As an example, we use the delay time-domain channel estimation approach, in which a primitive ZF channel estimate is transformed into the time domain channel impulse response. Then, only the cyclic prefix (called guard interval in some references) part of the channel impulse response is extracted and transformed again into the frequency domain[2.14] . This technique utilizes the fact that the channel elements in the channel impulse response are mainly present only in the cyclic prefix part, while the interference and noise elements are distributed evenly in the time domain.

In the second step, a replica signal is generated by using the channel estimate and canceled from the original received signal in the time domain. The replica signal cancellation can be conducted in the frequency domain if the received timings of signals from both BSs are close, within the cyclic prefix length; this can be realized by synchronizing the transmissions of BSs. To allow asynchronous BS operation, it is necessary to conduct replica signal cancellation in the time domain.

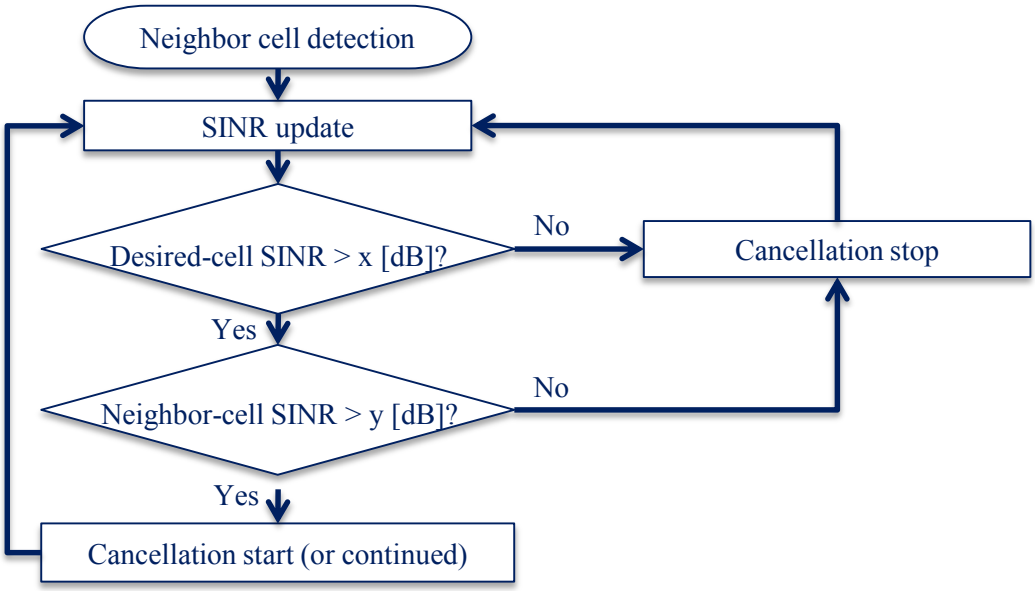

Figure 2. 3: Control algorithm of RS interference canceller

As the third, and final step, the refined signal is demodulated to yield the received data from BS1.

2.2.2.2 Control Algorithm of RS Interference Canceller

If the channel estimation accuracy for BS2 is poor, applying the RS interference canceller can be counterproductive. Therefore, the RS interference canceller should be properly activated. Accordingly, we propose a control algorithm for the RS interference canceller. The proposed algorithm considers both the SINR of the RS received from BS2 and the received SINR for BS1. The latter is necessary because the RS interference canceller offers little gain if the received SINR is too low, which means that there is a lot of interference and the effect of cancelling only RS is limited. The proposed control algorithm has five steps. Its flow chart is shown in Fig. 2.3.

(i) Neighbor cell is detected when its RS is observed by UE.

(ii) The SINRs for the desired BS and the neighbor BS are measured periodically.

(iii) The SINR for the desired BS is checked and RS interference cancellation is not conducted when the SINR is lower than or equal to a certain threshold, x [dB].

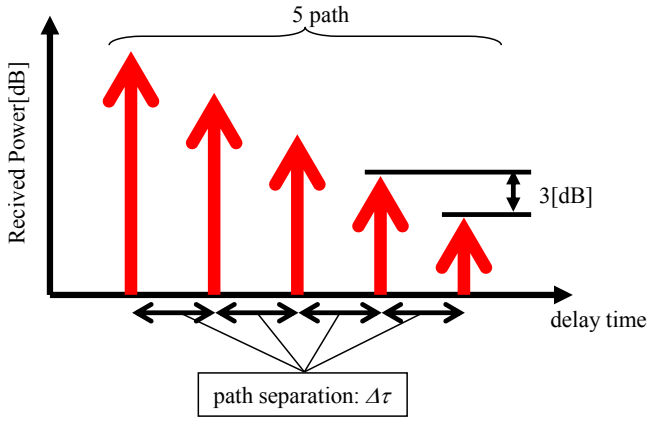

Figure 2. 4: Path model

(iv) The SINR for the neighbor BS is checked and RS interference cancellation is not conducted when the SINR is lower than or equal to a certain threshold, y [dB].

(v) If both conditions, (iii) and (iv), are satisfied, RS interference cancellation is started; the process from (ii) is repeated every time SINR measurement is updated, which is conducted periodically.

2.2.3 Evaluation

2.2.3.1 Simulation Conditions

We evaluated the proposed RS interference canceller by computer simulation. We assumed the two-cell model shown in Fig. 2.2. Simulation conditions are summarized in Table 2.1. We assumed a frame format, which is not exactly the same but as close as LTE system. The number of subcarriers is 1024 and the subcarrier spacing is 15 kHz; the OFDM symbol length is 66.7 μs. The cyclic prefix length is 4.69 μs. We used the path model shown in Fig. 2.4. This model represents a 5-path Rayleigh fading environment exhibiting exponential decay of averaged received power with equal interval of $\Delta\tau$ between adjacent paths. Its decay factor is 3dB per path, and each path is subjected to independent Rayleigh fading. We set the delay spread at 1.0 μs by adjusting $\Delta\tau$. We assumed quasi-static fading channel in this evaluation.

We used a frame structure shown in Fig. 2.2. The channel estimation technique explained in Sec. III-1 was used for both desired and neighbor BSs; the channel estimates are obtained on

Table 2. 1: Simulation conditions

Number of subcarriers	1024(15.36MHz)
OFDM symbol length	66.67μs (Subcarrier spacing: 15kHz)
Cyclic prefix length	4.69μs
Path model	Independent Rayleigh fading channel with exponential decay (Number of paths: 5, decay factor: 3dB)
Delay spread	1.0μs

four OFDM symbols per subframe because RSs are transmitted on the OFDM symbols, and these channel estimates are averaged in the time domain within a subframe.

We evaluated the spectral efficiency as a function of signal-to-interference ratio (SIR). We assumed that the UE was always served by BS1 and handover was not considered. The SIR is defined as the ratio of the received desired signal power from BS1 to the received interference power from BS2; the SIR is defined by assuming BS2 is transmitting at its maximum power regardless of muting. SNR is set at 20 dB at the cell border and SIR is changed by changing the received desired power. Therefore, when SIR is 10dB, SNR is 30 dB because the received desired power is increased by 10 dB.

We assumed Single Input Single Output (SISO) as the antenna configuration and calculated spectral efficiency from the ratio of the received power of desired signal to the sum of the residual received power of interference signal and noise power after RS interference cancellation; this SINR calculation is conducted per subframe. The spectral efficiency is calculated as the Shannon capacity multiplied by 0.75 by taking a realistic AMC (Adaptive Modulation and Coding) into account [2.20].

2.2.3.2 Evaluation Results

Evaluation results are shown in Fig. 2.5. We evaluated following four methods.

(i) Without canceller (BS2 is not muted)

(ii) Without canceller (BS2 is muted)

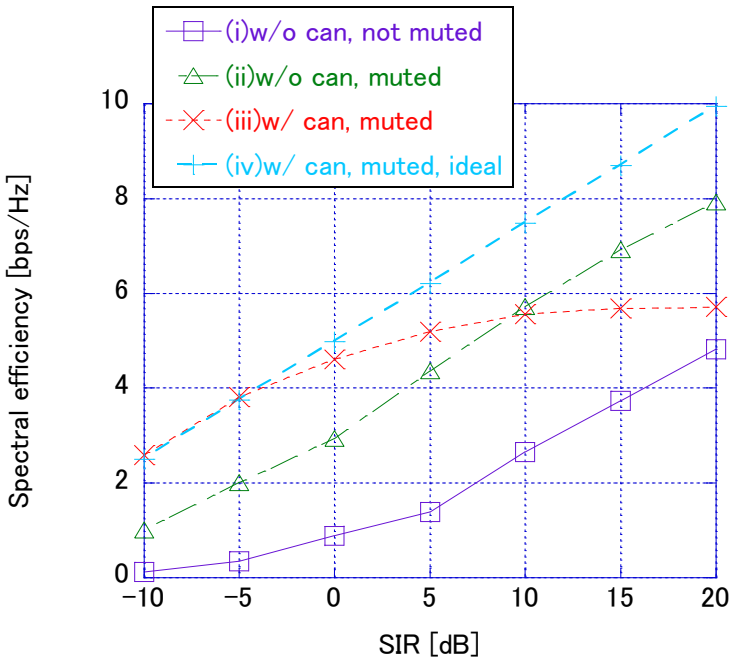

Figure 2. 5: Spectral efficiency

(iii) With canceller (BS2 is muted)

(iv) With canceller (BS2 is muted, ideal channel estimation is assumed.)

As shown in Fig. 2.5, the spectral efficiency of (ii) is improved by muting BS2, but this performance gain is limited by the RS transmission from BS2. (iii) shows the spectral efficiency with the proposed RS interference canceller, and we can observe that the spectral efficiency is further improved. When SIR is 0 dB, the spectral efficiency is further improved, by 1.6 times, compared to (ii). While the RS interference canceller is effective near the cell border, the spectral efficiency with the RS interference canceller becomes inferior to that without it when SIR becomes larger than 10 dB. This is due to the channel estimation accuracy. When SIR is high, it is difficult to obtain accurate channel estimates for BS2 because the SIR of RS from BS2 is strongly suppressed by the interference from the BS1 data signal. Therefore, it is important to apply the control algorithm described in Section 2.2.2.2 to prevent the drop in spectral efficiency by keeping the RS interference canceller active at all times. (iv) shows the performance assuming ideal channel estimation instead of the channel estimation described in

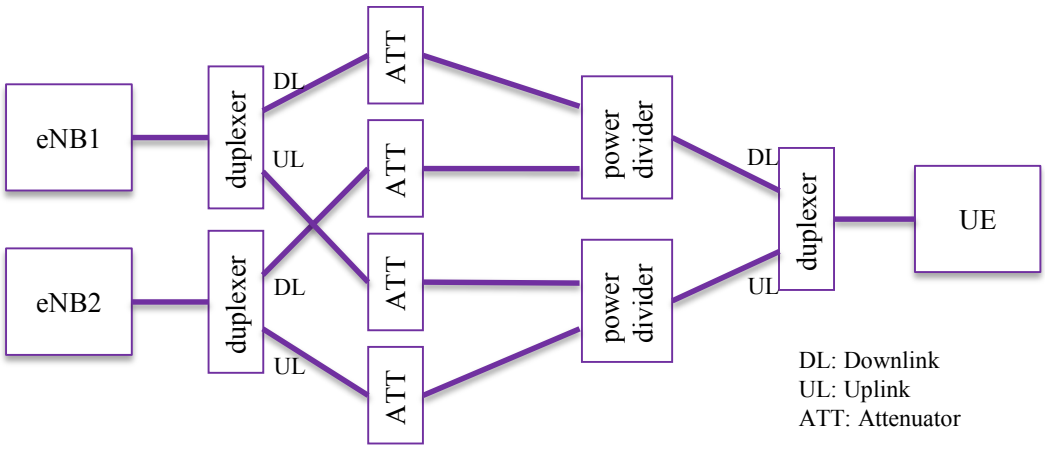

Figure 2. 6: Laboratory configuration

Section 2.2.2.1. This means that the spectral efficiency obtained by using the RS interference canceller can be further improved by applying more advanced channel estimation techniques; the SIR range, in which the RS interference canceller is effective, can also be extended to beyond 10 dB.

2.2.3.3 Basic lab experiment

We also conducted a basic lab experiment to confirm the effect of the proposed RS interference canceller with 3GPP Rel. 8-compliant LTE equipment. The same configuration as in Fig. 2.2 was used and the detailed configuration of the lab experiment is shown in Fig. 2.6. The downlink and uplink signal of each eNB, which is an BS equipment in LTE, are separated by a duplexer, and the downlink signals from both eNBs are combined at a power divider and received by a UE. The received power was controlled by attenuators so as to make the same setting as the simulation evaluation. The received power of the uplink was controlled by attenuators so as to realize high quality received environment, which does not give any impact on the downlink performance.

The difference in parameters between the lab experiment and the simulation was the number of subcarriers and the path models. The number of subcarriers was 600 following the setting of 5MHz in LTE, and the evaluation was conducted under an AWGN channel. The simulation conditions were the same as those in Table 1 except path model and that there exists

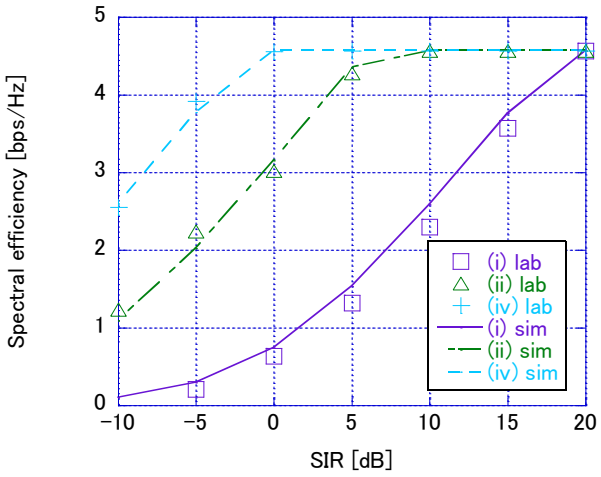

Figure 2. 7: Laboratory experiment results

an upper bound on spectral efficiency considering the realistic modulation and coding in LTE; the upper bound was set at 4.57 bps/Hz.

The UE used in this experiment was not equipped with the RS interference canceller, so that we evaluated the performance of the RS interference canceller virtually by stopping the transmission of RS signal from eNB2, which means that there was no signal transmission from eNB2. This corresponds to case (iv), "With canceller (BS2 is muted, ideal channel estimation is assumed.)", because there is no interference by the ideal interference canceller in this case.

The lab experiment results are shown in Fig. 2.7. The experiment results are shown with marks and the simulation results are shown with lines. We evaluated the cases (i), (ii) and (iv), which correspond to the same cases in Sec. 2.2.3.2. From the results, it is clearly shown that the lab experiment results are almost the same as the simulation results. Therefore, we can say that the proposed RS interference canceller will achieve performance improvement as shown in the difference between the cases (ii) and (iv) even with 3GPP Rel-8 LTE-compliant equipment if the cancellation algorithm with accurate channel estimator is properly implemented.

2.3 Multi-BS Cooperative Signal Transmission

Multi-BS cooperative signal transmission has been attracting much attention as an effective way to improve cell-edge throughput. It is referred to as Coordinated Multi-Point (CoMP)

transmission and reception in LTE-Advanced standardization activities. In the multi-BS cooperative signal transmission, multiple BSs jointly transmit signals to the same UE by coordinating desired and interference signals [2.8] [2.10] . Considering the burden of information exchange among the BSs, inter-sector cooperation is an easy way to implement multi-BS cooperative signal transmission. The common approach to the evolved Node B (eNB), which is BS equipment in LTE, has each eNB perform the signal processing for the three sectors belonging to the eNB. Therefore, channel state information (CSI) gathered for each sector does not have to be exchanged among eNBs, and the multi-sector cooperative transmission signal can be generated within the eNB. One drawback of this approach is that only UEs located in the areas between sectors can benefit from the cooperative transmission, and UEs located at the cell edges between sites rarely enjoy the benefits of cooperative transmission.

To solve the cell-edge weakness of inter-sector cooperation, we proposed a novel sector configuration, in which three sectors belonging to the same eNB are located at different sites that are linked by optical fiber, e.g. remote radio head (RRH) or radio on fiber (RoF)[2.14] . With this sector configuration that we call distributed sector configuration after here, UEs located at the cell edges between sites can benefit from the function of inter-sector cooperation. That is, we can realize the same effect as inter-cell cooperation, which usually requires information exchange among eNBs, by using the easy-to-implement inter-sector cooperation. We have clarified that inter-sector cooperation with the proposed distributed sector configuration provides throughput performance superior to that of the conventional sector configuration, in which the three sectors are located at the same site by a computer simulation [2.14] .

To clarify the benefits of inter-sector cooperation applied on the distributed sector configuration in actual environments, we implemented the function on 3GPP Release 8 LTE-compliant equipments and conducted a field trial in Kitakyushu, Fukuoka prefecture, Japan. In this field trial, we set up the above distributed sector configuration with RoF and evaluated the performance provided by multi-cell cooperative transmission; two BSs were arranged to transmit signals simultaneously to a UE at the cell edge between them. We evaluated three different types of cooperative transmission: “cooperative power combining”, “cooperative SFBC”, and “cooperative SDM”. In cooperative power combining, the same signal is

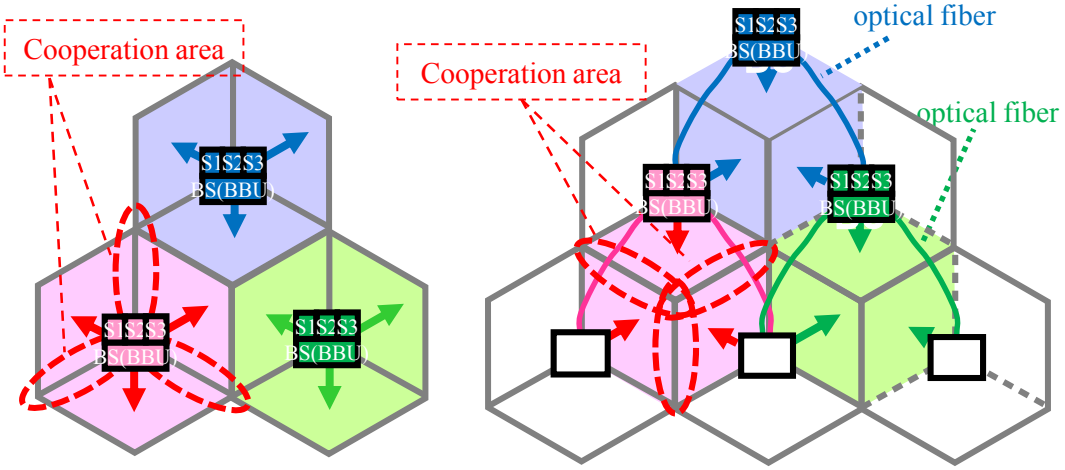

(a) Conventional sector configuration (b) Distributed sector configuration with fiber optics

Figure 2. 8: Sector configuration

transmitted simultaneously from the two BSs and the UE receives the signals by spatial power combining. In cooperative SFBC and cooperative SDM, the two BSs use transmit/receive diversity based on SFBC (Space Frequency Block Coding) (MIMO-SFBC) and spatial division multiplexing (MIMO-SDM), respectively.

In this section, we show the field trial results of multi-cell cooperative transmission and clarify that multi-cell cooperative transmission can improve cell-edge throughput dramatically.

2.3.1 Inter-sector cooperation on distributed sector configuration using optical fiber

Fig. 2.8 shows the distributed sector configuration using optical fiber; each cell comprises three sectors. Fig. 2.8 (a) shows the conventional sector configuration. In this configuration, a BS consisting of a base band unit (BBU) and three radio frequency units (RFUs) is placed at each site. BBU and RFU are responsible for base-band signal processing and RF processing, respectively. With the conventional sector configuration, in which the three RFUs are placed at the same site, UEs located in areas between sectors (indicated by the dotted line in the figure) are the mainly recipients of inter-sector cooperation. Fig. 2.8 (b) shows the distributed sector configuration with optical fiber. In this configuration, three RFUs belonging to the same BBU

Table 2. 2: Major parameters of eNB and UE

	Downlink	Uplink
Access system	OFDMA	SC-FDMA
Carrier frequency	1495.9MHz	1447.9MHz
System bandwidth	10MHz	
Number of subcarriers	600 (Sub-carrier spacing is 15kHz.)	
Symbol length	66.67μs + Cyclic Prefix 4.69μs	
Sub-frame length	1ms	
Number of transmitter antennas	1 or 2	1
Number of receiver antennas	2	2
Transmit power	43dBm/antenna	23dBm
Modulation	QPSK, 16QAM, 64QAM	QPSK, 16QAM
Channel coding/decoding	Turbo code/ Max-Log-MAP decoding	

are placed at different sites that are linked by optical fiber. Each RFU is located at the vertex of a hexagonal cell. With this sector configuration, UEs located at the cell edge between sites (indicated by the dotted line in the figure), can enjoy the benefits of inter-sector cooperation. They normally suffer poor received signal quality because the desired signal is weak while the interference signals are strong. We have clarified that the inter-sector cooperation on the distributed sector configuration achieves better performance in both average and cell edge throughput compared to the conventional centralized sector configuration[2.14] . Especially, the cell edge throughput is 20 percent higher than that of the conventional sector configuration [2.14] .

2.3.2 Field trial system configuration

In this field trial, we used 3GPP Release 8 LTE-compliant eNB and UE as the BSs and mobile station, respectively. Major device parameters are summarized in Table 2. 1Table 2. 2. Carrier frequency of the downlink and the uplink is 1495.9MHz and 1447.9MHz, respectively. The system bandwidth is 10MHz. The downlink wireless access system is OFDMA and the number of sub-carriers is 600; the sub-carrier spacing is 15 kHz and the symbol length is 66.67 μs. Normal cyclic prefix is used with length of 4.69 μs. 1x2 single input multiple output (SIMO)

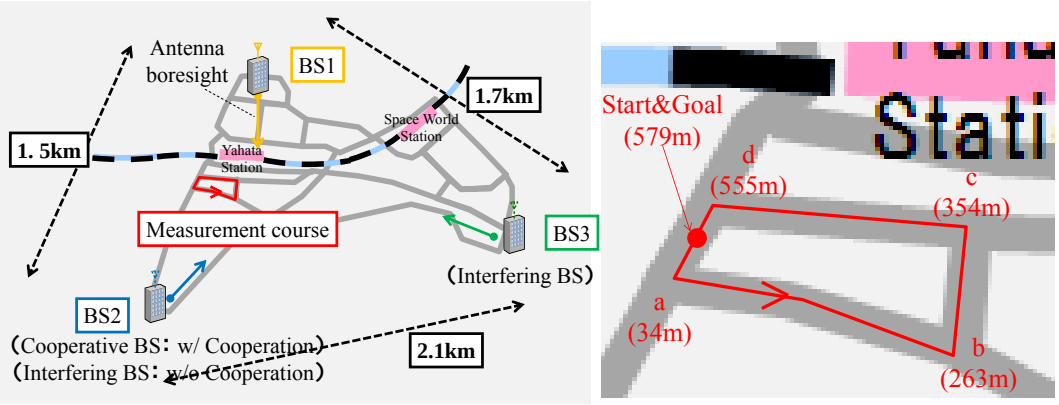

(a) Area map (b) Measurement course (extended figure)

Figure 2. 9: Field trial area

and 2x2 MIMO can be used as the downlink antenna configuration and MIMO-SFBC and MIMO-SDM are supported. For the uplink, 1x2 SIMO is used. For both downlink and uplink, adaptive modulation and channel coding (AMC), hybrid automatic repeat request (HARQ), and radio link control (RLC) layer retransmission are used. Transmit power of eNB and UE are set at 20 W per transmitter antenna and 200 mW, respectively.

2.3.3 Field Trial

2.3.3.1 Field Trial Configuration

We conducted the field trial in the area shown in Fig. 2.9 (a). We used three BSs, with the following separations: BS1-BS2 1.5 km, BS1-BS3 1.7 km, and BS2-BS3 2.1 km. One eNB responsible for three sectors was placed in the building of BS1. RFUs on BS2 and BS3 were connected to eNB by RoF. The transmit power of each BS was 20 W per transmitter antenna and sector antennas with the gain of 14 dBi (including cable loss) and half-value angle of 90 degrees were used. When we denote North as 0 degrees, the boresight orientation was 180 degrees for BS1, 60 degrees for BS2, and 270 degrees for BS3. The tilt angle was 4 degrees for all BSs. We conducted measurements on a rectangular course located roughly midway between BS1 and BS2. Fig. 2.9 (b) shows an extended figure of the measurement course. Its total length was around 600 m. The received signal powers from BS1 and BS2 were almost the same at “b” point in the figure. The received signal power from BS3 was around 20 dB lower at the same point.

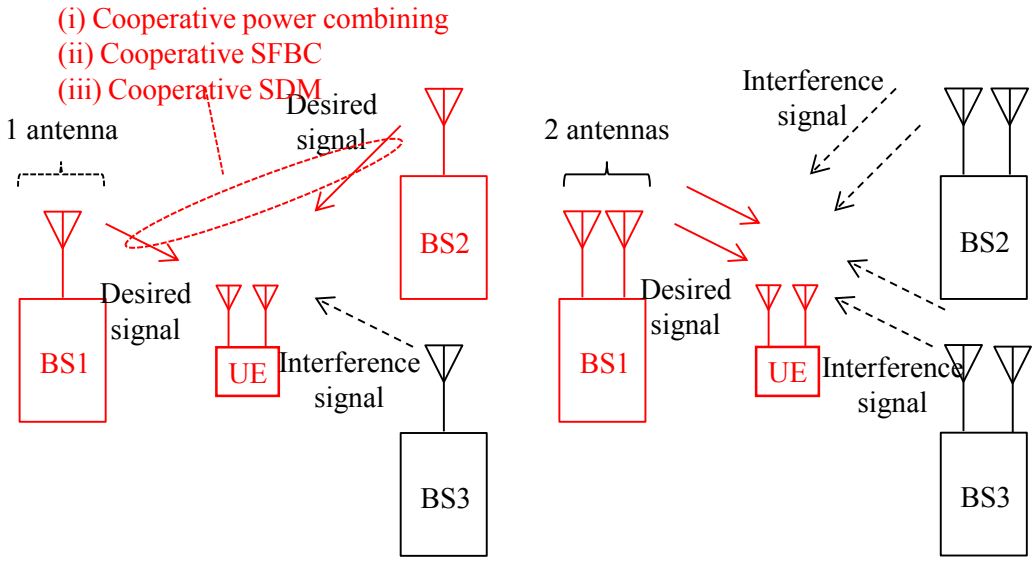

(a) Multi-cell cooperative transmission (b) Without cooperation

Figure 2. 10: Transmission schemes

The measurement course is basically non-line of sight (NLOS) for all BSs. The delay spread of the propagation channel between the course and BS1 ranged from 0.2 μs to 0.3 μs; it ranged from 0.4 μs to 0.6 μs for BS2. We drove around the course at about 30 km/h (maximum Doppler frequency was about 40 Hz).

2.3.3.2 Configuration of multi-cell cooperative transmission

Fig. 2.10 (a) and (b) show the test configurations with and without multi-cell cooperative transmission, respectively. When multi-cell cooperative transmission is used, each BS has one antenna, and the antennas of BS1 and BS2 are used to realize cooperative transmission. Without cooperative transmission, only BS1 transmits to the UE by MIMO-SDM. In the evaluation of cooperative transmission, we evaluated (i) cooperative power combining, (ii) cooperative SFBC, (iii) cooperative SDM, and (iv) without cooperation. Details are as follows.

1. Cooperative power combining

   Same signal is transmitted from the two BSs simultaneously and power combining is used at UE as in SFN (Single Frequency Network).

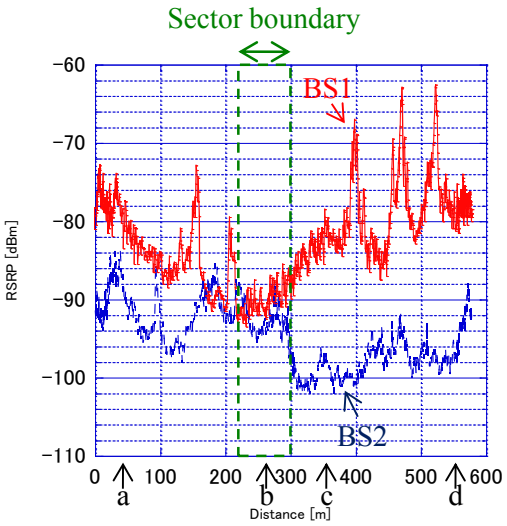

Figure 2. 11: RSRP from BS1 and BS2

2. Cooperative SFBC

   The two BSs form 2x2 MIMO antenna configuration and transmit one stream based on MIMO-SFBC.

3. Cooperative SDM

   The two BSs form 2x2 MIMO antenna configuration and transmit two streams based on MIMO-SDM.

4. Without cooperation

With cooperative transmission, the signal from BS3 is the sole interference signal; without cooperative transmission, the signals from BS2 and BS3 are interference signals. In this field trial, both with and without cooperative transmission, we used the 2x2 MIMO antenna configuration for desired signal transmission. The transmit power of each antenna was set at 20 W for all antennas. As MIMO-SDM, we used open-loop MIMO, which is defined in LTE [2.16] .

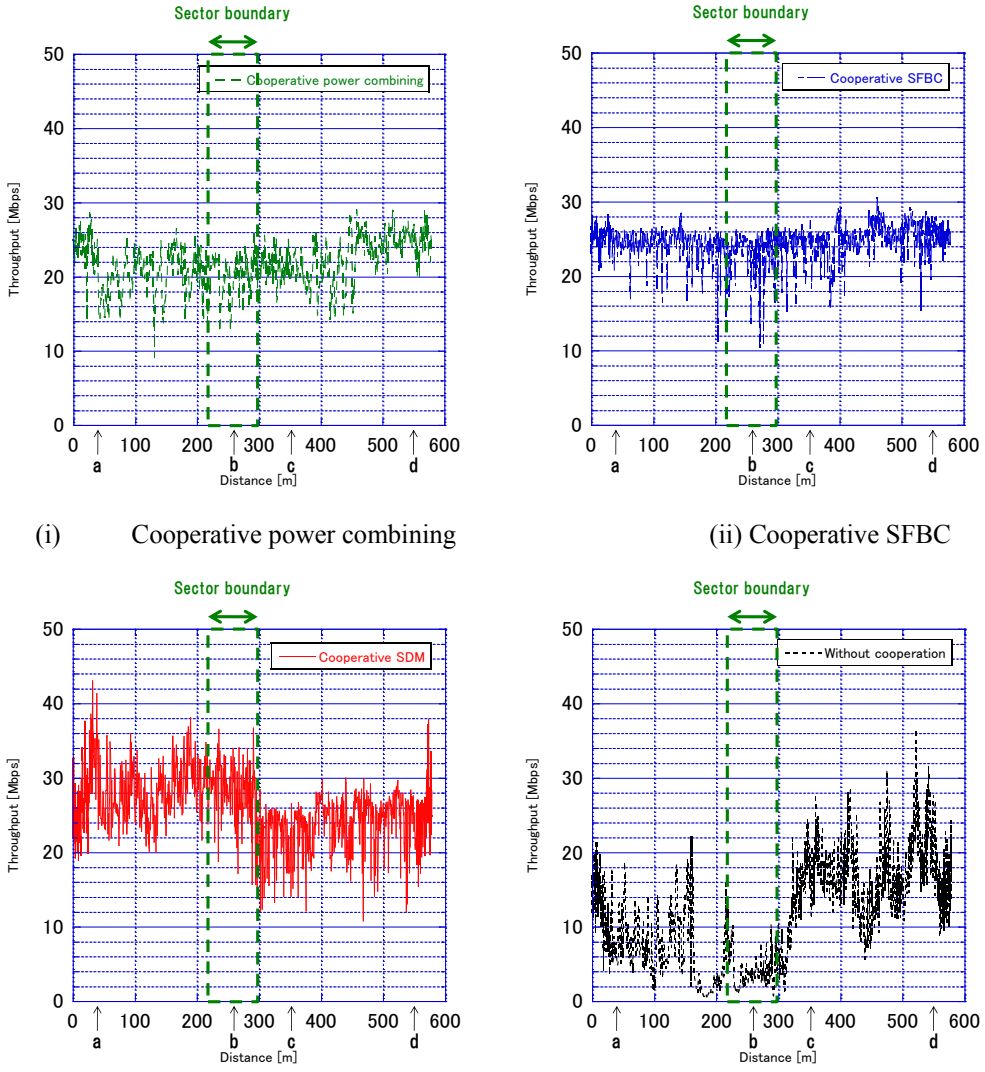

Figure 2. 12: Throughput characteristics

2.3.3.3 Results of Field Trial

Fig. 2.11 through Fig. 2.13 show the results of the field trial. Fig. 2.11 shows reference signal received power (RSRP), which means the received power of the reference signal used as the pilot signal for channel estimation in LTE. The figure shows RSRP when cooperative SDM is used, and each RSRP from BS1 and BS2 is shown. In cooperative SDM, “power boosting” is used, that is, the transmit power of RS from one transmitter antenna is higher than that of the

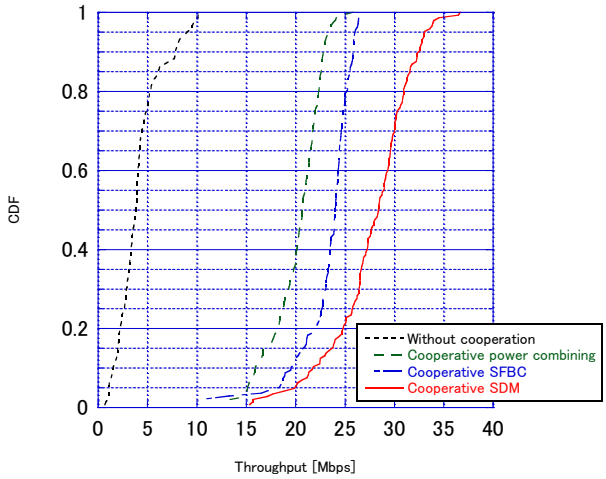

Figure 2. 13: CDF of sector boundary throughput

data channel by 3 dB. Therefore, the RSRP value is higher by 3 dB than the transmit power of data channel per sub-carrier per transmitter antenna. The x-axis shows the distance from the start point, see Fig. 2.9 (b). In the section within 40 m from b point, which is the section from 220 m to 300m, the received powers from BS1 and BS2 differ by less than 2 dB or so. Hereafter, we denote this region as “sector boundary”.

Fig. 2.12 shows the throughput characteristics when we drove around the measurement course. We also show the CDF of the throughput of the sector boundary in Fig. 2.13. From Fig. 2.12, it is clear that cooperative transmission improves throughput performance compared to the case without cooperation. When we do not use cooperative transmission, the throughput degrades to the minimum of 1 Mbps due to the strong interference signal from BS2. On the other hand, with cooperative transmission, because the interference signal from BS2 changes to a desired signal for the cell-edge UE, the throughput improves drastically. While the 50 % median throughput is 4 Mbps without cooperative transmission, that with cooperative power combining improves to 21 Mbps. With cooperative SFBC, the throughput becomes 24 Mbps due to the benefits of transmit diversity; with cooperative SDM, the throughput improves further to 28 Mbps due to the two-stream transmission. It is clear that cooperative transmission is made even more effective by introducing more advanced signal processing schemes such as SFBC and SDM.

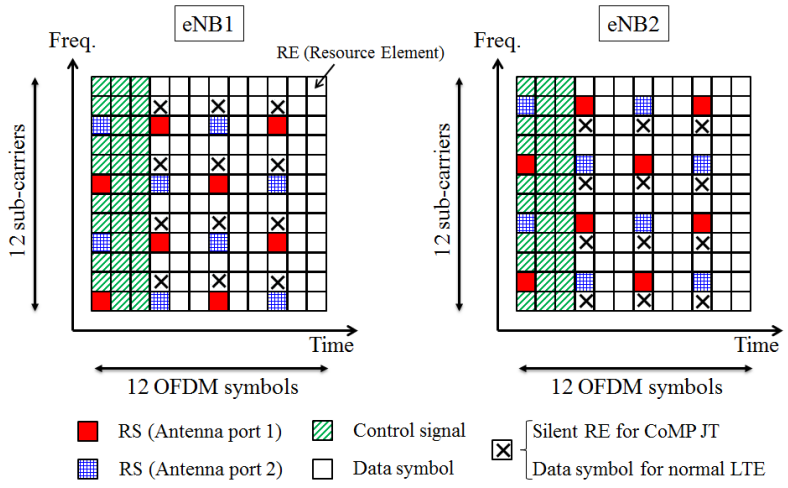

Figure 2. 14: Downlink frame format

2.4 X2-based Multi-BS Cooperative Signal Transmission

Multi-BS cooperative signal transmission with fiber optics shown in previous section makes it possible to improve cell-edge throughput different from inter-sector cooperation. Although the number of antenna sites being able to be connected to the same eNB can be infinite in theory, it is usually a few due to the limitation of the signal processing capability of eNB. Therefore, when we define a set of RRHs connected to the same eNB as “cluster”, CoMP JT can be used only within the cluster and the cell-edge UEs located at the “cluster” border cannot enjoy the merit of CoMP JT, which results in poor throughput.

As a solution to the issue, CoMP JT based on a distributed cooperation approach using inter-eNB interface such as X2 interface has been proposed [2.17, 2.18]. In the distributed cooperation, joint signal transmission is conducted from the geographically-separated eNBs; this is realized by achieving accurate synchronization based on Global Positioning System (GPS). Cooperating scheduling is also conducted through the negotiation between cooperating eNBs via inter-eNB interface. In the distributed cooperation approach, because there is no cluster unlike the centralized cooperation, CoMP JT can be used at any cell border, which gives all cell-edge UEs a chance to improve their throughput by CoMP JT.

However, the previous studies mainly showed only the concept or evaluated the basic

Table 2. 3: Major parameters of the prototype system

	Downlink	Uplink
Access system	OFDMA	SC-FDMA
Carrier frequency	3385MHz	3315MHz
System bandwidth	10MHz	
Number of subcarriers	600	
Symbol length	66.67μs+Cyclic Prefix 16.67μs	
Sub-frame length	1ms	
Number of transmitter antennas	2	1
Number of receiver antennas	2	2
Transmit power	43dBm/antenna	23dBm
Modulation	QPSK, 16QAM	QPSK
Channel coding/decoding	Turbo code/Max-Log-MAP decoding	

performance through computer simulations and feasibility study with a real system has not been conducted. In this section, we develop first-ever prototype system of CoMP JT based on distributed cooperation approach using inter-eNB interface. The detailed specifications and techniques for the prototype system are described. We also conduct laboratory and field experiments to verify the feasibility in a real system and clarify the performance improvement in cell-edge throughput.

2.4.1 CoMP joint transmission over X2 interface

2.4.1.1 System configuration

The major parameters of the prototype system are summarized in Table 2.3. We developed the prototype system based on LTE system. The carrier frequency of the downlink and the uplink is 3385MHz and 3315MHz, respectively. The system bandwidth is 10MHz. The downlink wireless access system is Orthogonal Frequency Division Multiple Access (OFDMA) and the number of sub-carriers is 600; the sub-carrier spacing is 15 kHz and the symbol length is 66.67 μs. Extended cyclic prefix, the length of which is 16.67 μs, is used. The downlink and uplink antenna configurations without CoMP are 2x2 Multiple Input Multiple Output (MIMO) and 1x2 Single Input Multiple Output (SIMO), respectively. The transmit power of eNB and UE are set at 20W (43dBm) per transmitter antenna are 200mW (23dBm), respectively.

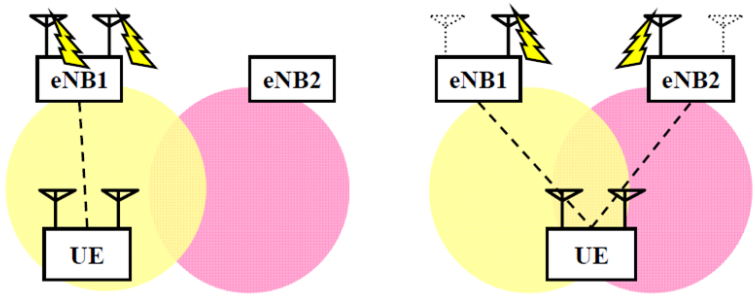

(a) normal LTE (w/o CoMP JT) (b) CoMP JT

Figure 2. 15: Antenna configuration

Fig. 2.14 shows the downlink frame format of the prototype system. The frame formats of neighboring two eNBs are shown for the explanation below. One subframe consists of 12 OFDM symbols and the duration is 1ms. In the frequency domain, the minimum resource allocation unit is 12 sub-carriers and the bandwidth is 180kHz. Control signal is transmitted in the first three OFDM symbols in each subframe. Reference Signal (RS) for channel estimation is transmitted per three OFDM symbols in the time domain. In the OFDM symbols including RS, RS is inserted every 6 sub-carriers in the frequency domain per transmit antenna; RSs from different antenna ports are mapped on different sub-carrier (RE: Resource Element) with three sub-carrier separation. Please note that the RE with the mark "X" is used for data symbol transmission in normal LTE transmission without CoMP JT.

In CoMP JT, as an initial implementation, the antenna configuration of 2x2 MIMO is used. The antenna configuration is shown in Fig. 2.15. Only one transmit antenna is used in each eNB in CoMP JT and a total of two transmit antennas are used. With this configuration, MIMO-Space Division Multiplexing (MIMO-SDM) is implemented and two-stream transmission is realized. In this implementation, one data stream is transmitted from each antenna. As shown in Fig. 2.14, in the downlink frame format of CoMP JT, the concept of "silent RE" is used[2.19] . With this technique, in CoMP JT, no data symbol is transmitted in the RE where RS is transmitted in the cooperating neighbor eNB. Therefore, the channel estimation accuracy can be drastically improved by eliminating the neighbor interference on RS. In CoMP JT, the SINR of the data channel can be improved because the interfering neighbor eNB is turned into an eNB also transmitting desired signal for the UE. However, as the RS still receives

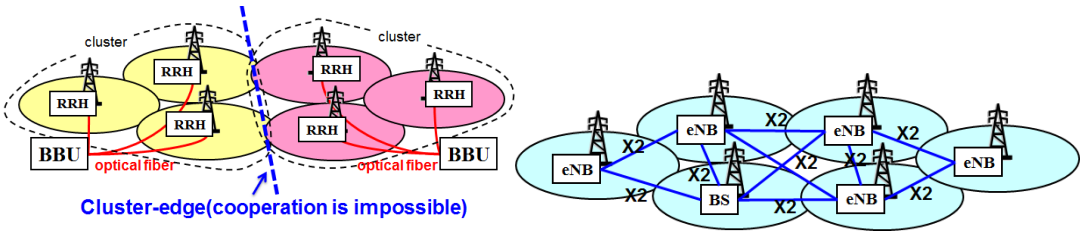

(a) Centralized cooperation (b) Distributed cooperation

Figure 2. 16: Network configuration

strong interference from the neighbor data symbol, the channel estimation accuracy remains low, which leads to poor throughput performance in spite of the high SINR of the data channel. Therefore, this silent RE is one of the key techniques to achieve high throughput performance in CoMP JT. In the uplink, the signal is transmitted for only the serving eNB and 1x2 SIMO receiver diversity is used.

For the downlink, adaptive modulation and channel coding (AMC) is used. As an initial implementation, only QPSK and 16QAM are implemented and the maximum Modulation and Coding Scheme (MCS) is limited to 13, so that the maximum throughput is around 23Mbps in normal LTE. Channel Quality Indicator (CQI) is fed back from a UE every 1 ms to notify its received signal quality such as Signal-to-Interference plus Noise Ratio (SINR); eNB decides MCS based on the fed-back CQI. Regarding retransmission, Hybrid Automatic Repeat reQuest (HARQ) in Medium Access Control (MAC) layer and Automatic Repeat request (ARQ) in Radio Link Control (RLC) layer is used. In CoMP JT, different from normal LTE, the number of HARQ process is set at 20 to cover the forwarding delay over inter-eNB interface. The details of HARQ for CoMP JT are described in [2.20] .

2.4.1.2 Network configuration

Fig. 2.16 shows the network configuration for centralized and distributed cooperation. In centralized cooperation shown in Fig. 2.16 (a), optical fiber systems such as RRH or RoF are utilized to realize the cooperation. The RRHs located at the center of the cells are centralized to a central signal processing unit, Base Band Unit (BBU). Therefore, CoMP JT can be realized easily because the joint signal transmission is conducted within one BBU. Also, the cooperating

scheduling such as resource allocation and the decision to adaptively start and end CoMP JT can be conducted in a centralized manner. However, CoMP JT can be used only within each cluster and the cooperation beyond a cluster border is impossible.

On the other hand, distributed cooperation in Fig. 2.16 (b) enables CoMP JT at any cell border by utilizing inter-eNB interface such as X2 interface. Because no central signal processing unit is necessary, every eNB can cooperate with any neighbor eNB to realize CoMP JT for cell-edge UEs. One challenge to realize this distributed cooperation is to realize joint signal transmission from neighboring eNBs, which are connected over asynchronous IP network; this is realized by achieving highly accurate synchronization between them based on GPS. The details of the synchronization are described in [2.19] .

2.4.1.3 Cooperative scheduling

Another challenge is to achieve cooperative scheduling on distributed configuration. Unlike centralized cooperation, necessary information to decide resource allocation or to start and end CoMP JT is not gathered at one place. Therefore, a control algorithm to conduct cooperating scheduling effectively on distributed cooperation is necessary. The flow chart of the control algorithm is shown in Fig. 2.17. This is the flow chart to decide the start of CoMP JT. For simplicity, we assume a two-cell model consisting of eNB1 and eNB2 and each eNB has one UE, UE1 and UE2; UE1 is located at the cell border and communicates with eNB1 in normal LTE. When UE1 nears cell border, it sends a Measurement Report (MR) to notify eNB1 the receiving environment of UE1 to prompt handover or CoMP JT. The threshold to start to send MR is instructed in advance by eNB and is based on RSRP difference from the serving and neighbor eNBs. In MR, RSRPs from eNB1 and eNB2 are included. When eNB1 receives a MR, it first makes a handover decision. When the neighbor RSRP is higher than the serving RSRP plus handover threshold, UE1 is handed over to eNB2. If the handover criterion is not satisfied, the decision to start CoMP JT is conducted.

When in CoMP JT, the UE enjoying the merit of CoMP JT can improve throughput drastically, while no UE can receive data in the neighbor eNB. Therefore, CoMP JT may degrade sum throughput of both eNBs. When we denote the throughput of UE1 and UE2 without CoMP JT as C_1 and C_2, the sum throughput is C_1+C_2. Therefore, when the throughput of

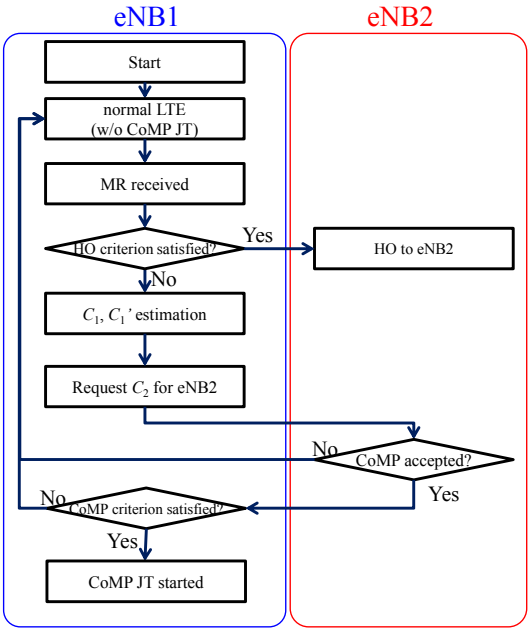

Figure 2. 17: Flow chart of control algorithm

UE1 with CoMP JT is defined as C_1', if the following condition is satisfied, sum throughput is not degraded when ρ is 1.

$$\rho(C_1 + C_2) \leq C_1' \tag{2.1}$$

Here, ρ is a parameter to adjust the priority of cell-edge throughput. When ρ is set at lower than 1, CoMP JT is started even when C_1' is not larger than C_1+C_2, which means cell-edge throughput is prioritized.

In order to improve cell-edge throughput without degrading sum throughput by using this condition, it is necessary to estimate throughput with and without CoMP JT. This estimation can be done by using feedback information from UE such as CQI and RSRP in MR. From the feedback information, we first estimate SINR with and without CoMP JT and then throughput is estimated based on Shannon capacity [2.21] .

Going back to the flow chart, in eNB1, C_1 and C_1' are calculated based on the feedback from UE1. Unlike centralized cooperation, in distributed cooperation, eNB1 does not know the throughput of UE2, C_2. Therefore, eNB1 requests C_2 for eNB2. In eNB2, except when its degree of congestion is quite high, it approves eNB1 (UE1) to start CoMP JT; C_2 is sent to eNB1 with the approval. After that, the condition in (1) is checked in eNB1 and final decision whether to

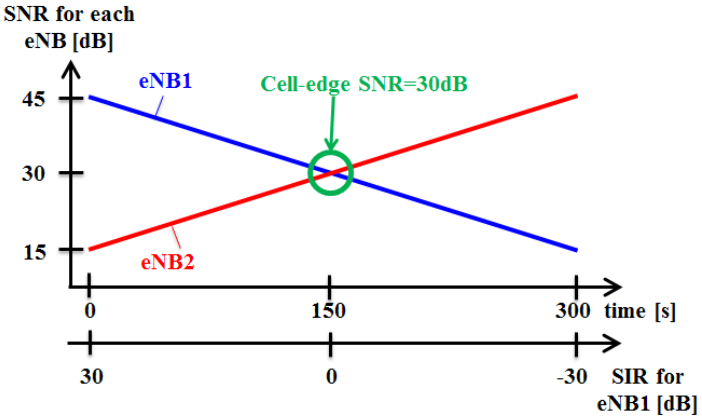

Figure 2. 18: Received power setting

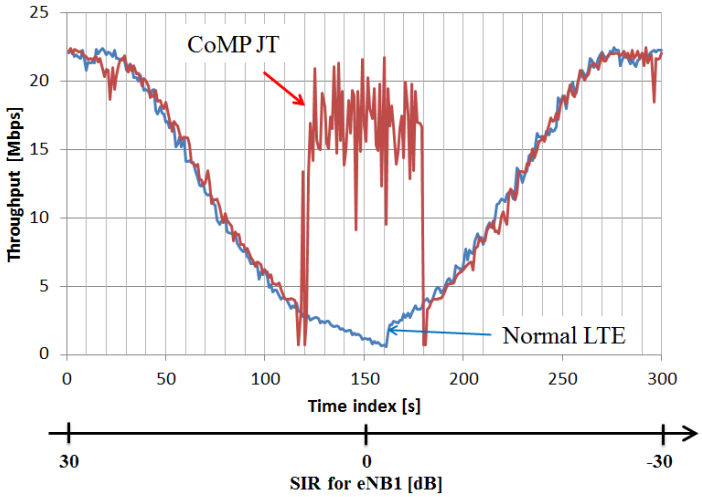

Figure 2. 19: Throughput performance

start CoMP JT or not is made. The decision to continue or end CoMP JT is conducted similarly.

In the prototype system, as an initial implementation, a simplified control algorithm is used. The CoMP request is issued based on the RSRP difference from the serving and the neighbor eNBs instead of calculating throughput with and without CoMP JT. And, the neighbor eNB unconditionally accepts CoMP JT request regardless of the congestion in the eNB. The end of CoMP JT is also conducted based on RSRP difference. Another way to end CoMP JT is handover as described in Fig. 2.17.

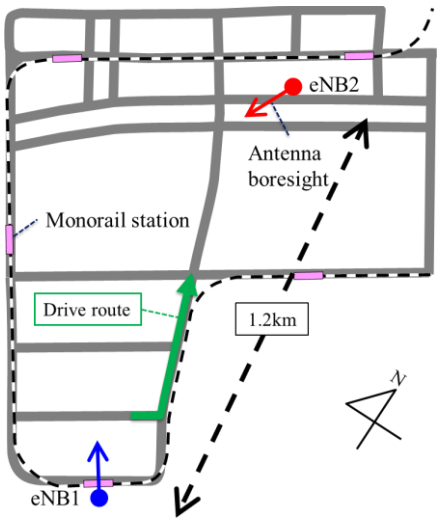

Figure 2. 20: Field trial area and drive route

2.4.2 Laboratory experiment

We first conducted a laboratory experiment. We used two eNBs and assumed a model that a UE moves from the neighborhood of one eNB to the neighborhood of the other eNB. Relative received powers from both eNBs were set as shown in Fig. 2.18. The y-axis shows SNR for each eNB; the SNR at cell edge was set at 30dB. We used Extended Vehicular A (EVA) channel model, the delay spread of which was 0.36μs. The maximum Doppler frequency was set at 70Hz. The received level was changed by a fading simulator continuously at the rate of 1dB per 10 seconds.

CoMP JT is started when the RSRP difference becomes smaller than or equal to 6dB; CoMP JT is ended when the difference becomes larger than or equal to 9dB. The 3dB difference between the start and end threshold is set to avoid so-called ping-pong effect. The handover threshold is set at 6dB.

Fig. 2.19 shows the throughputs with and without CoMP JT. Without CoMP JT, the throughput decreases as the UE approaches the cell border. When SIR becomes -3dB, i.e. the neighbor RSRP becomes 3dB higher than the serving RSRP, a handover is conducted and the UE gets served by eNB2. On the other hand, with CoMP JT, when SIR becomes 6dB, i.e. the

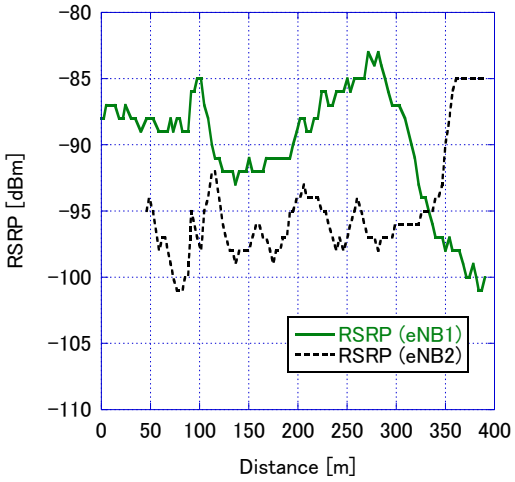

Figure 2. 21: RSRP

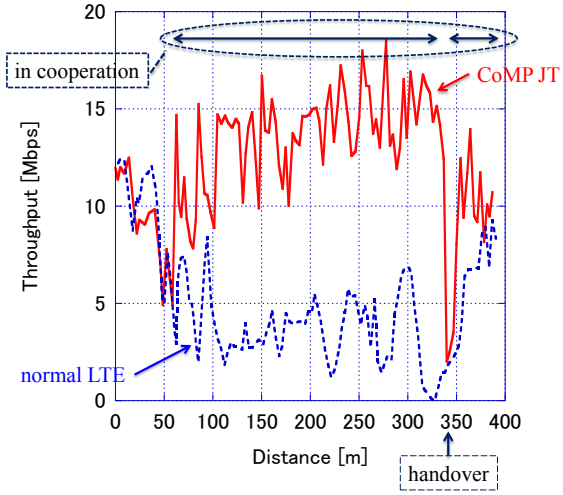

Figure 2. 22: Throughput performance

RSRP difference becomes 6dB, CoMP JT is started and throughput is improved drastically from 2.5Mbps to beyond 15Mbps. Then, when SIR becomes -6dB, handover is conducted and the UE gets served by eNB2. In CoMP JT, regardless of the delay as long as 20ms between eNBs, both AMC and HARQ worked well and the throughput reached its maximum, around 20Mbps.

2.4.3 Field experiment

2.4.3.1 Field experiment environment

We conducted a field experiment in an urban area in Tokyo, Japan. The area map is shown in Fig. 2.20. We used two eNBs; the separation of them is 1.2km. The eNBs were connected to each other by an inter-eNB interface on an asynchronous IP network. The transmit power of each eNB was 20 W per transmitter antenna and +45/-45 degree dual-polarized sector antennas were used; the gain was 16dBi and the half-value angle was 90 degrees. Denoting magnetic north as 0 degrees, the antenna boresights were 330 degrees for eNB1 and 210 degrees for eNB2 in a clockwise fashion. Each antenna was placed on top of a building and antenna height was around 90m. UE antennas were placed on top of a test car at a height of around 3m.

We conducted measurements on a driving course located between eNB1 and eNB2 as shown in Fig. 2.21. The total length was around 400 m. RSRP from both eNBs are shown in Fig. 8. The x-axis shows the distance from the start point of the driving course. RSRPs of eNB1 and eNB2 cross at around 330m and this is the handover point. The driving course was mostly Non-Line Of Sight (NLOS) for both eNBs. The delay spread of the propagation channel ranged from 0.2 μs to 0.7 μs for eNB1 and from 0.3 μs to 0.8 μs for eNB2. UE movement speed was around 10 km/h (maximum Doppler frequency was about 30 Hz).

2.4.3.2 Field experiment results

We compared the throughput performance with and without CoMP JT. CoMP JT start and end threshold were set at 6dB and 12dB, respectively. The handover threshold was set at 1dB. The throughput is shown in Fig. 2.22. In the case without CoMP JT, throughput decreases gradually as the UE approaches the cell border and a handover is conducted at the distance of 330m. On the other hand, with CoMP JT, when the UE reaches the distance of 60m, CoMP JT is started as the RSRP difference becomes smaller than 6dB. Then, the cooperation continues to the handover point. After the handover, CoMP JT is started again because the RSRP difference is smaller than 6dB. In this time, the serving cell is not eNB1 but eNB2. During CoMP JT, throughput is around 14Mbps on average, while the throughput without JT is around 3Mbps, that is around 5 times throughput improvement was confirmed.

2.5 Summary

We first proposed an RS interference canceller for ICIC. In ICIC, the data signal transmission from a BS is stopped when it improves the throughput of cell-edge UE belonging to the neighbor BS without degrading overall system throughput. However, even when the data signal transmission is stopped, RS is still transmitted from the muted BS and the interference to the cell-edge UE in the neighbor BS limits the throughput improvement. In our proposed RS interference canceller, the RS received from the muted BS is cancelled at the active UE; this is easily done because RS is a broadcast common signal that can be detected by any UE. We also propose a control algorithm for the RS interference signal canceller. This algorithm deactivates the RS interference canceller when being active would be counterproductive. To reduce signal processing cost, the algorithm halts the canceller when there is no performance gain. We conducted a computer simulation and clarified that the proposed canceller improves spectral efficiency by 60 percent when SIR is 0 dB and SNR is 20 dB. We also clarified that the canceller is effective as long as SIR does not exceed 10 dB. We also conducted a basic lab experiment to confirm the effect of the proposed RS interference canceller, and it was clearly shown that the lab experiment results are almost the same as the simulation results.

We then conducted a field trial to clarify the performance of multi-cell cooperative transmission by implementing the function on 3GPP Release 8 LTE-compliant equipments. The field trial was conducted on a distributed sector configuration, in which three sectors belonging to the same eNB are placed at different sites and linked by optical fiber. With this sector configuration, it becomes possible for UEs at the cell edges between sites to benefit from inter-sector cooperation, which is easy to implement. In the field trial, we set up the sector configuration with a RoF system. We examined several types of cooperative transmission: cooperative power boosting, cooperative SFBC, and cooperative SDM. While the 50 % median throughput of the UE at cell edge degrades to around 4 Mbps without cooperation, that with cooperative power combining reaches 21 Mbps. With cooperative SFBC and cooperative SDM, the median throughput becomes much higher, 24Mbps and 28Mbps, respectively, which shows that advanced signal processing leads to better performance.

Finally, we also developed first-ever CoMP JT prototype system based on a distributed

cooperation approach using inter-eNB interface. The details of its system configuration, network configuration and cooperative scheduling which is a key to realize effective cooperation on a distributed scheme were described. We also conducted laboratory and field experiments and verified the feasibility in a real system and confirmed that cell-edge throughput can be drastically improved.

Chapter 3

Multi-Link Signal Transmission

3.1 Issues and approaches for multi-link signal transmission

The received signal power becomes quite low at cell edge in a service area with large cells such as rural area, so the throughput of cell-edge MSs is affected by thermal noise as well as the interference from neighbor BSs. It is an effective way to concentrate transmit power in a part of its system bandwidth in order to improve the tolerance to thermal noise. Three-cell reuse is a way to achieve this, and the influence of thermal noise and the interference power from neighbor BSs can be simultaneously mitigated [3.1] . Fractional frequency reuse is another type of cell reuse, in which cell reuse is applied in a part of system bandwidth to improve cell-edge performance while one-cell reuse is used in remaining part of system bandwidth to increase spectral efficiency [3.2-3.5].

In these schemes, cell-edge MSs basically have access to only a part of the system bandwidth where the transmit power at BS is boosted by the power concentration; this becomes a bottleneck for improving cell-edge performance because of the limited resource allocation bandwidth. Here, it should be noted that cell-edge MSs can receive signals from both neighboring BSs with almost the same power because they are located at cell border. Multi-link signal transmission has been proposed as a way to improve cell-edge throughput by taking into account this nature of cell-edge MSs [3.6-3.8]. Especially in OFDM systems, when the signals to a cell-edge MS from both neighboring BSs are multiplexing in the frequency domain, i.e. each signal is transmitted on different sub-carriers, it is beneficial for the MS from the view point of signal processing because it can receive both signals similarly as single-cell reception [3.9] .

In multi-link signal transmission for OFDM systems, given timing synchronization among BSs and sufficient guard interval length, the orthogonality among signals from adjacent BSs can

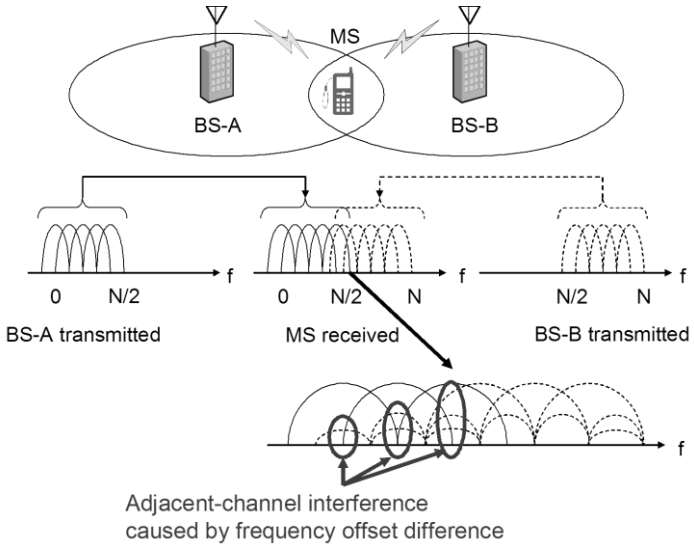

Figure 3. 1: System model of multi-link signal transmission

be retained as it is in normal OFDM communications. However, it is generally true that BSs have different frequency errors caused by the inaccuracies of their oscillators. Demand for high frequency bands and using cheaper oscillators to reduce costs are likely to strengthen the impact of these frequency errors. Unfortunately, in multi-link signal transmission, this will collapse the orthogonality among signals causing adjacent-channel interference to degrade the communication quality.

To solve this problem, we propose a novel interference canceller that mitigates the adjacent-channel interference caused by the frequency-offset differences [3.10, 3.11]. If the BSs have different frequency offsets, signals received from multiple BSs are not orthogonal to each other, and adjacent-channel interference is generated. The proposed method makes, in advance, a replica of the adjacent-channel signal and removes it from the original received signal to prevent harmful adjacent-channel interference.

In the proposed canceller, it is important to achieve accurate channel estimation to make sure the accuracy of the replica signal. The channel estimation accuracy is usually improved by averaging channel estimate values over both time and frequency. It is also possible to further improve the channel estimation accuracy by using time-domain channel estimation based on the characteristics of channel impulse response as in [3.12] . Considering that the above accurate channel estimation techniques are applicable to the proposed canceller, we assume ideal channel

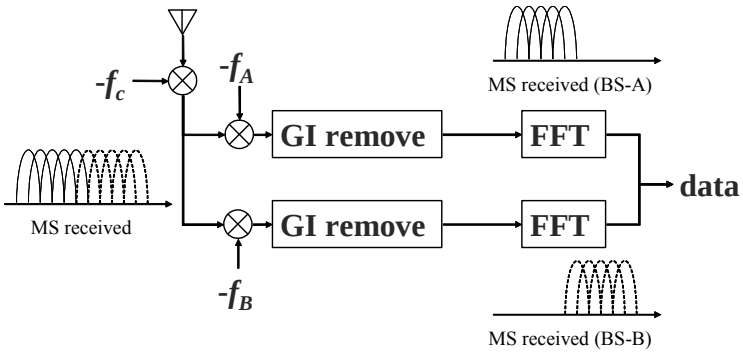

Figure 3. 2: Block diagram of the receiver for multi-link signal transmission

estimation in this chapter in order to focus on the impact of adjacent-channel interference. We evaluate both residual interference and BER performance by numerical analysis and computer simulations.

This chapter is organized as follows. Section 3.2 outlines multi-link transmission in OFDM systems. Section 3.3 describes the proposed interference canceller. Section 3.4 explains our approach to numerically analyzing the proposed canceller. Section 3.5 shows the results of our numerical analysis and computer simulations. Finally, we summarize this chapter in Section 3.6.

3.2 Multi-link signal transmission in OFDM systems

To simplify the evaluation, we assume the simple two-cell model shown in Fig. 3.1. In multi-link OFDM transmission, we assume that base station A (BS-A) transmits its signal on sub-carriers 0 to N/2−1. Similarly, BS-B transmits its signal on sub-carriers N/2 to N−1. The mobile station (MS) receives signals from both base stations. To focus on the impact of an adjacent-channel interference, we assume that the remaining sub-carriers in each base station are not used.

As described in the previous section, adjacent base stations have different frequency errors, so it is impossible to realize accurate frequency-offset compensation when using one frequency-offset compensator. Therefore, we have to compensate the frequency offset separately for each base station. A block diagram of this is shown in Fig. 3.2. Here, we denote the frequency offset between BS-A (or BS-B) and MS as f_A (or f_B). First, we duplicate the received

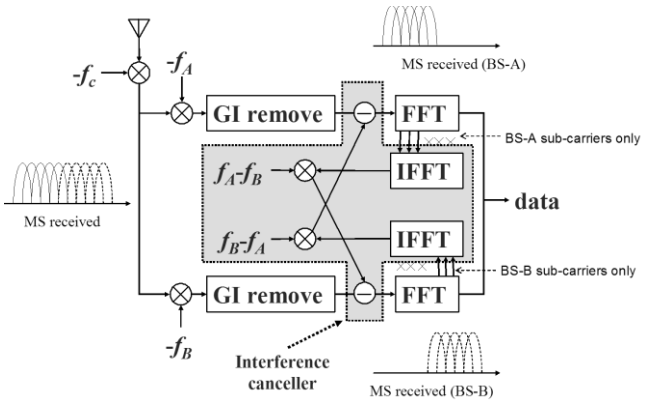

(a) Canceller using replica generation without decision (RG)

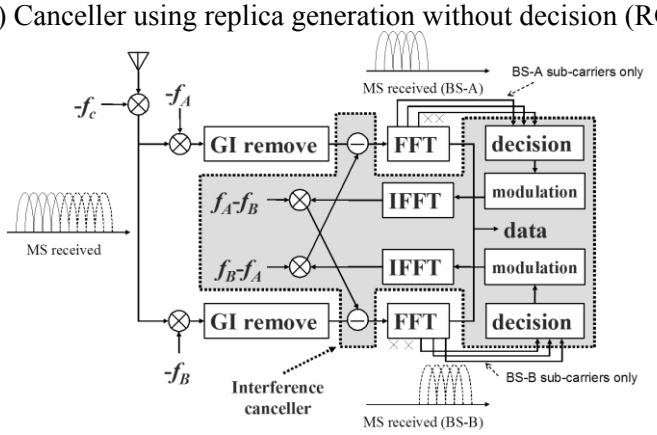

(b) Canceller using replica generation with decision (RGd)

Figure 3. 3: Block diagram of proposed canceller

base-band signal, which is down-converted at the center frequency, f_c, and compensate each frequency offset. Next, after removing the guard interval, we retrieve the sub-carriers by Fourier transform. Finally, we combine the sub-carriers and demodulate them. In this process, even if the frequency-offset compensation for each BS is perfect, the difference in frequency offsets among the BSs yields adjacent-channel interference as shown in Fig. 3.1.

3.3 Frequency-offset interference canceller

Fig. 3.3 shows the block diagram of the proposed interference canceller. Cancellation must be conducted for both signals, but to simplify the explanation, we focus on BS-A signal reception. In the figure, the blocks inside the dotted line represent the proposed interference canceller. Other blocks are the same as those in Fig. 3.2.

The interference canceller must accurately generate the replica needed for cancellation. In this paper, we propose two methods: 1) Replica generation without decision (RG) and 2) Replica generation with decision (RGd).

The basic replica generation process estimates the frequency offset for BS-B, f_B, compensates the frequency offset, and decomposes the received signal into sub-carrier elements by Fourier transform after the GI is removed. In RG method, only BS-B sub-carrier elements at the output of FFT are used directly as the replica. In RGd method, on the other hand, first, only BS-B sub-carrier elements are demodulated. Next, the decided symbol is re-modulated and multiplied by the corresponding frequency responses to generate the replica.

After the replica is generated, it is converted into a time-domain signal by inverse Fourier transform, followed by the frequency adjustment of f_B-f_A. Finally, the cancellation signal is subtracted from the received signal.

3.4 Numerical analysis of frequency-offset interference canceller

3.4.1 Analysis model

In this section, we analyze the performance of the proposed interference canceller by assuming the following analysis model. As in Fig. 3.1, we consider OFDM as the wireless access system and denote the sub-carrier spacing as Δf and the number of sub-carriers as N. Two adjacent BSs, BS-A and BS-B, split the sub-carriers. BS-A uses the sub-carriers from 0 to $N/2-1$, and BS-B uses the remaining sub-carriers from N/2 to N−1. We also assume that the frequency of BS-B is offset from that of BS-A by Δf_{off}.

3.4.2 Adjacent-channel interference caused by frequency-offset difference

Before analyzing the performance of the proposed methods, we first clarify the impact of the adjacent channel interference caused by the frequency-offset difference between the two base stations. The signal transmitted from each base station, $s_A(k)$ and $s_B(k)$, can be expressed as follows.

$$s_A(k) = \sum_{n=0}^{N/2-1} d_n e^{j2\pi nk/N} \tag{3.1}$$

$$s_B(k) = \sum_{n=N/2}^{N-1} d_n e^{j2\pi nk/N} e^{j2\pi\alpha k/N} \tag{3.2}$$

Here, n is the sub-carrier index, d_n is the modulated symbol for the n-th sub-carrier, k is the sample number index, and α is the frequency offset difference between base stations, which is normalized by the sub-carrier spacing. That is, $\alpha = \Delta f_{off}/\Delta f$.

We assume that the propagation channel consists of N_p discrete paths experiencing independent Rayleigh fading. The complex path gains of the p-th path are denoted as $h_A(p)$ and $h_B(p)$ for BS-A and BS-B, respectively. Here, $\mathrm{E}\left[\sum_{p=0}^{N_p-1} |h_A(p)|^2\right] = 1$. E[.] is the ensemble average operation. The same definitions are used for $h_B(p)$. The time delays of the p-th path for each BS are assumed to be the same and are denoted as τ_p, i.e. sample-space delay. The received signal at the mobile station, $r(k)$, can be written as follows.

$$r(k) = \sum_{p=0}^{N_p-1} h_A(p) s_A(k-\tau_p) + \sum_{p=0}^{N_p-1} h_B(p) s_B(k-\tau_p) \tag{3.3}$$

In this equation, we ignore the noise to focus on the adjacent-channel interference power. The signals from both base stations suffer adjacent channel interference from each other and the impact is symmetrical. Accordingly, we consider hereafter only the impact of interference from BS-B on the BS-A signal. The l-th sub-carrier element of BS-A obtained by Fourier transform, $R_{noc}(l)$, which includes interference element, $I_{noc}(l)$, can be written as follows.

$$\begin{aligned} R_{noc}(l) &= \frac{1}{N}\sum_{k=0}^{N-1} r(k) e^{-j2\pi lk/N} \\ &= d_l H_A(l) + I_{noc}(l) \qquad ;0 \le l < N/2 \end{aligned} \tag{3.4}$$

where

$$
\begin{aligned}
I_{noc}(l) &= \frac{1}{N}\sum_{k=0}^{N-1}\sum_{p=0}^{N_p-1} h_B(p)s_B(k-\tau_p)e^{-j2\pi lk/N} \\
&= \frac{1}{N}\sum_{n=N/2}^{N-1} d_n \sum_{p=0}^{N_p-1} h_B(p)e^{-j2\pi mp\Delta\tau/N}\sum_{k=0}^{N-1} e^{j2\pi(n-l+\alpha)k/N} \\
&= \frac{1}{N}\sum_{n=N/2}^{N-1} d_n H_B(n+\alpha)\frac{1-e^{j2\pi(n-l+\alpha)}}{1-e^{j2\pi(n-l+\alpha)/N}} \\
&= \frac{1}{N}\sum_{n=N/2}^{N-1} d_n H_B(n+\alpha)\frac{\sin(\pi(n-l+\alpha))}{\sin(\pi(n-l+\alpha)/N)}e^{j\pi\frac{N-1}{N}(n-l+\alpha)}
\end{aligned}
\tag{3.5}
$$

The frequency response for each base station, $H_A(l)$ and $H_B(n+\alpha)$, can be expressed as follows.

$$
H_A(l) = \sum_{p=0}^{N_p-1} h_A(p)e^{-j2\pi l\tau_p/N} \tag{3.6}
$$

$$
H_B(n+\alpha) = \sum_{p=0}^{N_p-1} h_B(p)e^{-j2\pi(n+\alpha)\tau_p/N} \tag{3.7}
$$

Taking the ensemble average of the above equations yields the average interference power, $P_{noc}(l)$.

$$
P_{noc}(l) = E\left[|I_{noc}(l)|^2\right] = \frac{1}{N^2}\sum_{n=N/2}^{N-1}\frac{\sin^2(\pi\alpha)}{\sin^2(\pi(n-l+\alpha)/N)} \tag{3.8}
$$

Here, the ensemble average of the transmitted symbols, $E[|d_n|^2]$, is denoted as 1.

3.4.3 Interference canceller (Without decision)

In our interference canceller, it is important to generate an accurate replica of the adjacent-channel signal. When we denote the generated replica symbol on *n*-th sub-carrier as $\tilde{d}_n$, and the corresponding channel estimate as $\tilde{H}_B(n+\alpha)$, the residual adjacent-channel interference power, $I_{can}(l)$, can be expressed, following Eqn. 3.5, as

$$
\begin{aligned}
I_{can}(l) = \frac{1}{N}\sum_{n=N/2}^{N-1}&\left(d_n H_B(n+\alpha) - \tilde{d}_n\tilde{H}_B(n+\alpha)\right) \\
&\cdot\frac{\sin(\pi(n-l+\alpha))}{\sin(\pi(n-l+\alpha)/N)}e^{j\pi\frac{N-1}{N}(n-l+\alpha)}
\end{aligned}
\tag{3.9}
$$

The replica including the channel estimate, $\tilde{d}_n\tilde{H}_B(n+\alpha)$, can be obtained by Fourier

transforming the received signal as follows.

$$\begin{aligned}\tilde{d}_n\tilde{H}_B(n+\alpha) &= \frac{1}{N}\sum_{k=0}^{N-1}(r(k)+z(k))e^{-j2\pi nk/N}e^{-j2\pi\alpha k/N} \\ &= d_nH_B(n+\alpha) \\ &+ \frac{1}{N}\sum_{n'=0}^{N/2-1}d_{n'}H_A(n'-\alpha)\frac{\sin(\pi(n'-n-\alpha))}{\sin(\pi(n'-n-\alpha)/N)}e^{j\pi\frac{N-1}{N}(n'-n-\alpha)} \\ &+ Z(n)\end{aligned} \tag{3.10}$$

where $z(k)$ is a zero-mean complex Gaussian noise and $Z(n)$ is the corresponding noise element on n-th sub-carrier; $E[|Z(n)|^2]$ is denoted as σ_n^2. As shown in the above equation, the channel estimate for d_n, $\tilde{H}_B(n+\alpha)$, is included just by Fourier transforming the received signal after the frequency-offset adjustment of $-\alpha$. By substituting Eqn. 3.10 into Eqn. 3.9, the residual adjacent-channel interference power, $I_{can}(l)$, can be rewritten as follows.

$$\begin{aligned}I_{can}(l) = -\frac{1}{N^2}&\sum_{n'=0}^{N/2-1}d_{n'}H_A(n'-\alpha)e^{j\pi\frac{N-1}{N}(n'-l)} \\ &\cdot\sum_{n=N/2}^{N-1}\frac{\sin(\pi(n'-n-\alpha))\sin(\pi(n-l+\alpha))}{\sin(\pi(n'-n-\alpha)/N)\sin(\pi(n-l+\alpha)/N)} \\ &-\frac{1}{N}\sum_{n=N/2}^{N-1}Z(n)\frac{\sin(\pi(n-l+\alpha))}{\sin(\pi(n-l+\alpha)/N)}e^{j\pi\frac{N-1}{N}(n-l+\alpha)}\end{aligned} \tag{3.11}$$

Taking the ensemble average of the above equation yields the average interference power, $P_{can}(l)$.

$$\begin{aligned}P_{can}(l) = \frac{1}{N^4}&\sum_{n'=0}^{N/2-1}\left|\sum_{n=N/2}^{N-1}\frac{\sin(\pi(n'-n-\alpha))\sin(\pi(n-l+\alpha))}{\sin(\pi(n'-n-\alpha)/N)\sin(\pi(n-l+\alpha)/N)}\right|^2 \\ &+\frac{\sigma_n^2}{N^2}\sum_{n=N/2}^{N-1}\frac{\sin^2(\pi(n-l+\alpha))}{\sin^2(\pi(n-l+\alpha)/N)}\end{aligned} \tag{3.12}$$

3.4.4 Interference canceller (With decision)

The residual adjacent-channel interference power when the interference canceller with decision is used is the same as Eqn. 3.9, however the accuracy of the replica is much improved. When we denote the transmitted symbol as $d_n=d_{xn}+jd_{yn}$, the estimated symbol as $\tilde{d}_n=\tilde{d}_{xn}+j\tilde{d}_{yn}$,

and the difference between them as Δd_n, Δd_n can be expressed as follows.

$$\Delta d_n = d_n - \tilde{d}_n = \left(d_{xn} - \tilde{d}_{xn}\right) + j\left(d_{yn} - \tilde{d}_{yn}\right) \tag{3.13}$$

(a) QPSK case

Assuming QPSK modulation, if an error occurs in either I or Q channel, the difference vector power, $|\Delta d_n|^2$, can be expressed as follows.

$$\left|\Delta d_n\right|^2 = \begin{cases} \left|d_{xn} - \tilde{d}_{xn}\right|^2 = \left|\dfrac{\sigma_d}{\sqrt{2}} - \left(-\dfrac{\sigma_d}{\sqrt{2}}\right)\right|^2 = 2\sigma_d^2 \text{ ; Ich error} \\ \left|d_{yn} - \tilde{d}_{yn}\right|^2 = \left|\dfrac{\sigma_d}{\sqrt{2}} - \left(-\dfrac{\sigma_d}{\sqrt{2}}\right)\right|^2 = 2\sigma_d^2 \text{ ; Qch error} \end{cases} \tag{3.14}$$

Here, σ_d^2 denotes the power of d_n (σ_d^2=1). Assuming that only one bit error occurs in a symbol simultaneously, which means that only I channel or Q channel has an error, the residual adjacent-channel interference, $I_{dec}(l)$, can be written as follows based on Eqn. 3.9; channel estimation is assumed to be ideal.

$$I_{dec}(l) = \frac{1}{N}\sum_{n=N/2}^{N-1} \Delta d_n H_B(n+\alpha) \frac{\sin(\pi(n-l+\alpha))}{\sin(\pi(n-l+\alpha)/N)} e^{j\pi\frac{N-1}{N}(n-l+\alpha)} \tag{3.15}$$

where

$$\left|\Delta d_n\right|^2 = \begin{cases} 0 & (w/o \quad signal \quad error) \\ 2\sigma_d^2 = 2 & (w/ \quad signal \quad error) \end{cases} \tag{3.16}$$

To clarify the average interference power, it is necessary to calculate the BER characteristics of the received symbol. The adjacent-channel interference is the sum of interference from many independent sub-carriers, so the interference can be approximated as complex Gaussian noise based on the central limit theorem. Therefore, in the following, we take the interference to be thermal noise and calculate the BER characteristics. When coherent detection is assumed, the BER of sub-carrier n, $P_e(\gamma_n)$, can be written as follows from theoretical BER formula of AWGN channels as in [11].

$$P_e(\gamma_n) = \frac{1}{2} erfc\left(\sqrt{\frac{\gamma_n}{2}}\right) \tag{3.17}$$

Here, γ_n means the average received CINR; it is given as follows.

$$\gamma_n = |H_B(n+\alpha)|^2 / \left(P_{A2B}(n) + \sigma_n^2\right) \tag{3.18}$$

where

$$P_{A2B}(n) = \frac{1}{N^2} \sum_{n=N/2}^{N-1} \frac{\sin^2(\pi\alpha)}{\sin^2(\pi(n-l-\alpha)/N)} \tag{3.19}$$

We assume that only one-bit error occurs at the same time in a symbol, so that the symbol error rate, $f_{QPSK}(\gamma_n)$, can be approximated as twice the theoretical BER of QPSK.

$$f_{QPSK}(\gamma_n) \approx 2P_e(\gamma_n) = erfc\left(\sqrt{\frac{\gamma_n}{2}}\right) \tag{3.20}$$

The frequency response of each sub-carrier, $|H_B(n+\alpha)|$, follows a Rayleigh distribution as follows.

$$f(|H_B(n+\alpha)|) = \frac{|H_B(n+\alpha)|}{\delta^2} \exp\left(-\frac{|H_B(n+\alpha)|^2}{2\delta^2}\right) \tag{3.21}$$

Here, $2\delta^2$ means the variance of $|H_B(n+\alpha)|$. When the frequency response varies from 0 to infinity following the above Rayleigh distribution, the average adjacent-channel interference power, $P_{dec}(l)$, can be expressed as follows.

$$\begin{aligned} P_{dec}(l) = & \frac{1}{N^2} \sum_{n=N/2}^{N-1} \frac{\sin^2(\pi(n-l+\alpha))}{\sin^2(\pi(n-l+\alpha)/N)} \\ & \cdot \int_0^{\infty} 2\sigma_d^2 |H_B(n+\alpha)|^2 f_{QPSK}(\gamma_n) f(|H_B(n+\alpha)|) d|H_B(n+\alpha)| \end{aligned} \tag{3.22}$$

(b) 16QAM case

When 16QAM is used, if one-bit error occurs, $|\Delta d_{n,16QAM}|^2$ becomes $2\sigma_d^2/5$. That is,

$$\left|\Delta d_{n,16QAM}\right|^2 = \begin{cases} 0 & (w/o \quad signal \quad error) \\ 2\sigma_d^2/5 = 2/5 & (w/ \quad signal \quad error) \end{cases} \tag{3.23}$$

The BER for 16QAM, $P_{e,16QAM}(\gamma_n)$, can be calculated as follows by assuming coherent detection from approximated theoretical BER formula of AWGN channels as in [11].

$$P_{e,16QAM}(\gamma_n) \approx \frac{3}{8} erfc\left(\sqrt{\frac{\gamma_n}{10}}\right) \tag{3.24}$$

The symbol error rate of 16QAM can be approximated as the quadruple of the theoretical BER of 16QAM.

$$f_{16QAM}(\gamma_n) \approx 4P_{e,16QAM}(\gamma_n) = \frac{3}{2} erfc\left(\sqrt{\frac{\gamma_n}{10}}\right) \tag{3.25}$$

When the frequency response varies from 0 to infinity following a Rayleigh distribution, the average adjacent-channel interference power, $P_{dec,16QAM}(l)$, can be expressed as follows.

$$\begin{aligned} P_{dec,16QAM}(l) = & \frac{1}{N^2} \sum_{n=N/2}^{N-1} \frac{\sin^2(\pi(n-l+\alpha))}{\sin^2(\pi(n-l+\alpha)/N)} \\ & \cdot \int_0^{\infty} \frac{2\sigma_d^2}{5} |H_B(n+\alpha)|^2 f_{16QAM}(\gamma_n) f(|H_B(n+\alpha)|) d|H_B(n+\alpha)| \end{aligned} \tag{3.26}$$

3.4.5 BER performance

We calculate the average BER performance for QPSK and 16QAM. As the propagation channel, we assume a multi-path fading channel wherein many delay waves are combined. This means that the propagation channel is frequency-selective. When the delay spread is relatively high, the fading correlation between sub-carriers becomes small, so we assume that there is no fading correlation between sub-carriers.

As shown in Eqn. 3.8, 3.12, and 3.22, the adjacent-channel interference signals are expressed as the sum of interference from many sub-carriers, so they are, by the central limit theorem, taken to be a complex Gaussian noise. We assume the adjacent channel interference to be thermal noise and calculate the average BER.

When we denote the average noise power per sub-carrier as σ_n^2, the average CINR of l-th sub-carrier, γ_l, can be expressed as follows by denoting the received desired signal level as $P_s(l)$.

$$\gamma_l = \begin{cases} P_s(l)/\left(P_{noc}(l) + \sigma_n^2\right) & ;w/o \quad canceller \\ P_s(l)/\left(P_{can}(l) + \sigma_n^2\right) & ;canceller\ w/o\ decision \\ P_s(l)/\left(P_{dec}(l) + \sigma_n^2\right) & ;canceller\ w/\ decision \end{cases} \tag{3.27}$$

Table 3. 1: Simulation parameters of multi-link signal transmission

Sub-carrier spacing	15 kHz
Number of sub-carriers	64
Guard interval length	1/4 symbol length
Number of OFDM symbols	1
Modulation	QPSK, 16QAM
maximum Doppler frequency	0 Hz

Given coherent detection and quasi-static fading, the average BER for QPSK and 16QAM, $P_{f,\mathrm{QPSK}}$ and $P_{f,16\mathrm{QAM}}$, respectively, can be derived as follows.

$$P_{f,QPSK}(l) = \frac{1}{2}\left(1 - \frac{1}{\sqrt{1+2/\gamma_l}}\right) \tag{3.28}$$

$$P_{f,16QAM}(l) \approx \frac{3}{8}\left(1 - \frac{1}{\sqrt{1+10/\gamma_l}}\right) \tag{3.29}$$

3.5 Evaluation results

3.5.1 Simulation conditions

We evaluated the proposed methods by analyses and computer simulations. Simulation parameters are summarized in Table 3.1. We assumed the two-cell model shown in Fig. 3.1. Both base stations transmit their signal at the same power. The sub-carrier spacing is 15 kHz, and 64 sub-carriers are used; 32 sub-carriers are used by each base station. The guard interval length is set at 1/4 the OFDM symbol length, and one OFDM symbol is used for the evaluation. QPSK and 16QAM are used and the maximum Doppler frequency is set at 0Hz. For the path model, we used a five-path Rayleigh fading channel with exponential decay of the average received power. The path intervals between adjacent paths are equal and the decay factor is 3 dB per path. Each path experiences independent Rayleigh fading. The delay spread is set at 1.1μs. The channel estimation, the timing-offset estimation, and the frequency-offset estimation are assumed to be ideal.

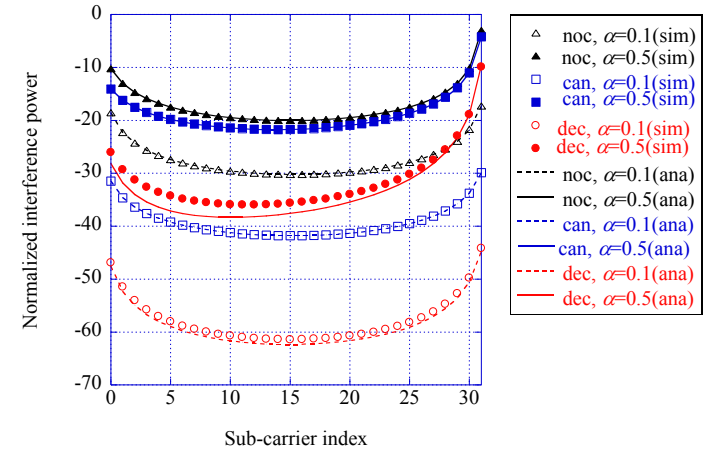

(a) QPSK

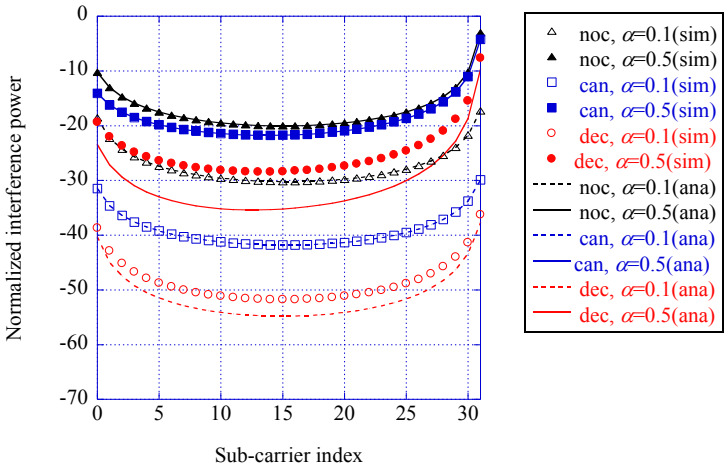

(b) 16QAM

Figure 3. 4: Adjacent-channel interference power

3.5.2 Evaluation results

First, we evaluated the adjacent-channel interference power through analyses and computer simulations. The evaluation results are shown in Fig. 3.4. The horizontal-axis is the sub-carrier index for the BS-A sub-band, and the vertical-axis is the interference power, which is normalized by the power of the received desired signal. The analysis results are shown by lines and the simulation results are shown by marks. The results of the conventional method, cancellers without and with decision are identified by the labels, “noc”, “can”, and “dec”, respectively. The frequency offset difference between the two base stations, normalized by the sub-carrier spacing, α, is used as the parameter; α values examined are -0.1 and -0.5. To

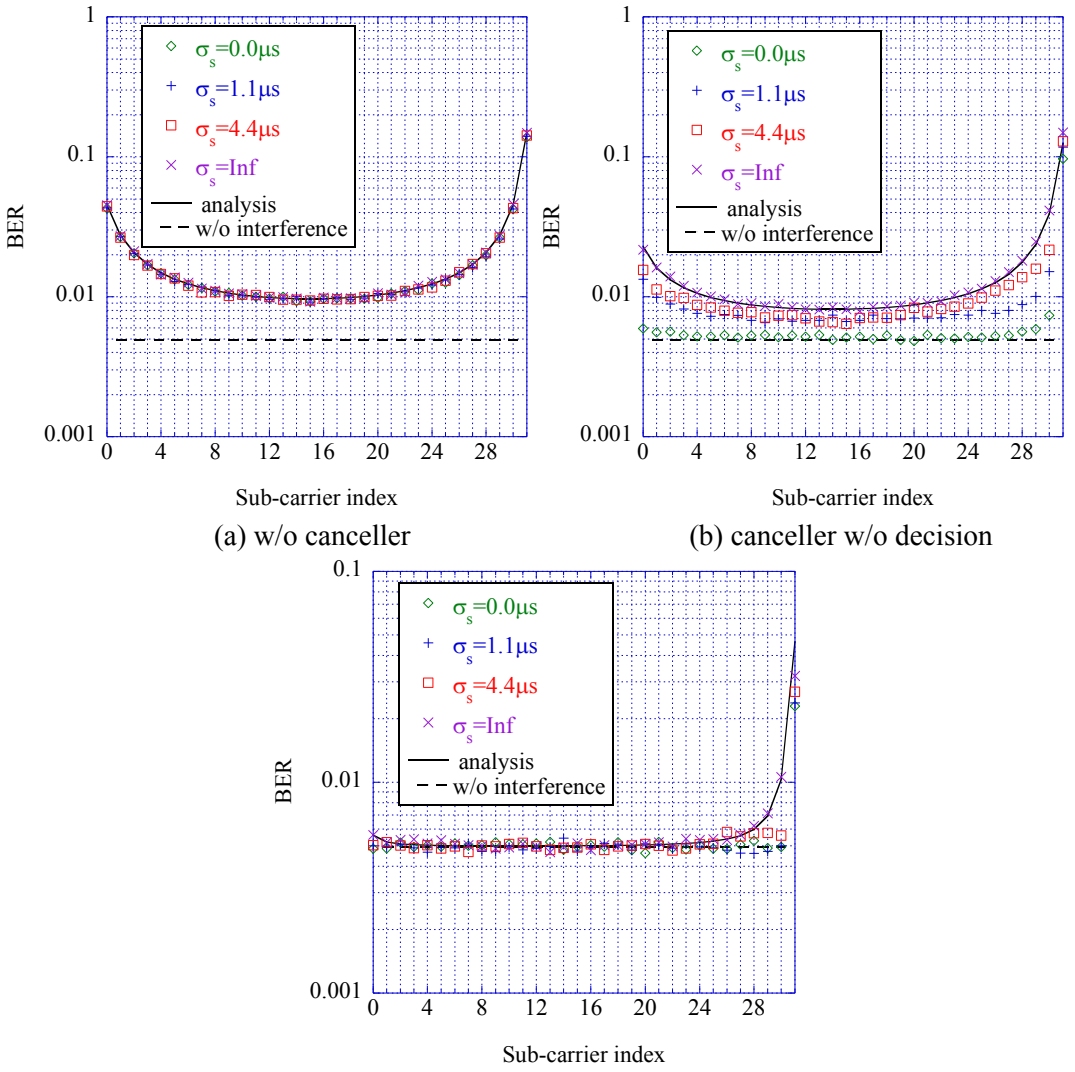

(a) w/o canceller

(b) canceller w/o decision

(c) canceller w/ decision

Figure 3. 5: BER performance

evaluate the proposed canceller with decision, QPSK and 16QAM are used, and the SNR is set at 20dB.

The above results clearly show that the proposed methods reduce the interference level compared to the conventional method regardless of the frequency offset or the sub-carrier index. The addition of the decision process provides a further reduction in the interference level. Note that the analysis results are very close to the simulation results.

When the canceller with decision (RGd) is used with 16QAM, the analysis and simulation

results have some difference. In the analysis in Section 3.4, we assumed that only one-bit error occurs at the same time in a symbol for simplicity, so that the error vector power $|\Delta d_{n,16\mathrm{QAM}}|^2$ is assumed as $2\sigma_d^2/5$ as in Eqn. 23. However, several bit errors sometimes occur in a symbol. In this case, the error vector power can be larger than $2\sigma_d^2/5$ multiplied by the number of error bits. This causes that interference power obtained by analysis is smaller than the simulation values.

In all methods, the interference power becomes worse as the sub-carrier index approaches the edge, i.e. the 0-th or 31-st sub-carrier. This reflects the impact of the inter-sub-band interference caused by the collapse of orthogonality; the sub-carriers near the BS-B sub-band receive higher interference power. Comparing the interference power of the 0-th and 31-st sub-carriers, the latter has worse interference power, because the frequency offset values take minus values such as -0.1 or -0.5, which means the BS-B sub-band approaches the BS-A sub-band. In realistic implementations, interference on the sub-carriers near the 0-th sub-carrier can be avoided by setting the FFT size larger than the number of sub-carriers.

Next, we evaluated the BER performance through numerical analysis and computer simulations. In the evaluation, we assumed QPSK and set SNR at 20dB and the frequency offset difference at -0.5. In figures, we also added theoretical BER of QPSK in Rayleigh fading channels by assuming no interference case. The BER performance becomes different depending on the delay spread. In the computer simulations, we set the delay spread at 0μs, 1.1μs, and 4.4μs. We also evaluated the case when there is no fading correlation between sub-carriers, which corresponds to severe frequency selective fading; this case is shown in the figure with the label “Inf”. Fig. 3.5 (a), (b), and (c) show the evaluation results for no canceller, canceller without decision and canceller with decision, respectively.

Fig. 3.5(a) shows that the BERs are the same regardless of the delay spread when the canceller is not used; the analytical result is almost identical. As shown in Fig. 3.5 (b) and (c), the BER performance changes depending on the delay spread when the cancellers are used. As the delay spread increases, the BER performance deteriorates and approaches the analytical values. This can be explained as follows. In the numerical analysis, we assumed that the correlation between sub-carriers was 0. Thus, as the delay spread increases, the fading correlation approaches 0, which corresponds to the condition we assumed in the numerical analysis. Therefore, we can regard the analyzed BER performance as the upper bound of the

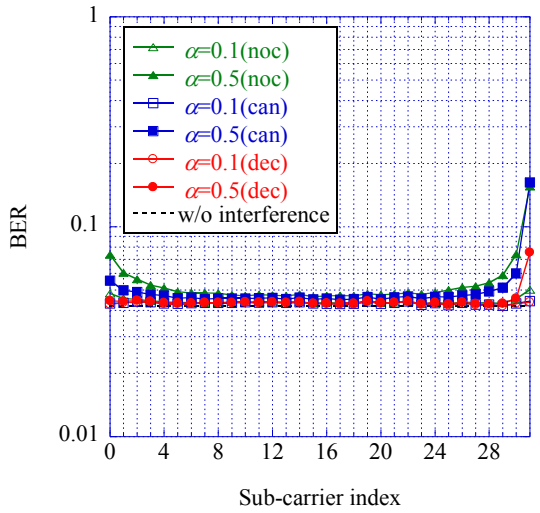

(a) SNR=10dB

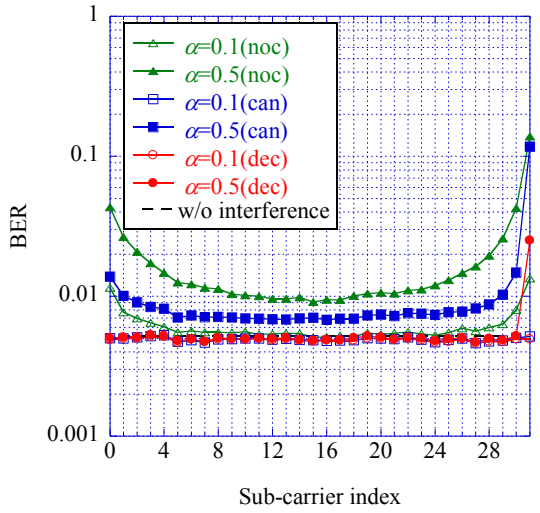

(b) SNR=20dB

Figure 3. 6: BER performance (QPSK)

BER performance when the cancellers are applied. Also, the analysis results are almost the same as the simulation results when the delay spread is relatively large.

The impact of delay spread on the performance of the cancellers can be explained as follows. When considering the interference caused by frequency-offset difference, the average interference power from the received signal from BS-A (hereafter, BS-A portion) to BS-B band is the same regardless of delay spread. However correlation between instant received signal level of BS-A portion and interference power differs depending on delay spread. When delay

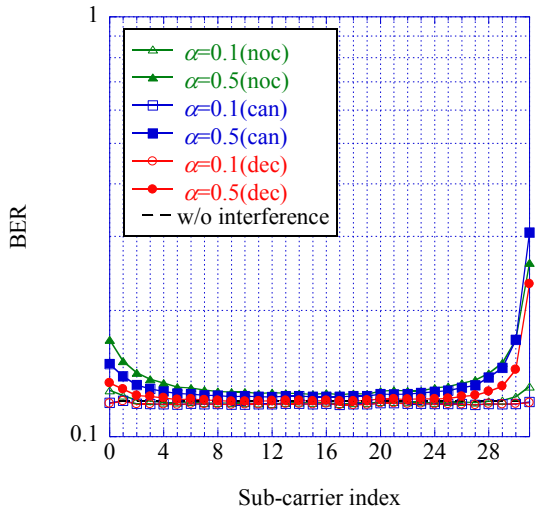

(a) SNR=10dB

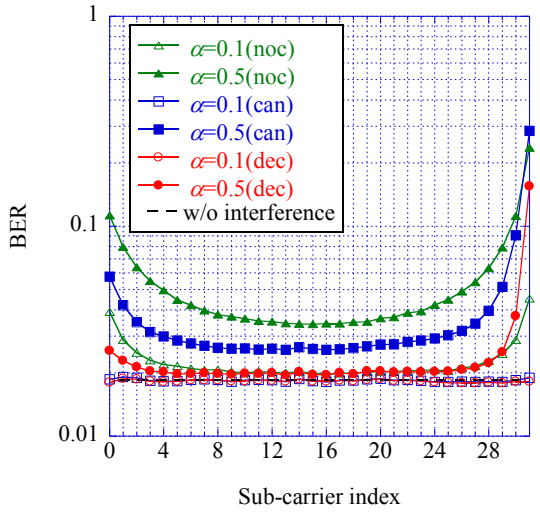

(b) SNR=20dB

Figure 3. 7: BER performance (16QAM)

spread is small, the received signal level of BS-A portion is close to flat on all sub-carriers and correlation between the received signal level and interference power is high. Therefore, even when the accuracy of BS-B signal replica is low by the high interference power, bit error unlikely occurs by the high received signal power of BS-A portion. On the other hand, when delay spread is large, the received signal level of BS-A portion is not flat by frequency selective fading, which leads that correlation between the received signal level and interference power on

BS-B band is low on per sub-carrier basis. Therefore, bit error of BS-A portion tends to occur more frequently compared with low delay-spread case. The above discussion on the influence of delay spread is applicable to both cancellers. However, when the canceller with decision (RGd) is used, the replica accuracy is sufficiently high regardless of delay spread due to the decision, so that the impact of delay spread on BER is relatively small compared to the canceller without decision.

As discussed in Sec. 3.1, the impact from channel estimation error can be prevented by introducing accurate channel estimation, and we assume ideal channel estimation in this paper. In the following, we give qualitative explanation of channel estimation impact on the methods with and without decision. In the canceller with decision (RGd), the channel estimation accuracy has impact on replica accuracy because it affects the decision accuracy. The decision process of desired received signal, which is conducted after replica subtraction, is of course affected by channel estimation accuracy. On the other hand, in the canceller without decision (RG), channel estimation accuracy has no impact on replica generation. However, these impacts arise only when channel estimation accuracy is not sufficient. Therefore, they can be prevented by using accurate channel estimation techniques as described in Sec. 3.1.

Finally, we show the BER performances obtained by computer simulations; the delay spread is set at 1.1 μs. Fig. 3.6 and Fig. 3.7 show the results for QPSK and 16QAM, respectively. In the figures, we also added theoretical BER in Rayleigh fading channels by assuming no interference case. In both evaluations, (a) shows the results for the SNR of 10dB, and (b) shows the results for the SNR of 20dB. These figures clearly show that the BER performance is also improved by the proposed methods regardless of the frequency offset or the modulation method. This advantage strengthens as the SNR increases. This is because the interference power from the adjacent sub-band overwhelms the noise power.

3.6 Summary

In this chapter, we proposed an interference canceller for multi-link signal transmission that mitigates the interference caused by the frequency-offset difference between two BSs; the goal is to improve the cell-edge downlink throughput. The proposed method mitigates the

adjacent-channel interference by canceling the signal transmitted on the adjacent sub-band. Moreover, by adding a decision process, a further improvement in performance can be gained. We evaluated the proposed canceller and its extended form with decision by computer simulations and numerical analysis, and confirmed that both offered a significant performance improvement in terms of the interference power and BER performance. In this chapter, although we assumed maximum Doppler frequency of 0Hz in order to simplify numerical analysis, we believe similar performance gain can be obtained even with mobility environment. This is because typical maximum Doppler frequency is less than a few hundreds of Hz and much less than the impact of frequency offset, which is 1500Hz and 7500Hz for α=0.1 and 0.5, respectively.

Chapter 4

Channel Estimation

4.1 Issues and Approaches for Channel Estimation

In order to improve communication quality at cell edge, accurate fading compensation as well as inter-cell interference are important. At cell edge, we need to conduct channel estimation under the influence of high interference power from neighbor BSs, so advanced accurate channel estimation techniques are highly required.

Currently, both Direct Sequence Code Division Multiple Access (DS-CDMA) systems and OFDMA systems are widely used all over the world. Multi-carrier CDMA (MC-CDMA) is a technology, which combines the virtues of CDMA and OFDMA, and has attracted much attention as a candidate for next generation mobile communication systems [4.1-4.6, 4.18-4.20]. In MC-CDMA systems, data symbols can be spread in the frequency or time domain by using a given spreading code [1-6, 18-20]. It has been reported that time-domain spreading MC-CDMA systems have superior BER performance to frequency-domain spreading MC-CDMA systems, which are degraded by multiple access interference in severe frequency selective fading environments, especially when a lot of multiplexing codes are used [4.5] . Moreover, the time-domain spreading systems can enjoy frequency diversity effect similar to the frequency-domain spreading systems by applying forward error correction with bit-interleaving in the frequency domain. In time-domain spreading MC-CDMA systems, it is usual to spread data and pilot symbols in the time domain and code-multiplex them [4.5, 4.6]. Utilizing those code-multiplexed pilot symbols, we need to realize accurate channel estimation. As to the multiplexing of pilot symbols, there are various ways to multiplex them such as time-domain multiplexing or more-sophisticated scattered-type multiplexing [4.21, 4.22]. In OFDM systems, it is difficult to introduce code-multiplexed pilot symbols, so that it is reasonable to adopt scattered-type pilot symbols. On the other hand, in time-domain spreading MC-CDMA systems,

by the nature of code multiplexing, it is possible to multiplex pilot symbols in code domain. In this case, pilot symbols are transmitted on every sub-carrier and in every symbol, so that we can improve channel estimation accuracy by averaging many pilot symbols with high fading correlation. In the following, we concentrate on this pilot symbol format and describe the channel estimation methods.

In mobile communication systems, the mobile terminals generally move around at high speed. Therefore, the fading environment changes so fast that channel estimation is a serious issue to be resolved. Taking into account the current congestion in UHF band, next generation mobile communication systems are expected to use the microwave band, which is higher than the band used by 3rd generation mobile communication systems. This yields higher maximum Doppler frequencies so that a more powerful channel estimation method is needed for next generation systems. However, until now, sufficient studies on channel estimation methods for time-domain spreading MC-CDMA systems have not been published. Considering this, we combine a two-dimensional channel estimation method and an impulse response-based channel estimation method to propose a channel estimation method that offers high accuracy.

In DS-CDMA systems, which are used for 3rd generation mobile communication systems, it is usual to coherently add some pilot symbols in the time domain to improve the signal-to-noise ratio (SNR) of the pilot symbols. To combat fading variation in the time domain, the weighted multi-slot averaging (WMSA) channel estimation filter has been proposed [4.7, 4.8]. This filter adds several pilot symbols by giving a weight to each pilot symbol according to fading variation in the time domain. This channel estimation method is effective because the chip rate of DS-CDMA is very high, a few mega chips per second in W-CDMA or CDMA2000. On the other hand, the chip rate of MC-CDMA is relatively slow. In MC-CDMA systems, the guard interval is used to offset delay paths. To minimize the overhead of the guard interval, a relatively long symbol period is used. Therefore, we cannot expect the same effect if we apply the channel estimation method similar to that of DS-CDMA systems to MC-CDMA systems.

MC-CDMA systems consist of a lot of sub-carriers, and there is fading correlation among adjacent sub-carriers. Considering this feature, we expand the above channel estimation method into a new method that utilizes adjacent pilot symbols in both time and frequency domains. The method improves the SNR by coherently adding pilot symbols in both domains. To combat the

variation in fading correlation among pilot symbols, which is determined by propagation attributes such as the maximum Doppler frequency in the time domain and delay spread in the frequency domain, we introduce a two-dimensional filter that adaptively weights the pilot symbols in both domains. The weight can be assessed by measuring the changes in received power in the time domain (maximum Doppler frequency) and the frequency domain (delay spread) at the mobile station.

To further improve the channel estimation accuracy, we combine an impulse response-based channel estimation method with the above two-dimensional method. The time domain signals, which are obtained by inversely Fourier transforming the channel estimates in the frequency domain (estimated frequency responses), represent the impulse response. In the impulse response, the path elements are included in the guard interval duration so that the impulse response outside the guard interval can be eliminated. Therefore, the proposed method can improve the SINR of the pilot symbols. The improved impulse response is then Fourier transformed to yield new channel estimates in the frequency domain at the cost of a slight increase in signal processing power [4.9, 4.10].

It is important for adaptive channel estimation methods like our proposal to determine the appropriate weight factor for each fading environment. Various adaptive channel estimation methods and optimized weight factors have been proposed. For example, for direct sequence CDMA systems, the optimization of the weight factors for the time-domain averaging of the channel estimates has been conducted [4.7, 4.8]. Also, for OFDM systems, some studies have examined the weight factors for the frequency-domain averaging of the channel estimates as in [4.17] and its references. However, the integration of time-domain averaging, frequency-domain averaging and impulse response-based channel estimation method has not been proposed. Moreover, the optimization of the forgetting factors considering the characteristics of time-domain spreading MC-CDMA has not been conducted. When applying the two-dimensional channel estimation method, an appropriate weight factor should be prepared in advance for each fading environment. With the predetermined weight factors, mobile terminals can apply the two-dimensional channel estimation method simply by calculating the propagation attributes such as maximum Doppler frequency and delay spread. The weight factors should be determined by considering the improvement in channel estimation accuracy

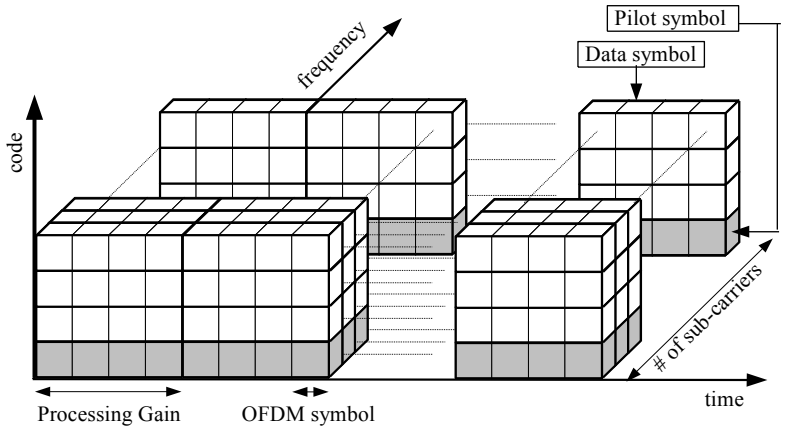

tems

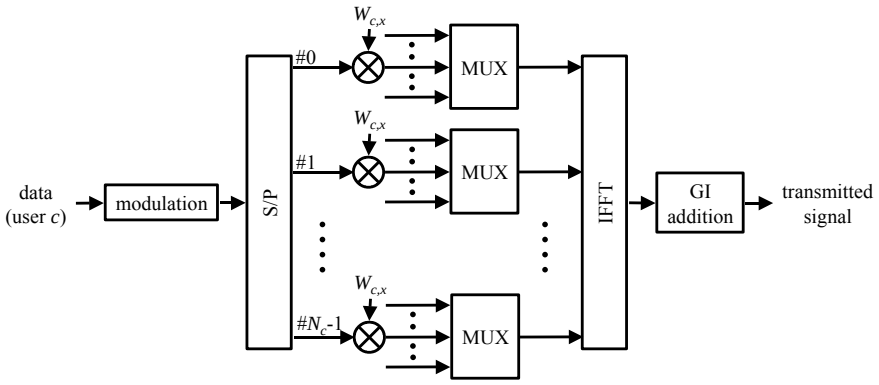

ems

produced by both the two-dimensional channel estimation method and the impulse response-based channel estimation method. We calculate the appropriate weight factors by computer simulations.

This chapter is organized as follows. Section 4.2 outlines time-domain spreading MC-CDMA systems. Section 4.3 and 4.4 explain our proposed channel estimation method. Section 4.5 demonstrates the BER performance of our proposed method and introduces an easy method of implementing the proposed methods. Finally, Section 4.6 draws summary.

4.2 Time-domain spreading MC-CDMA systems

The frame format of time-domain spreading MC-CDMA systems is shown in Fig. 4.1. On

each sub-carrier, data and pilot symbols are spread in the time domain, and code-multiplexed. A guard interval, which is a copy of the tail part of the following OFDM symbol, is transmitted before each OFDM symbol to avoid the inter symbol interference (ISI) caused by multipath fading. The transmitter structure is shown in Fig. 4.2. The complex equivalent low-pass transmitted signal of the m-th sample in the x-th chip's OFDM symbol, $s_{x,m}$, is expressed as

$$s_{x,m} = \sum_{k=0}^{N_c-1} y_{k,x} e^{j2\pi \frac{km}{N_c}} \tag{4.1}$$

$$y_{k,x} = \sum_{c=0}^{N_m-1} d_{k,c} W_{c,x} \tag{4.2}$$

where N_c is the number of sub-carriers, N_m is the number of multiplexed codes, $d_{k,c}$ is the data symbol of sub-carrier k for the c-th user, and $W_{c,x}$ is the x-th chip of the spreading code for the c-th user. Here, the spreading code for the 0-th user $W_{0,x}$ is applied to pilot symbols.

The received signal, $r_{x,m}$, is expressed as

$$r_{x,m} = \sum_{p=0}^{N_p-1} s_{x,m-p\Delta\tau} h_{x,p} + n_{x,m} \tag{4.3}$$

where N_p is the number of received paths, $h_{x,p}$ is the complex amplitude of the p-th path in the x-th OFDM symbol, $\Delta\tau$ is the interval between any two adjoining paths, and $n_{x,m}$ is the noise signal. Here, fading fluctuation in time domain is assumed to be negligible during symbol duration. The received code-multiplexed symbol of sub-carrier k' in the x-th OFDM symbol, $y'_{k',x}$, is expressed as

$$\begin{aligned} y'_{k',x} &= \frac{1}{N_c} \sum_{m=0}^{N_c-1} r_{x,m} e^{-j2\pi \frac{k'm}{N_c}} \\ &= \frac{1}{N_c} \sum_{m=0}^{N_c-1} \sum_{p=0}^{N_p-1} \sum_{k=0}^{N_c-1} h_{x,p} y_{k,x} e^{j2\pi \frac{(k-k')m - kp\Delta\tau}{N_c}} \\ &\quad + \frac{1}{N_c} \sum_{m=0}^{N_c-1} n_{x,m} e^{-j2\pi \frac{k'm}{N_c}} \\ &= y_{k',x} H_{k',x} + N_{k',x} \end{aligned} \tag{4.4}$$

where

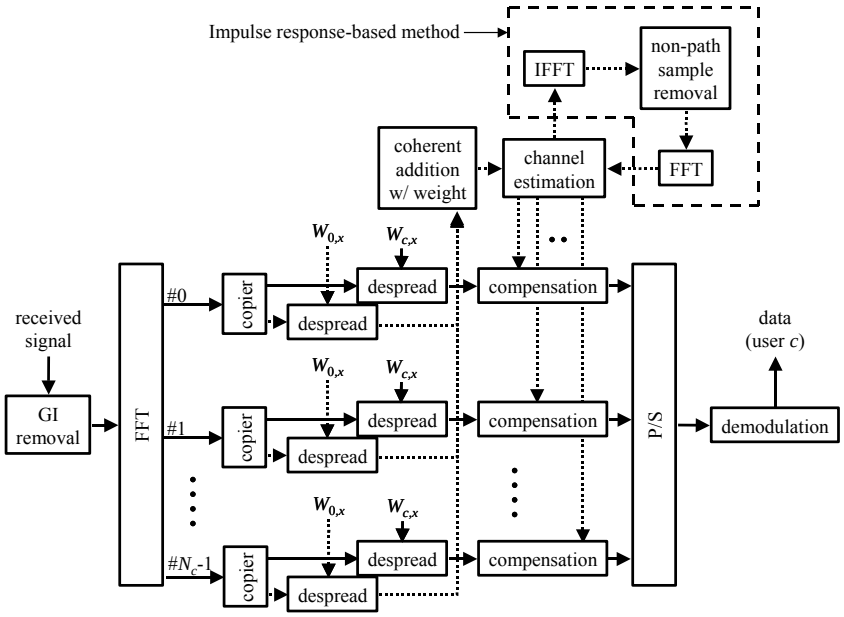

Figure 4. 3: Receiver structure of time-domain spreading MC-CDMA systems

$$H_{k',x} = \sum_{p=0}^{N_p-1} h_{x,p} e^{-j2\pi \frac{k'p\Delta\tau}{N_c}} \tag{4.5}$$

$$N_{k',x} = \frac{1}{N_c} \sum_{m=0}^{N_c-1} n_{x,m} e^{-j2\pi \frac{k'm}{N_c}} \tag{4.6}$$

Here, we assume that $H_{k',x}=H_{k'}$ ($0<=x<P_G$) to simplify the explanation. In the evaluation shown in Section 4.5, we do not use this assumption. The received symbol of sub-carrier k' for the c'-th user, $d'_{k',c'}$, is expressed as

$$\begin{aligned} d'_{k',c'} &= \frac{1}{P_G} \sum_{x=0}^{P_G-1} y'_{k',x} W_{c',x} \\ &= \frac{1}{P_G} \sum_{x=0}^{P_G-1} \left(H_{k',x} \sum_{c=0}^{N_m-1} d_{k',c} W_{c,x} + N_{k',x} \right) W_{c',x} \\ &= \frac{1}{P_G} \sum_{c=0}^{N_m-1} d_{k',c} \sum_{x=0}^{P_G-1} H_{k',x} W_{c,x} W_{c',x} + \frac{1}{P_G} \sum_{x=0}^{P_G-1} N_{k',x} W_{c',x} \\ &= d_{k',c'} H_{k'} + N'_{k',c'} \end{aligned} \tag{4.7}$$

where

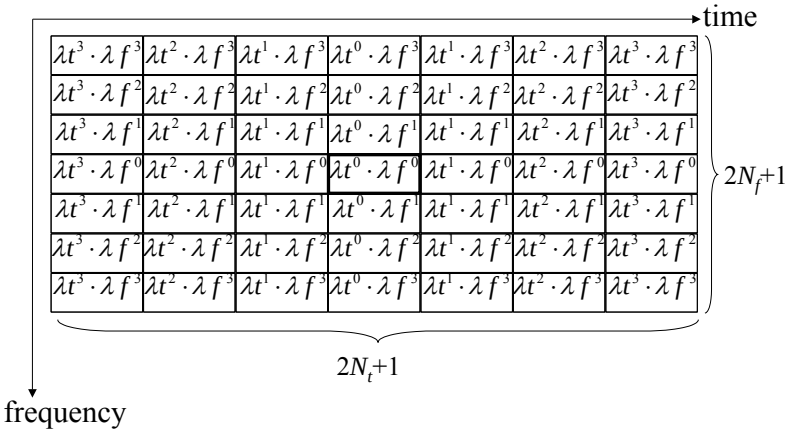

Figure 4. 4: Weighted pilot symbols for coherent addition (Stored method)

$$N'_{k',c'} = \frac{1}{P_G} \sum_{x=0}^{P_G-1} N_{k',x} W_{c',x} \tag{4.8}$$

The receiver structure is shown in Fig. 4.3. Here, the compensation of each received data symbol is conducted after the received data symbol is despread. The channel estimate $E_{k'}$ is expressed as

$$\begin{aligned} E_{k'} &= d'_{k',0} / d_{k',0} \\ &= H_{k'} + N'_{k',0} / d_{k',0} \end{aligned} \tag{4.9}$$

Here $d_{k',0}$ denotes the transmitted pilot symbol on sub-carrier k'.

4.3 Two-dimensional channel estimation method

We apply a two-dimensional channel estimation method that offers high accuracy for time-domain spreading MC-CDMA systems in variable propagation environments. The basic concept of this method is adaptively selecting the number of pilot symbols in both frequency and time domains according to the propagation environments and coherently adding those pilot symbols [4.6] . To realize this method, we use pilot symbols in a fixed area, which mean a fixed number of pilot symbols, and introduce weight factors and give weight each pilot symbol in the area differently according to the propagation environments. This method is equivalent to changing the number of pilot symbols adaptively. Note that this approach is easier to implement because the coherently added pilot symbols are fixed.

As for the area of pilot symbols for coherent addition, we investigate two channel estimation approaches. One is a stored method, which selects pilot symbols that have already been received and will be received as shown in Fig. 4.4. Here, each small block means a despread pilot symbol. The variable in each block represents the weight for the pilot symbol. The central heavy-line frame (hereafter target symbol) indicates where the channel estimate is applied to compensate the data symbols. In this method, we need a memory function to memorize the received data symbols until all pilot symbols for the channel estimation have been received. The other approach, a real-time method, selects only pilot symbols that have been received when the target symbol is received. This method eliminates the need for memory to hold the received data symbols, and we can demodulate data symbols in real time. The stored method provides more accurate channel estimation than the real-time method, because it can use more pilot symbols that have higher correlation.

4.3.1 Stored method

When we use $2N_t$+1 and $2N_f$+1 pilot symbols in the time and frequency domains, respectively, $(2N_t+1)(2N_f+1)$ pilot symbols are used in the channel estimation. Considering that the correlation falls in proportion to the distance between symbols, the weights should be given according to the distance. Here, λ_t and λ_f denote the weight factors (hereafter the forgetting factors) in the time and frequency domains as shown in Fig. 4.4. The channel estimate of the t_ith symbol on the f_ith sub-carrier, $E_s(t_i,f_i)$ is expressed as

$$E_s(t_i, f_i) = \frac{\sum_{t=t_i-N_t}^{t_i+N_t} \sum_{f=f_i-N_f}^{f_i+N_f} E_{t,f} \lambda_t^{|t-t_i|} \lambda_f^{|f-f_i|}}{\sum_{t=t_i-N_t}^{t_i+N_t} \sum_{f=f_i-N_f}^{f_i+N_f} \lambda_t^{|t-t_i|} \lambda_f^{|f-f_i|}} \tag{4.10}$$

where $E_{t,f}$ is the t-th channel estimate on the f-th sub-carrier obtained by Eqn. 4.9. Here, the conventional channel estimation method is the case of λ_t=1.0 and λ_f=1.0.

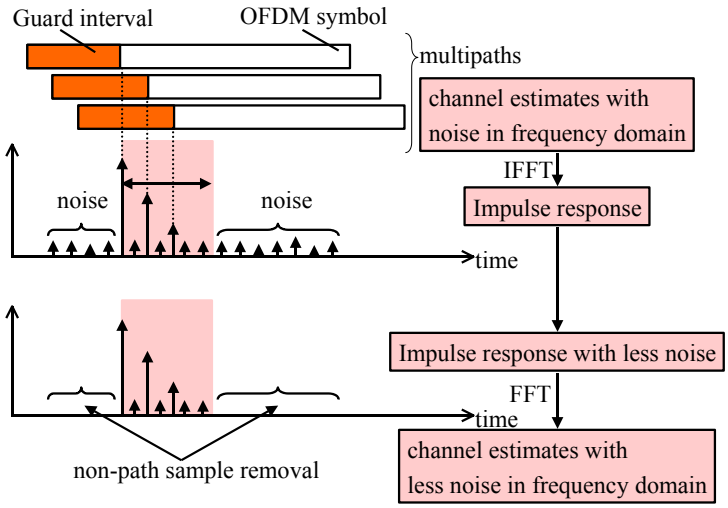

Figure 4. 5: Delay profile-based noise suppression method

4.3.2 Real-time method

In the real-time method, only pilot symbols that have already been received are used for channel estimation. Here, we use N_t+1 pilot symbols in the time domain, $2N_f$+1 pilot symbols in the frequency domain, so there are $(N_t+1)(2N_f+1)$ pilot symbols in total. The channel estimate obtained by this method, $E_r(t_i,f_i)$, is expressed as

$$E_r(t_i, f_i) = \frac{\sum_{t=t_i-N_t}^{t_i} \sum_{f=f_i-N_f}^{f_i+N_f} E_{t,f} \lambda_t^{|t-t_i|} \lambda_f^{|f-f_i|}}{\sum_{t=t_i-N_t}^{ti} \sum_{f=f_i-N_f}^{fi+N_f} \lambda_t^{|t-t_i|} \lambda_f^{|f-f_i|}} \tag{4.11}$$

4.4 Impulse response-based channel estimation method

To further improve channel estimation accuracy, we combine an impulse response-based method in combination with the two-dimensional method. Here, the first channel estimate (estimated frequency response) of the t_i-th symbol on the f_i-th sub-carrier, $E(t_i,f_i)$, which is obtained by our two-dimensional coherent addition method, is expressed as

$$E(t_i, f_i) = H_{t_i,f_i} + N_{t_i,f_i} \tag{4.12}$$

$N_{ti,fi}$ denotes the noise, which also includes channel estimation error raised in Eqn. 4.10 or 4.11. $H_{ti,fi}$ denotes the frequency response and is described as follows.

$$H_{t_i,f_i} = \sum_{p=0}^{N_p-1} h_{t_i,p} e^{-j2\pi \frac{f_i p \Delta\tau}{N_c}} \tag{4.13}$$

Here, N_p is the number of received paths, $\Delta\tau$ is the path interval, and $h_{t_i,p}$ is the impulse response of the p-th path at the t_i-th symbol. The inverse Fourier transformed signal of the channel estimates represents the estimated impulse response. In this method, we first obtain the estimated impulse response $T_{t_i,m}$ by inversely Fourier transforming the first channel estimates.

$$\begin{aligned} T_{t_i,m} &= \sum_{f_i=0}^{N_c-1} E(t_i, f_i) e^{j2\pi \frac{f_i m}{N_c}} \\ &= h_{t_i,m} + \sum_{f_i=0}^{N_c-1} N_{t_i,f_i} e^{j2\pi \frac{f_i m}{N_c}} \end{aligned} \tag{4.14}$$

As shown in the middle of Fig. 4.5, the path components are included only in the guard interval duration of the impulse response, when the longest delay path is shorter than the guard interval and the timing synchronization is accurate. In other words, elements of the estimated impulse response out of the guard interval duration consist of just noise. Therefore, a more accurate impulse response can be obtained by removing the noise as shown at the bottom of Fig. 4.5. As the final step, this refined impulse response is transformed into second channel estimates by FFT. Here, the SNR of the second channel estimates have been refined by the removal of noise from the original impulse response. When the number of samples for guard interval and OFDM symbol is N_G and N_c respectively, the SNRs of the second channel estimates are improved by N_c/N_G compared with the original ones. The second channel estimate of the t_i-th symbol on the f'_i-th sub-carrier, $E'(t_i,f'_i)$, is expressed as follows.

Table 4. 1: Simulation parameters of channel estimation

Bandwidth	40.96[MHz]
Number of sub-carriers: N_c	1024
Guard interval length	1/4 symbol length
Processing gain: P_G	16
Spreading code	OVSF
Modulation	QPSK

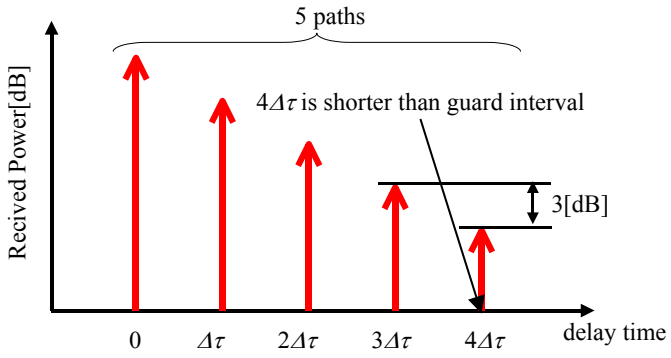

Figure 4. 6: Path model

$$
\begin{aligned}
E'(t_i, f_i') &= \frac{1}{N_c}\sum_{m=0}^{N_G-1} T_{t_i,m} e^{-j2\pi\frac{f_i' m}{N_c}} \\
&= \sum_{p=0}^{N_p-1} h_{t_i,p} \sum_{m=0}^{N_G-1} e^{-j2\pi\frac{f_i' m}{N_c}} \frac{1}{N_c}\sum_{f_i=0}^{N_c-1} e^{j2\pi\frac{(m-p\Delta\tau)f_i}{N_c}} + N'_{t_i,f_i'} \\
&= H_{t_i,f_i'} + N'_{t_i,f_i'}
\end{aligned}
\tag{4.15}
$$

where

$$
N'_{t_i,f_i'} = \frac{1}{N_c}\sum_{m=0}^{N_G-1}\sum_{f_i=0}^{N_c-1} N_{t_i,f_i} e^{j2\pi\frac{(f_i-f_i')m}{N_c}} \tag{4.16}
$$

As shown in Fig. 4.3, this impulse response-based method can be added to the two-dimensional method easily, and can improve accuracy of the channel estimates output by either the stored or the real-time method in exchange for a slight increase in signal processing cost.

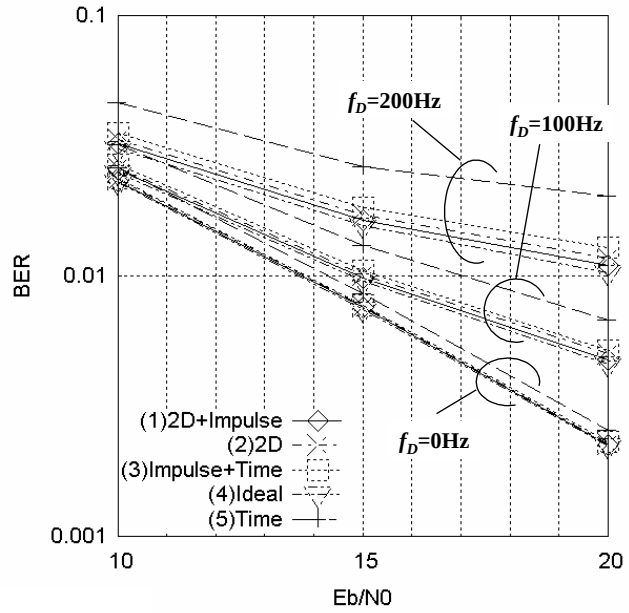

Figure 4. 7: BER performance comparison (σ_s=0.0μs)

4.5 simulations and discussions

4.5.1 Simulation conditions

We evaluate our proposed method by computer simulations. The parameters used in the computer simulations are shown in Table 4.1. The processing gain, P_G, is 16 for both pilot and data symbols, and 15 codes for users and one code for pilot symbol are used. Figure 6 shows the path model, i.e. the delay profile, used to represent propagation. This model has 5-path Rayleigh fading channels exhibiting exponential decay of average received power with equal interval of $\Delta\tau$ between adjacent paths. Its decay factor is 3dB per path, and each path is subjected to independent Rayleigh fading with maximum Doppler frequency f_D. In this model, we change the delay spread, i.e. fading correlation in the frequency domain, by changing the interval between paths, $\Delta\tau$; the longest delay path does not exceed the guard interval. In this chapter, we use this 5-path path model regardless of delay spread. In MC-CDMA systems, different from DS-CDMA systems, multi-path fading can simply be regarded as frequency-selective fading by the usage of guard interval. Therefore, in the evaluation of MC-CDMA systems, fading correlation in the frequency domain is important. In our path model, by changing the interval

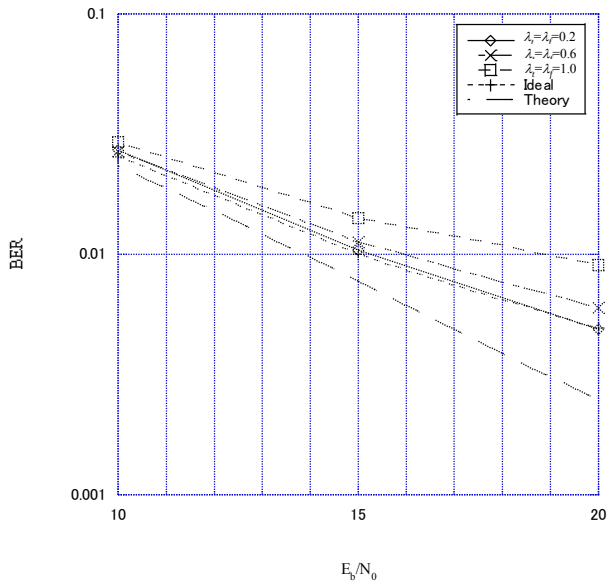

Figure 4. 8: BER performance of our proposed method (f_D=100 Hz, σ_s=0.4μs)

between paths, we can change the fading correlation, so that this simple path model is adequate to evaluate MC-CDMA systems and the channel estimation methods for them. We also assume that the frequency synchronization and the timing synchronization are ideal. Further, we assume the despread interference from adjacent cells as equivalent white noise, so N_0 includes white noise and equivalent white noise. In our simulation, the received power of pilot symbols is not considered when calculating the received E_b/N_0 of data symbols.

In the following, we show the evaluation results of our proposed method, which combines a two-dimensional method and an impulse response-based method. Concerning the two-dimensional method, results of the stored method are used, and we assume that the number of pilot symbols used in the time and frequency domains is N_t=N_f=3; 7x7=49 pilot symbols in total are used for coherent addition.

4.5.2 An example of the evaluation of the proposed method

We compared the performance of the proposed method to other methods. We set the maximum Doppler frequency to 0, 100 and 200Hz, and the delay spread to 0.0μs. Fig. 4.7

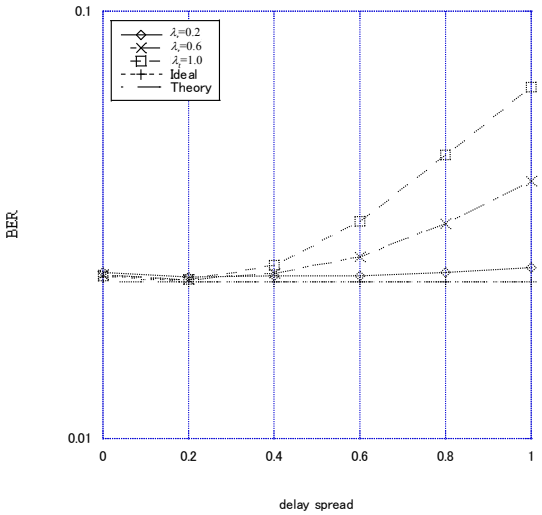

(a) f_D=50Hz, λ_t=0.8

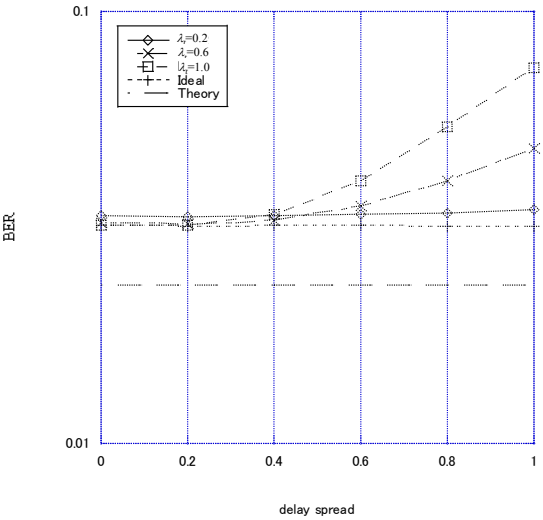

(b) f_D=200Hz, λ_t=0.2

Figure 4. 9: Relation between delay spread and forgetting factors

shows the BER performance of (1) the proposed method, (2) two-dimensional method without impulse response-based method, (3) impulse response-based method with time domain averaging with weight and (4) ideal channel estimation case. We also show (5) time domain averaging with weight as an example of DS-CDMA-like channel estimation. In the method (3), only the time-domain averaging with weights is used after applying the impulse response-based

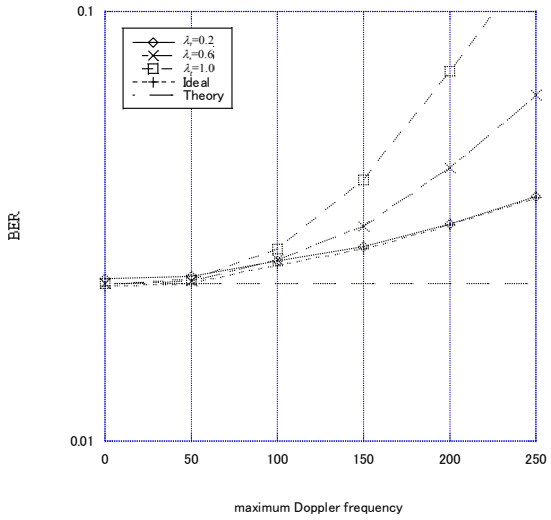

(a) σ_s=0.2μs, λ_f=0.8

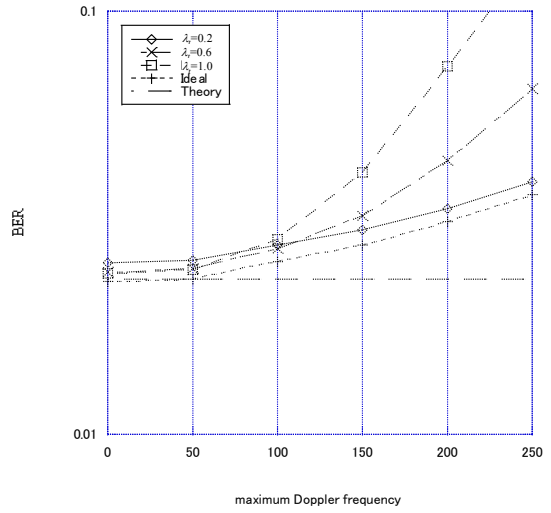

(b) σ_s=0.8μs, λ_f=0.2

Figure 4. 10: Relation between maximum Doppler frequency and forgetting factor

method. The weighting factors for the methods from (1) to (3) and (5) were optimized. As can be seen in the figure, the proposed method offers better performance than the other methods, (2), (3), and (5) at all maximum Doppler frequencies examined. This is because the proposed method can fully utilize time-domain averaging, frequency-domain averaging, and the impulse-response based method. Detailed comparison results are shown in Section 4.5.5.

4.5.3 Evaluation with regard to the optimum forgetting factors in the proposed method

First, we show the impact of forgetting factors. Fig. 4.8 shows the BER performance of our proposed method when the maximum Doppler frequency is 100 Hz and the delay spread is 0.4 μs. Several forgetting factors were used. We also show the result assuming ideal channel estimation to indicate the channel estimation accuracy. The theoretical BER of QPSK in a Rayleigh fading environment is also shown as a reference [4.14] . In the figure, it is clearly shown that the forgetting factor significantly alters the results and there exists an optimal set of forgetting factors. For example, when comparing the case of λ_t=λ_f=0.2 to the case of λ_t=λ_f= 1.0, the former achieves 3.8dB over that of the latter when the BER is 0.01. Comparing the results of our method to that of the ideal channel estimation case, when the appropriate forgetting factors are selected, the BER degradation is as small as 0.2 dB. When the E_b/N_0 is high, the BER performance degrades compared to the theoretical BER. This is because the inter-code interference occurs due to the high Doppler frequency. At very high Doppler frequencies, this degradation can be offset by introducing MMSE (Minimum Mean Square Error) combining [4.11-4.13].

Next, we clarified the relation between delay spread σ_s and the forgetting factor for the frequency domain λ_f. Fig. 4.10(a) plots BER performance versus σ_s for several values of λ_f; E_b/N_0=10dB. The maximum Doppler frequency, f_D, is 50Hz and the forgetting factor for the time domain, λ_t, is fixed at 0.8. Fig. 4.10(b) shows the BER performance when f_D is 200Hz. Here, λ_t is fixed at 0.2. These figures show that BER performance improves as λ_f increases if the delay spread is small; the reverse is true if the delay spread is large. Moreover, it is shown that the optimal λ_f changes with f_D.

We also calculated the relation between f_D and λ_t. Fig. 4.10(a) plots the BER performance versus f_D with λ_t as a parameter. Here, σ_s is 0.2μs. λ_f is fixed at 0.8. Fig. 4.10(b) shows the BER performance when σ_s is 0.8μs. Here, λ_f is fixed at 0.2. These figures show that BER performance improves as λ_t increases if the maximum Doppler frequency is low; the reverse is true if the maximum Doppler frequency is high.

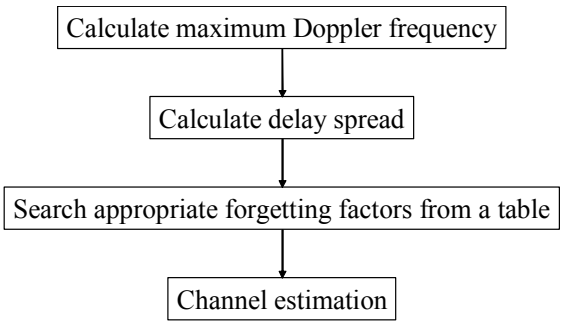

Figure 4. 11: Control algorithm

4.5.4 Control Algorithm

From these results, it is clear that the accuracy of channel estimation can be improved by optimizing the forgetting factors according to f_D and σ_s. Figure 4.11 shows how to realize the two-dimensional methods. First, we generate a table that lists optimal forgetting factors according to f_D and σ_s. MS selects the optimal forgetting factors according to f_D and σ_s as measured by MS. The two-dimensional methods improve the accuracy of channel estimation, that is, the BER can be improved. Nevertheless, they are very simple because the MS needs only the forgetting factor table to be able to sele ct the optimal forgetting factors according to f_D and σ_s. The optimal forgetting factors were obtained through computer simulations. Table 4.2 (a) and (b) show the optimal forgetting factors for E_b/N_0 of 10 and 20 dB, respectively. The BER performance evaluation shown in Fig. 4.7 used these forgetting factors. When E_b/N_0 is 15 dB, linearly interpolated forgetting factors were used. More ramified parameters could be expected to offer better BER performance, so we examined the use of 0.1-spaced forgetting factors. However, the improvement does not exceed 0.1 dB compared to 0.2-spaced forgetting factors. Therefore, 0.2-spaced forgetting factors are sufficient for our proposed method. Also, in this chapter, we showed the results for E_b/N_0 of 10dB to 20dB, while it is also necessary to consider that E_b/N_0 becomes under 10dB or larger than 20dB depending on the receiver environments. In most mobile communication systems, E_b/N_0 of 0dB to 30dB is realistic. Therefore, we consider that it can be one possible approach that we prepare 4 forgetting factor tables for each 0, 10, 20, and 30dB of E_b/N_0 and use interpolation for other intermediate E_b/N_0.

Table 4. 2: Optimum forgetting factors for combined method

(a) E_b/N_0=10dB

f_D \ σ_s	0.0	0.2	0.4	0.6	0.8	1.0
0	λ_f=1.0 λ_t=1.0	λ_f=0.8 λ_t=1.0	λ_f=0.2 λ_t=1.0	λ_f=0.2 λ_t=1.0	λ_f=0.0 λ_t=1.0	λ_f=0.0 λ_t=1.0
50	λ_f=1.0 λ_t=0.8	λ_f=0.8 λ_t=0.8	λ_f=0.2 λ_t=0.8	λ_f=0.2 λ_t=0.8	λ_f=0.0 λ_t=0.8	λ_f=0.0 λ_t=0.8
100	λ_f=1.0 λ_t=0.4	λ_f=0.8 λ_t=0.4	λ_f=0.4 λ_t=0.4	λ_f=0.2 λ_t=0.4	λ_f=0.0 λ_t=0.6	λ_f=0.0 λ_t=0.6
150	λ_f=1.0 λ_t=0.2	λ_f=1.0 λ_t=0.2	λ_f=0.6 λ_t=0.2	λ_f=0.2 λ_t=0.2	λ_f=0.2 λ_t=0.2	λ_f=0.0 λ_t=0.4
200	λ_f=1.0 λ_t=0.2	λ_f=0.8 λ_t=0.2	λ_f=0.6 λ_t=0.2	λ_f=0.2 λ_t=0.2	λ_f=0.2 λ_t=0.2	λ_f=0.0 λ_t=0.2
250	λ_f=1.0 λ_t=0.0	λ_f=1.0 λ_t=0.0	λ_f=0.6 λ_t=0.0	λ_f=0.4 λ_t=0.2	λ_f=0.2 λ_t=0.2	λ_f=0.0 λ_t=0.2

(b) E_b/N_0=20dB

f_D \ σ_s	0.0	0.2	0.4	0.6	0.8	1.0
0	λ_f=1.0 λ_t=1.0	λ_f=0.2 λ_t=1.0	λ_f=0.0 λ_t=1.0	λ_f=0.0 λ_t=1.0	λ_f=0.0 λ_t=1.0	λ_f=0.0 λ_t=1.0
50	λ_f=1.0 λ_t=0.4	λ_f=0.6 λ_t=0.4	λ_f=0.0 λ_t=0.6	λ_f=0.0 λ_t=0.6	λ_f=0.0 λ_t=0.6	λ_f=0.0 λ_t=0.6
100	λ_f=1.0 λ_t=0.2	λ_f=0.6 λ_t=0.2	λ_f=0.2 λ_t=0.2	λ_f=0.0 λ_t=0.2	λ_f=0.0 λ_t=0.2	λ_f=0.0 λ_t=0.2
150	λ_f=1.0 λ_t=0.2	λ_f=0.8 λ_t=0.0	λ_f=0.2 λ_t=0.2	λ_f=0.2 λ_t=0.2	λ_f=0.0 λ_t=0.2	λ_f=0.0 λ_t=0.2
200	λ_f=1.0 λ_t=0.0	λ_f=0.8 λ_t=0.0	λ_f=0.4 λ_t=0.0	λ_f=0.2 λ_t=0.2	λ_f=0.2 λ_t=0.2	λ_f=0.0 λ_t=0.0
250	λ_f=1.0 λ_t=0.0	λ_f=1.0 λ_t=0.0	λ_f=0.4 λ_t=0.0	λ_f=0.2 λ_t=0.0	λ_f=0.2 λ_t=0.0	λ_f=0.0 λ_t=0.0

Basically, forgetting factor for the time domain, λ_t, depends on the maximum Doppler frequency, not on the delay spread. The reverse can be said for the forgetting factor for the frequency domain, λ_f. We note, however, that if f_D is 100Hz, optimal λ_t is 0.4 when σ_s is 0-0.6μs and 0.6 when σ_s is over 0.6μs in Table 4.2(a). When σ_s is small enough, accurate channel estimates can be obtained by coherently adding pilot symbols only to the frequency domain. On the other hand, when σ_s becomes large, the accuracy of channel estimation degrades if pilot symbols are coherently added only to the frequency domain. Therefore, the coherent addition of pilot symbols in the time domain is useful even if the correlation in the time domain is not so high. Accordingly, using an N-by-N table is the best way to ensure highly accurate channel

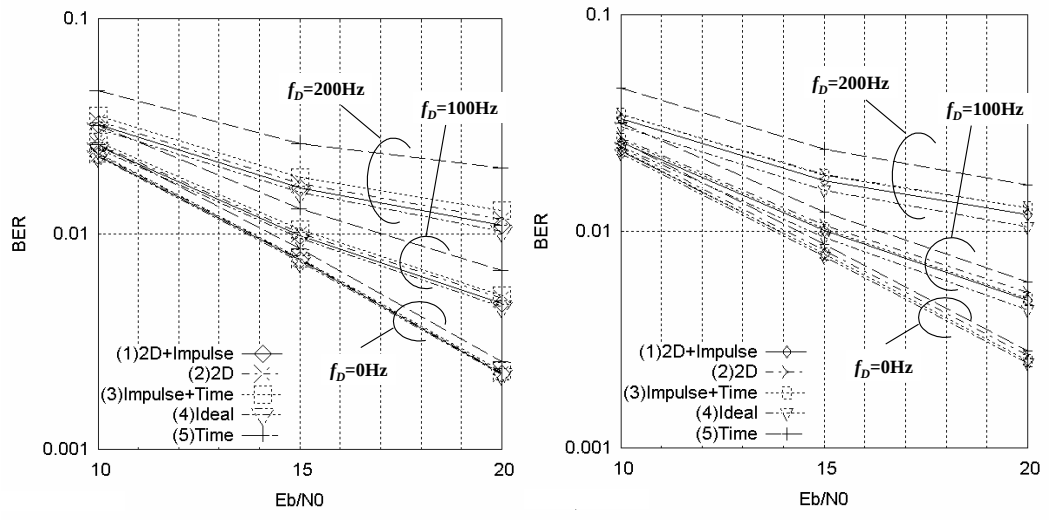

(a) σ_S=0.0μs (b) σ_S=0.4μs

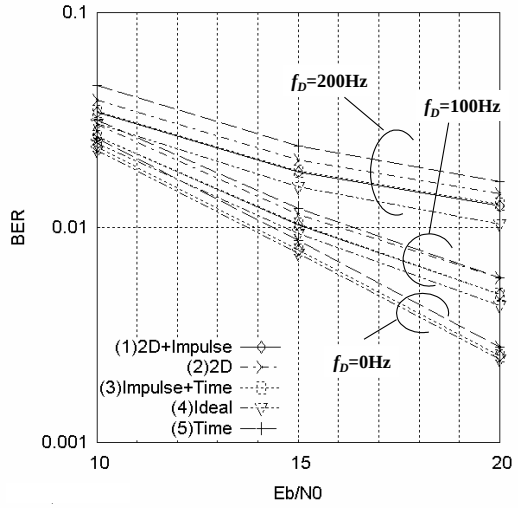

(c) σ_S=0.8μs

Figure 4. 12: BER performance comparison

estimation and simplicity.

To implement this method in actual systems, we need methods that can estimate the maximum Doppler frequency and the delay spread; examples of such methods are shown in references [4.14-4.16].

4.5.5 Comparison with other methods

We clarify the performance of our proposed method and compare it to other methods in detail. The delay spreads are 0.0 μs, 0.4 μs and 0.8 μs, respectively, in Fig. 4.12(a), 4.12(b) and 4.12(c). In each figure, the maximum Doppler frequencies were set at 0, 100 and 200 Hz. The BER performance was evaluated for the five methods described in Section 4.5.2.

Method (2) does not include the impulse response-based method. When both the maximum Doppler frequency and the delay spread are small, the BER performance is almost identical to that of method (1). This is because the channel estimation accuracy is high enough even if the impulse response-based method is not used. However, when both the maximum Doppler frequency and the delay spread are large, the channel estimation accuracy obtained by just the two-dimensional method is so low that the BER performance is inferior to that of method (1). For example, when the maximum Doppler frequency is 100 Hz and the delay spread is 0.4 μs, the BER performance is 0.6 dB worse than that of method (1) at the BER of 0.01.

Method (3) applies only one-dimensional averaging in the time domain combined with the impulse response-based method. When the maximum Doppler frequency is small, only the time-domain averaging has a significant impact on the channel estimation accuracy. However, when the maximum Doppler frequency becomes high, the averaging in the time domain does not work well and only the impulse response-based method is effective. For example, when the maximum Doppler frequency is 200 Hz and the delay spread is 0.4 μs, the BER performance is 0.4 dB worse than method (1) at the BER of 0.02.

Method (5) applies only one-dimensional averaging in the time domain without the impulse response-based method. Therefore, regardless of the delay spread, the method cannot obtain any average gain in the frequency domain. Also, as the maximum Doppler frequency becomes higher, the channel estimation accuracy becomes worse rapidly because the method can obtain little averaging gain.

From the results mentioned above, to achieve good BER performance, which is impacted by the channel estimation accuracy, it is very effective to use combining and optimizing the two-dimensional method and the impulse response-based method.

4.5.6 Summary

In this chapter, we proposed a channel estimation method, a combination of a two-dimensional method and an impulse response-based method, for next generation mobile communication systems in which highly accurate channel estimation is required. The two-dimensional method averages pilot symbols which are transmitted consecutively in both time and frequency domains, and each pilot symbol is weighted by considering the fading correlation in both domains. The impulse response-based channel estimation method further improves the channel estimation accuracy. The time domain signal, which is obtained by inversely Fourier transforming the channel estimates in the frequency domain, represents the impulse response. With regard to the impulse response, the path elements are included in the guard interval duration so that the impulse response outside the guard interval can be eliminated. Therefore, the method can further improve the channel estimation accuracy.

We first evaluated the optimized forgetting factors for combination of a range of maximum Doppler frequencies and delay spread values by considering the effects of the two-dimensional method and the impulse response-based method. Through an evaluation, we showed that spacing the forgetting factors by 0.2 yields virtually the best performance; using tighter spacing does not yield significantly better forgetting factors. We then evaluated the BER performance of our method in a comparison with other methods. Comparing with the two-dimensional method without impulse response-based method, the proposed method is 0.6 dB better when the maximum Doppler frequency is 100Hz and the delay spread is 0.4μs. Also, compared to the impulse response-based method with time-domain filtering, the proposed method offers a gain of 0.4dB when the maximum Doppler frequency is 200Hz and the delay spread is 0.4μs.

Chapter 5

Handover

5.1 Issues and approaches for handover

In CDMA mobile cellular systems, MSs can simultaneously connect with multiple BSs by a soft handover (hereafter, handoff in this chapter) technique. Soft handoff has following advantages over conventional hard handoff:

· Improving the radio channel quality by virtue of the decrease of total interference power [5.1]

· Avoiding the interruption resulting from the connection switching and frequent connection changes (known as “ping-pong effect”)

Its drawback is apparent; each MS in the soft handoff state occupies wired channels at multiple BSs. Therefore, we need to identify the influence of such a redundancy on the wired channels.

Past researches on soft handoff in CDMA have been mainly dedicated to the wireless channel quality. For example, the author in [5.4] evaluated the trade-off relationship between wireless quality of uplink and downlink, and proposed a way to decide the size of the soft handoff region. In [5.3] , the authors described that introducing soft handoff causes the decrease of shadow fade margin which leads to the increment of capacity or improvement of wireless quality.

However, in those studies, the limitation by the number of wired channels at each BS is not considered. If all of wired channels of one BS have already been occupied, some MSs cannot enjoy soft handoff because of lack of wired channels. The existence of such MSs must affect wireless channel quality. One of a few exceptions can be found in [5.2] where the authors have evaluated blocking probability for newly generated and handoff call as the performance measure of CDMA systems to discuss the influence of soft handoff on the quality of wired channels. They also presented the call control method by using those performance measures. To evaluate

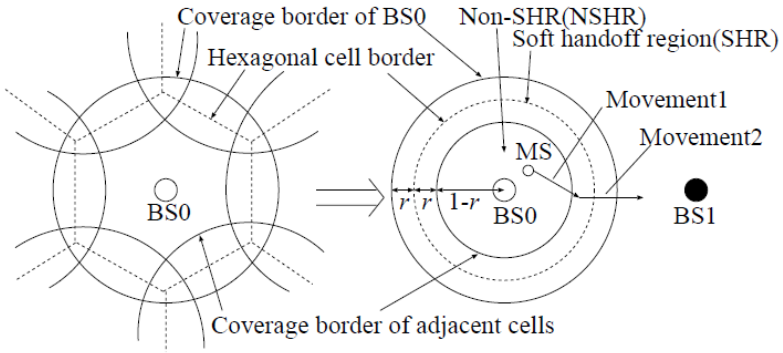

Figure 5. 1: Approximation model of CDMA cell

the performance of the call control method, however, its effect on wireless channel quality must be considered. Only such total evaluation of the soft handoff system makes it possible to decide the meaningful system parameters.

In this chapter, we evaluate the effect of the size of soft handoff region on qualities of both wired and wireless channels comprehensively. We adopt blocking probability for newly arriving calls and forced termination probability of handoff calls as performance measures of wired channels, and outage probability for wireless channel quality. We derive these performance measures by an approximate analytical method. Through numerical examples, we show the effect of the size of soft handoff region on the system performance. We also introduce one example which improves wireless channel quality by suppressing the interference power. This shows that appropriate call control methods may improve feeling of satisfaction of users. This paper is organized as follows. In Section 5.2, we explain the system model and performance measures for each wired and wireless quality. In Section 5.3, we propose an analysis method. Then we show numerical examples by applying our analysis method in Section 5.4. Finally, this chapter is summarized in Section 5.5.

5.2 System model and performance measures

5.2.1 Model of CDMA mobile cellular systems

As illustrated in Figure 5.1, we assume that the service area is divided into hexagonal cells,

and its shape is approximated by a circle for simplicity. We also assume that MSs are uniformly distributed within the service area. As shown in Figure 5.1, MSs in SHR (Soft Handoff Region) can connect with BS0 and one of the adjacent BSs, but we assume that each MS cannot connect with three or more BSs at the same time. MSs in NSHR (non-SHR) can connect with BS0 only. The width of SHR is denoted by $2r$, and the NSHR radius is defined as $1 - r$ by assuming that a cell radius is always 1.

5.2.2 Evaluation of wired channel assignment

As described before, we evaluate the quality of wired channels in terms of blocking and forced termination probabilities. Blocking probability is defined as the probability that a newly generated call is blocked. Such an event takes place due to two reasons; a newly generated call in NSHR is blocked when there is no available channel in the nearest BS. In SHR, it is blocked when there is no available channel in both of two BSs that it can connect with. We derive blocking probability by calculating a weighted average of blocking probability in each region. When a MS leaves a current cell, and find no available wired channel in the cells which it moves into, it is terminated forcibly. In Figure 5.1, the MS moving towards BS1 (Movement1) gets into the soft handoff state, if there is available wired channel at BS1. The MS can keep a call if it keeps to move for BS1 (Movement2). On the other hand, if there is no available wired channel at BS1, the MS that moves for BS1 (Movement1) has only a single connection with BS0 even in SHR. The call of the MS is forcedly terminated when the MS continues moving towards BS1 (Movement2), because it does not have a connection with BS1. As another performance measure of wired quality, we introduce forced termination probability which means the probability that a call is forcedly terminated before communication itself ends because of handoff failure. Note one assumption for simple analysis. We consider the case that one available channel generates in BS1 when a MS connects with BS0 only in SHR. In such a case, the MS cannot connect with BS1 as long as it is in the same region.

5.2.3 Evaluation of wireless channel quality

In this paper, we focus on the up link in examining the wireless channel quality since it is more important in investigating the effect of the soft handoff [5.1] . In evaluating the wireless channel quality, we consider outage probability which is defined as the probability that the signalto-interference ratio (SIR) is less than the threshold level realizing adequate transmission quality [5.5] . In the CDMA system, outage probability can appropriately evaluate wireless quality because SIR directly determines BER (Bit Error Rate). We assume that perfect power control is realized such that power from MS is steadily received at BS.

5.3 The analysis method

Here, we show our analysis method to obtain performance measures which we have explained in previous section. We first consider wired channels and derive blocking probability and forced termination probability. By the analysis, we will obtain the numbers of MSs in SHR and NSHR in steady state. We will then derive interference power, and obtain outage probability.

5.3.1 Blocking probability and forced termination probability

We assume that generation of new calls follows the Poisson process, and the arrival rate per one cell is denoted as λ. Call holding time and residual time per one cell are assumed to follow the exponential distribution, and denoted as $1/\mu$, $1/\mu_c$ respectively. Then, residual time in NSHR and SHR, $1/\mu_s$ and $1/\mu_m$, also follow exponential distribution. Those can be calculated from $1/\mu_c$ (See Appendix A of [5.6]).

We assume that MSs spread uniformly in the system. Therefore, we can derive performance measures by focusing on one cell. In the target cell, we denote the number of calls in NSHR as n_s, and in SHR as n_m. The state of occupied wired channels is then denoted as (n_s, n_m), and the steady state probability of (n_s, n_m) is denoted as $p(n_s, n_m)$. From call arrival rate per one cell λ, the call arrival rate in NSHR and SHR, λ_s and λ_m, are calculated by considering area

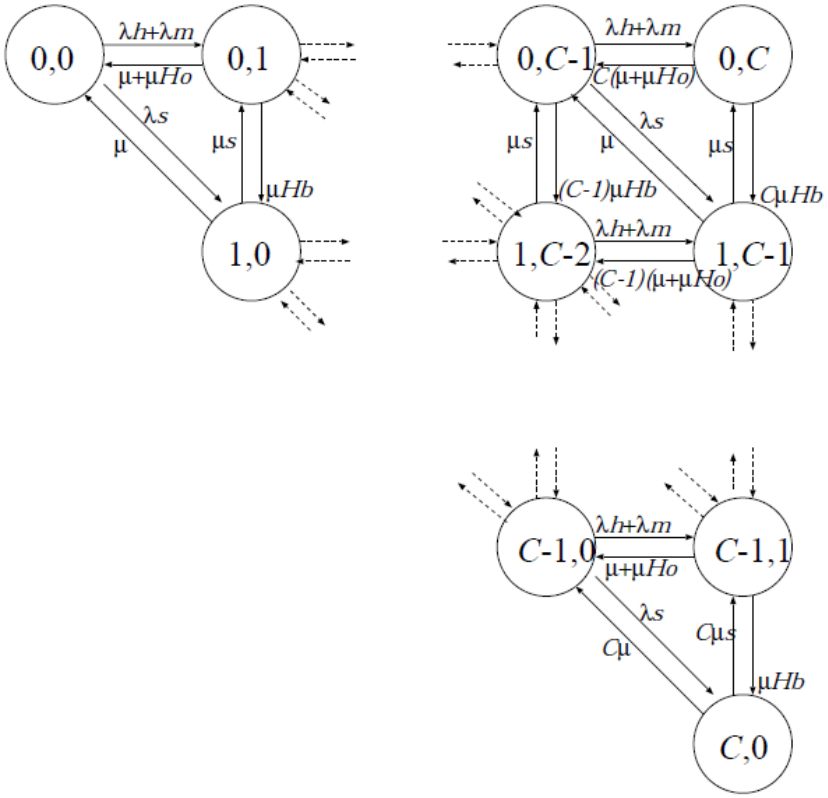

Figure 5. 2: State transition probability for occupied wired channels for SHR and NSHR

of each region.

$$\lambda_s = (1-r)^2\lambda, \quad \lambda_m = 4r\lambda \tag{5.1}$$

When MSs in SHR move out from the region, they are assumed to move into NSHR with the probability b_k (See Appendix B of[5.6]). With this assumption, the probabilities that MSs in SHR move out to NSHR, μ_{Hb}, and to out of the target cell, μ_{Ho} are given as follows.

$$\mu_{Hb} = b_k\mu_m, \quad \mu_{Ho} = (1-b_k)\mu_m \tag{5.2}$$

In steady state, the call arrival rate from other cells to the target cell and departure rate from the target cell to other cells are assumed to be equivalent. Therefore, we can calculate λ_h which means the call arrival rate from other cells to SHR of the target cell, as

$$\lambda_h = \sum_{n_s=0}^{C}\sum_{j=n_m}^{C-n_s} n_m \cdot \mu_{Ho} \cdot p(n_s, n_m) \tag{5.3}$$

With these assumptions and calculations, we can obtain the state transition probabilities

(see Figure 5.2). This transition can be expressed by following equilibrium state equation.

$$\begin{aligned}
&\{n_s(\mu+\mu_s)+n_m(\mu+\mu_{Hb}+\mu_{Ho})\\
&+\lambda_m+\lambda_h+\lambda_s\}p(n_s,n_m)\\
&=\lambda_s p(n_s-1,n_m)+(\lambda_m+\lambda_h)p(n_s,n_m-1)\\
&\quad+(n_m+1)\mu_{Hb}p(n_s-1,n_m+1)\\
&\quad+(n_s+1)\mu_s p(n_s+1,n_m-1)\\
&\quad+(n_s+1)\mu p(n_s+1,n_m)1_{\{n_s+n_m<C\}}\\
&\quad+(n_m+1)(\mu+\mu_{Ho})p(n_s,n_m+1)1_{\{n_s+n_m<C\}}
\end{aligned} \tag{5.4}$$

The steady state probability can then be obtained by applying the normalization condition;

$$\sum_{n_s=0}^{C}\sum_{n_m=0}^{C-n_s}p(n_s,n_m)=1 \tag{5.5}$$

However, as shown in Equation 5.3, call arrival rate from other cells depends on the steady state probabilities. Therefore, by repeating calculations, we can obtain its convergence as the steady state probabilities. The probability that the target cell has no available channels, p_f, is given by the sum of the probabilities of states with $n_s + n_m = C$, i.e.,

$$p_f=\sum_{(n_s,n_m);n_s+n_m=C}p(n_s,n_m) \tag{5.6}$$

To derive the blocking probability of users, we consider the users within hexagonal cell border of one cell (Figure 5.1). The call arrival rate in SHR within the border is given by $\lambda - \lambda_s$. Then, blocking probability P_B can be obtained by calculating a weighted average;

$$P_B=\lambda_s p_f+(\lambda-\lambda_s)p_f^2 \tag{5.7}$$

By letting the probability that users go out from coverage border (Figure 5.1) be μ_{cover}, the probability that users go out from coverage border before they terminate their call is given by $\left(\frac{\mu_{cover}}{\mu+\mu_{cover}}\right)$ Then, the forced termination probability is obtained by

$$P_T=\sum_{i=0}^{\infty}\left(\frac{\mu_{cover}}{\mu+\mu_{cover}}\right)^{i+1}(1-p_f)^i p_f \tag{5.8}$$

Note that derivation of μ_{cover} is found in [5.6] .

5.3.2 Calculation of outage probability

Here, we show the analysis method of outage probability that exhibits wireless channel quality. It can be obtained by calculating interference power that a BS receives from MSs. We

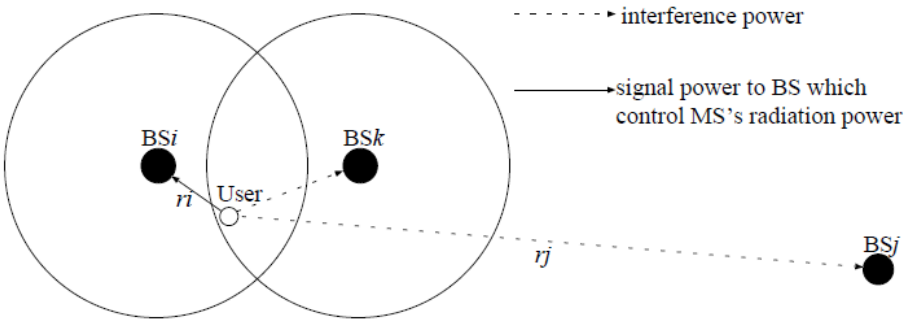

Figure 5. 3: Interference power from the user in soft handoff state

assume that the power that each MS radiates (denoted by E_{trans}) is ideally controlled and be received at same power, E_s, at the BS. Furthermore, let us introduce I_{BS} to represent the interference power that the BS receives from all MSs. In Figure 5.3, the user is in the soft handoff state, and connects with BS_i and BS_k . Then we assume that attenuation to BS_i is smaller than BS_k including distance and shadowing effect. That is, the required power from BS_i is smaller for the user than BS_k . As described before, the user can keep communication as long as it can connect with at least one BS. Therefore, the radiation power of the user is enough if it satisfies the required power from BS_i . To derive the radiation power for the user, we further introduce γ denoting the attenuation which is in inverse proportion to the distance [1]. Moreover, ζ_i represents the attenuation by the shadowing which follows the regular distribution. ζ_i has two parts; the one is a common element for whole system (denoted by ξ) and the other is the element dependent on each BS (ξ_i). It is then given by

$$\zeta_i = \frac{1}{\sqrt{2}}\xi + \frac{1}{\sqrt{2}}\xi_i \tag{5.9}$$

The radiation power for the user, Etrans, is given by using the above quantities as;

$$E_{trans} = E_s \cdot r_i^{\gamma} 10^{\zeta_i/10} \tag{5.10}$$

With these equations, interference power that BS_j receives from the user is calculated as;

$$I_{BSj} = \frac{E_{trans}}{r_j^{\gamma} 10^{\zeta_i/10}} = E_s \left(\frac{r_i}{r_j}\right)^{\gamma} 10^{\frac{\xi_i - \xi_j}{10\sqrt{2}}} \tag{5.11}$$

We introduce another assumption to calculate outage probability. If we want to take account of outage probability correctly, we should calculate interference power from all MSs in the service

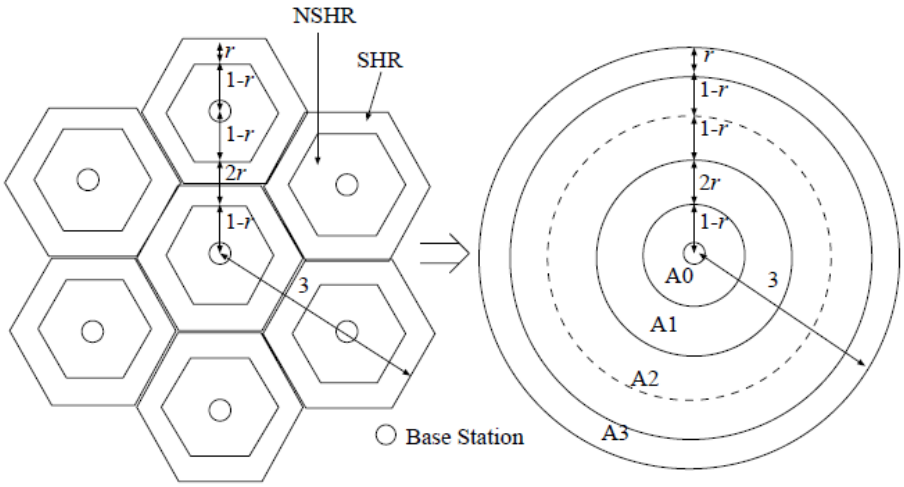

Figure 5. 4: Approximation model for calculating outage probability

area. However, interference power from MSs which is far from the target BS can be ignored because of attenuation by the distance. Therefore, we approximately obtain the outage probability by considering interference power from MSs in the target cell and the neighbor cells. For simple analysis, we approximate these cells are circular area as shown in Figure 5.4. We then calculate interference power from MSs in each region, from A0 to A3. The mean of the interference power from each MS in NSHR can be calculated as follows.

$$E[Is] = E_s \left(\frac{r_i}{r_j}\right)^{\gamma} E[10^{\frac{\xi_i - \xi_j}{10\sqrt{2}}}] \tag{5.12}$$

For MSs in SHR, it is given by;

$$\begin{aligned} E[Im] &= E_s \left(\frac{r_i}{r_j}\right)^{\gamma} E[10^{\frac{(\xi_i - \xi_j)}{10\sqrt{2}}}] \\ &\quad \cdot P(r_i^{\gamma} 10^{\zeta_i/10} < r_k^{\gamma} 10^{\zeta_k/10}) \\ &+ E_s \left(\frac{r_k}{r_j}\right)^{\gamma} E[10^{\frac{(\xi_k - \xi_j)}{10\sqrt{2}}}] \\ &\quad \cdot P(r_i^{\gamma} 10^{\zeta_i/10} > r_k^{\gamma} 10^{\zeta_k/10}) \end{aligned} \tag{5.13}$$

The mean interference power from all MSs in the target area is given by summing means of those from all MSs, because interference power from each MS is independent. In a similar manner, the variance is also calculated. The mean number of users in NSHR, Ns, is obtained by using the steady state probability, which was derived in Subsection 5.3.1.

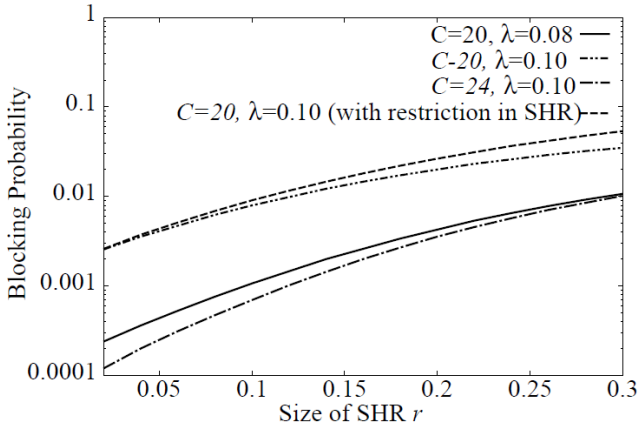

Figure 5. 5: The effect of size of SHR on blocking probability

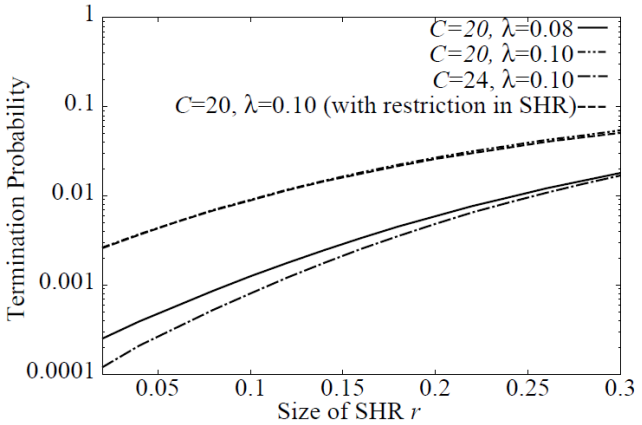

Figure 5. 6: The effect of size of SHR on forced termination probability

$$N_s = \sum_{n_s=0}^{C} \sum_{n_m=0}^{C-n_s} n_s p(n_s, n_m) \tag{5.14}$$

The mean number of users in SHR, Nm, is also obtained in a similar way. By multiplying the mean number of users by the area of region A0 (and A1, A2 and A3), we can obtain the average number of MSs in each region. SIR at the target BS is denoted as follows.

$$SIR = \frac{G_p E_b}{I_{BS}} \tag{5.15}$$

Here, G_p means process gain at BSs. By denoting required *SIR* as SIR_{req} and mean and variance of interference power from all MSs as $E[I_{BS}]$, $Var[I_{BS}]$, outage probability P_{out} is obtained as follows.

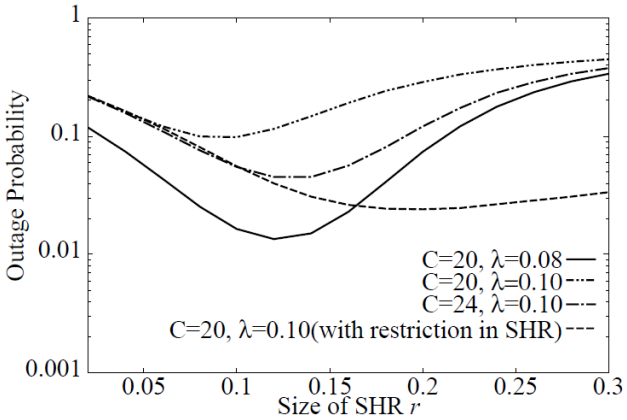

Figure 5. 7: The effect of size of SHR on outage probability

$$\begin{aligned} Pout &= P\left(I_{BS} > \frac{Gp}{SIR_{req}}\right) \\ &= Q\left(\frac{\frac{G_p}{SIR_{req}} - E[I_{BS}]}{\sqrt{Var[I_{BS}]}}\right) \end{aligned} \tag{5.16}$$

5.4 Numerical examples and discussions

In this section, we demonstrate the applicability of our method. An arrival rate of the new calls at each cell is denoted as λ. The number of wired channels of BS is denoted as C. System parameters are summarized in Table 1. We plot blocking and forced termination probabilities against the size of SHR, r, in Figures 5.5 and 5.6, respectively. Blocking and forced termination probabilities are increased as r gets larger. It is natural because the number of available wired channels becomes short as more MSs are allowed to be moved into the soft handoff state. The corresponding outage probabilities are shown in Figure 5.7. Outage probability is first improved against increased r. However, it is degraded when exceeding some value. It is because the SHR size gives different influences on outage probability. Due to the soft handoff, the interference power can be decreased. It contributes the decrease of outage probability and the effect is dominant when r is small. However, as r becomes larger, MSs connecting with single BS in SHR (which have failed to connect with another BS) is increased due to lack of the available wired channels. Those MSs must send the signal with stronger power to keep the connection

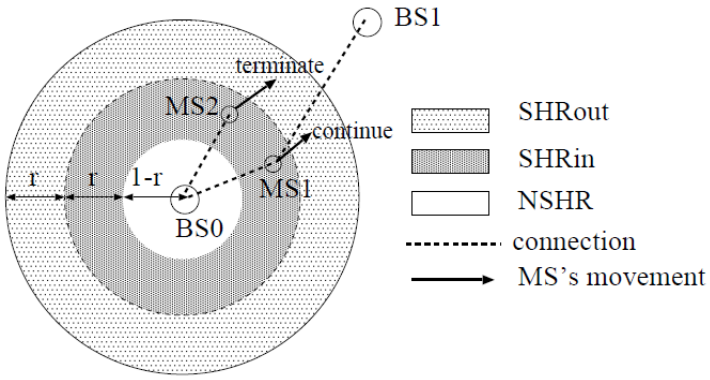

Figure 5. 8: Restriction of MSs in SHR for wireless quality improvement

with far BS. Then, outage probability becomes worse against the larger r. By comparing two lines (λ = 0.08 and 0.10), we can also observe that the increased load makes the performance worse. Then, increasing the number of wired channels can improve the performance again as expected. See the lines for C = 24 in three figures. One remarkable point observed in the figure is that the optimal value of r to minimize outage probability is shifted. Thus, we need to seek out the optimal value of the size of SHR by some appropriate method such as ours. If we look at the results more carefully, we can find another approach without more wired channels. By changing the load from λ = 0.08 to 0.10 (for C = 20), the performance (blocking and forced termination probabilities and outage probability) was degraded. It is because as the traffic load becomes high and the number of available wired channels becomes little, MSs are likely to fail to move into the soft handoff state within SHR. Then those MSs send strong interference power to BSs because they must keep connection with far BS. It results in that outage probability is degraded by increased SIR values. It suggests that we can expect performance improvement by following method. In Figure 5.8, MS1 has connections with both BS0 and BS1, and MS2 has only one connection with BS0. When MS1 moves to SHRout, it can keep connections with both BS0 and BS1. However, when MS2 moves to SHRout, its connection with BS0 is terminated forcibly because it radiates strong power and degrades wireless quality of other users. The results are also shown in the figures with the label "with restriction in SHR". Here, we set C = 20 and λ = 0.10. In our method, blocking and forced termination probabilities are not degraded,

while outage probability can much be improved.

5.5 Summary

In this chapter, we proposed evaluation method of soft handoff in CDMA mobile cellular systems. We have adopted blocking and forced termination probability as performance measures of wired channels, and outage probability as for wireless channels. Then, we have calculated these performance measures by analytical method. We have clarified the effect of the width of soft handoff region and the number of wired channels at a BS on these performance measures, by showing some numerical examples obtained from our analytical method. From our results, it is apparent that adjusting system parameters by considering both wired and wireless quality is needed for system design. This integrated evaluation is necessary to control a system after the operation of the system starts.

Chapter 6

Layered Cell Configuration

6.1 Issues and approaches for layered cell configuration

Layered cell configuration is recently attracting much attention as a tool to improve capacity, in which a large number of small cells are put in a macro-cell coverage area [6.1-6.6]. In the case of co-channel layered cell configuration, the co-channel interference between macro and small cells needs to be controlled effectively in order to increase spectral efficiency. In LTE-Advanced, enhanced Inter-Cell Interference Coordination (eICIC) has been standardized to resolve the co-channel interference. In eICIC, the interference is reduced by stopping some parts of the downlink signal transmission of a base station (hereafter, eNB: evolved Node B). This signal muting can be conducted subframe by subframe, which is 1ms long, in the time domain by applying Almost Blank Subframe (ABS), in which data and control signals are not transmitted.

Therefore, it is important to decide the amount and the position of ABSs effectively in order to increase system capacity. This decision is basically conducted in a distributed fashion at each eNB, so that it becomes more difficult to control the co-channel interference effectively as the interference among cells becomes more complicated. Recently, in urban areas, traffic is increasing rapidly especially in high-rise condominiums and office buildings. Therefore, the three-dimensionally overlaid cell structure (hereafter, 3D structure) is becoming essential where small cells are deployed in the vertical domain as well as in the horizontal domain as shown in Fig. 6.1. In order to solve the complicated interference among cells in 3D cell structure, we propose the network-based coordinated interference control system, in which all macro-cell and small-cell eNBs are connected to an IP backhaul network and the co-channel interference control is conducted in a centralized fashion. Although the burden of control information and signal processing increases, the amount and the position of ABSs are not required to be updated frequently and the centralized approach is sufficiently feasible.

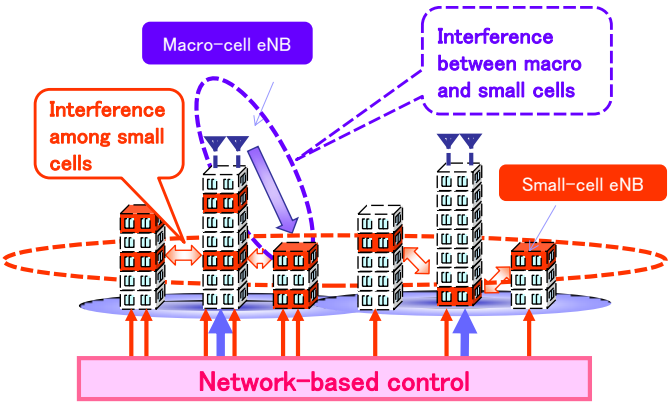

Figure 6. 1: Network-based coordinated interference control

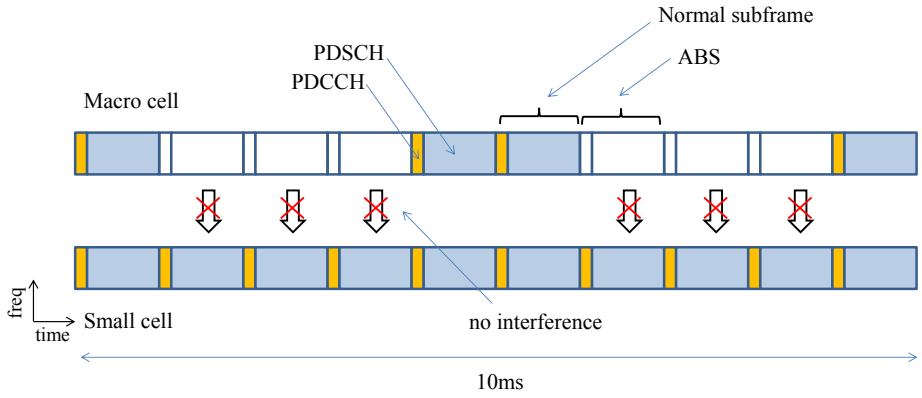

Figure 6. 2: Frame structure of eICIC

We also develop a prototype of the network-based coordinated interference control system in order to demonstrate its feasibility through laboratory and field experiments. In the past, the experimental evaluations of eICIC even with a distributed approach have not been well conducted, although some field experiments of an overlaid cell structure have been conducted [6.6] . We implement eICIC in our prototype system and the amount and the position of ABSs is controlled in a centralized fashion. We also implement three types of ABSs such as Non Multicast Broadcast Single Frequency Network ABS (Non-MBSFN ABS), MBSFN ABS and Blank subframe and clarify the difference of the three types of ABSs through laboratory experiments. Moreover, we conduct field experiments in order to demonstrate the feasibility and clarify the throughput performance of the network-based coordinated interference control system.

This coordinated interference control for layered cell configuration is presented in Section 6.2. Subsection 6.2.1 describes the overview of coordinated interference control. Subsection 6.2.2 details the prototype system of the coordinated interference control, which is followed by laboratory experiments in Subsection 6.2.3. The results of field experiments are also explained in Subsection 6.2.4.

In this chapter, radio resource allocation for layered cell configuration is also studied. Mobile data traffic is doubling every year recently and is expected to increase 1000-fold in ten years [6.12] . As a promising solution to cope with this rapidly increasing mobile data traffic, the layered cell configuration, which overlays the macro cell coverage area with a large number of small cells, is attracting much attention for 3rd Generation Partnership Project (3GPP) Long-Term Evolution Advanced (LTE-Advanced) and 5th Generation mobile communications systems (5G) [6.1, 6.2, 6.13]. With the layered cell configuration, we can install low-cost small cells in traffic hot spots and greatly improve user throughput by offloading the macro-cell traffic to the small cells.

This cell configuration yields a mixture of variously sized cells, from macro to small, and the Mobile Station (MS) and traffic distribution of each cell are quite different. Therefore, the distribution of the number and the received signal quality of the MSs is much wider than the conventional macro-cell homogeneous networks. This means that the cell-edge user throughput in a cell with large number of MSs is still expected to be low even in layered cell configuration.

Load balancing has been proposed as a way of mitigating MS distribution among cells [6.14, 6.15]. In load balancing, the number of MSs in a cell can be controlled by adjusting the transmit power, which increase and decrease cell size. MS redistribution can also be achieved by Cell Range Expansion (CRE) of 3GPP LTE-Advanced, which can increase and decrease the cell size by adjusting the effective handover threshold [6.15-6.18].

Even belonging to the same cell, the throughput of the connected MSs distributes, and the cell-edge MSs suffer relatively low throughput because they receive low signal power from their serving cell and high interference power from the neighboring cells. In order to improve the cell-edge user throughput, the multiple base-station cooperative transmission technique has been studied; neighboring multiple cells transmit to the cell-edge MS in a coordinated manner [6.19-6.21]. This technique has also been studied intensively under the name of Coordinated

Multi-Point (CoMP) transmission even in 3GPP [6.22].

By applying load balancing or CoMP transmission, the congestion of cells with large numbers of MSs can be mitigated, and the user throughput at cell edge can be improved. However, there is a limit to the mitigation of the congestion by load balancing because the adjustment of cell size by transmission power control or CRE has a certain restriction. In terms of CoMP transmission, the effect of the technique varies a lot depending on the interference power from the neighboring cells. Considering the above issues, this paper proposes a scheduling priority control scheme; it can further improve cell-edge user throughput in combination with load balancing and/or CoMP transmission.

The proposed scheme controls the scheduling priority individually per cell by taking into account its cell-edge throughput performance. This is conducted based on the Generalized Proportional Fair (GPF) scheduling algorithm, which is an extension of the widely-used Proportional Fair (PF) scheduling algorithm [6.23-6.25]. Because implementing the proposed scheme changes only the control algorithm of GPF, it is quite simple and can be applied simultaneously with conventional load balancing and/or CoMP transmission. We also propose a dynamic control algorithm in order to adaptively follow changes in the distribution over time. The performance of the proposed method is confirmed by computer simulations.

The rest of this section is organized as follows. Subsection 6.3.1 details the proposed adaptive scheduling priority control scheme. Subsection 6.3.2 shows the evaluation conditions of the computer simulations, which are followed by the evaluation results of the proposed method in Subsection 6.3.3. Finally, we give our summary in Section 6.4.

6.2 Coordinated interference control for layered cell configuration

6.2.1 Coordinated interference control

The concept of the network-based coordinated interference control for the co-channel overlaid cell structure is shown in Fig. 6.1. Small cells are deployed in buildings in a three-dimensional fashion in a macro-cell coverage area and receive the co-channel interference from macro-cell eNBs. As the number of small cells increases, the distance between small cells

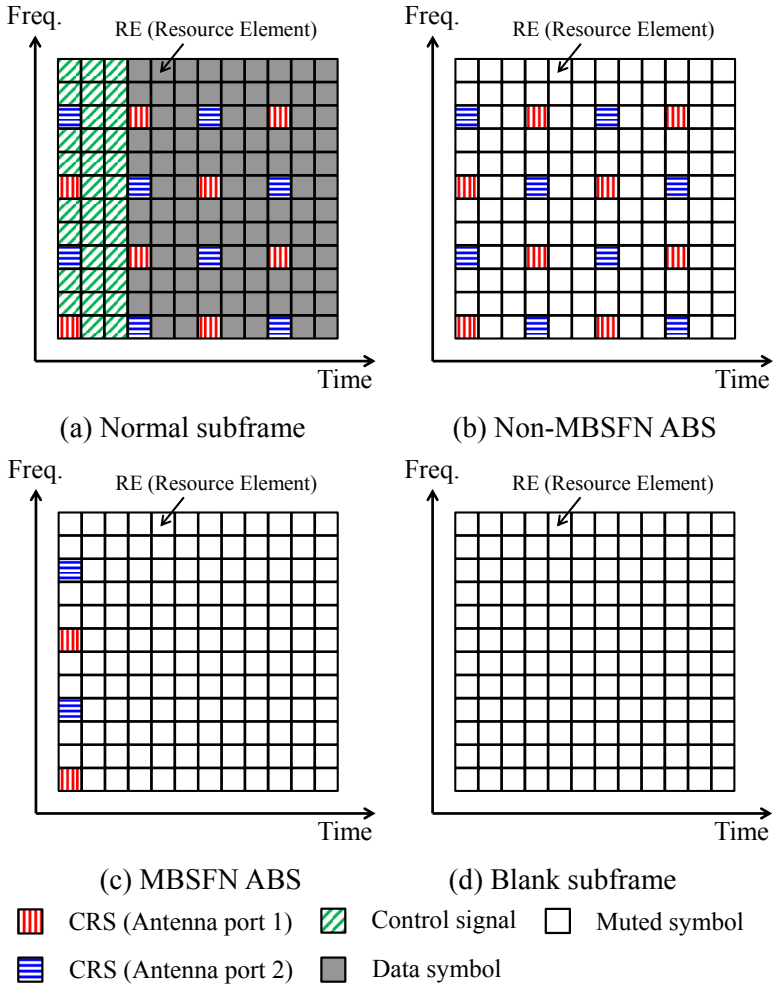

Figure 6. 3: Downlink subframe format

becomes closer and the interference between small cells also needs to be solved. The small-cell eNBs as well as the macro-cell eNBs are connected to an IP backhaul network, and the interferences are effectively controlled by utilizing network coordination.

The interference between macro and small cells can be avoided based on eICIC. Fig. 6.2 shows the frame format of LTE-Advanced. One radio frame consists of ten 1ms subframes. A subframe can be set as ABS in order to reduce interference. In Fig. 6.2, six subframes in a radio frame are set as ABS at the macro-cell eNB in order to reduce the interference to small cells. When there is interference from a small cell to a macro cell, the interference can be mitigated by applying ABSs at the small-cell eNB. In eICIC, the decision of the amount and the position of

ABSs are important in order to increase system capacity. However, the decision based on a distributed approach becomes more difficult as the number of eNBs in the system increases.

In order to solve this issue, in the network-based coordinated interference control system, the decision is conducted in a centralized approach. The important information to make the decision such as the traffic amount of each eNB and the received quality and the received desired and interference signal power of the User Equipments (UEs) in the cell is reported from each eNB to a centralized control equipment and the decision is made there. Although the amount of control information and signal processing becomes larger as the number of eNBs in the system increases, the centralized approach is feasible as the update of the decision does not need to be conducted so often. Although a kind of clustering is needed in the centralized approach, the performance degradation caused by the clustering can be mitigated by increasing the number of eNBs connected to the centralized control equipment and properly setting the cluster borders at areas where there is low traffic.

The subframe format of a normal subframe is shown in Fig. 6.3 (a). We assume the usage of extended cyclic prefix and the number of OFDM symbols per subframe is 12. Control signals (PDCCH: Physical Downlink Control CHannel) are transmitted in the first three OFDM symbols and data signals (PDSCH: Physical Downlink Shared CHannel) are transmitted in the remaining OFDM symbols. Cell-specific Reference Signal (CRS) for received-power measurement and channel estimation is inserted every six subcarriers in the frequency domain per transmit antenna in 0-th, 3rd, 6-th and 9-th OFDM symbols; we assume two transmit antennas.

In eICIC in LTE-Advanced, two types of ABSs can be used: Non-MBSFN ABS and MBSFN ABS, which are shown in Fig. 6.3 (b) and (c), respectively. In Non-MBSFN ABS, PDCCH and PDSCH are muted and only CRS remains. Although most part of the interference is reduced, the remaining CRS interference limits the throughput improvement in interfered cells. In MBSFN ABS, CRS in PDSCH region can also be stopped, which means there is no interference for the data signals in interfered cells. Although there is a limitation that MBSFN ABS can be set up to only six subframes in a radio frame, the throughput performance in the interfered cells can be improved drastically. However, the CRS in the 0-th OFDM symbol degrades the reception performance of PDCCH, which is transmitted in the first three OFDM

Table 6. 1: Major parameters of prototype system for coordinated interference control

	Downlink	Uplink
Access system	OFDMA	SC-FDMA
Carrier frequency	3385MHz	3315MHz
System bandwidth	10MHz	
Number of subcarriers (Subcarrier spacing)	600 (15kHz)	
Symbol length	66.67μs+Cyclic Prefix 16.67μs	
Sub-frame length	1ms	
Number of transmitter antennas	2	1
Number of receiver antennas	2	2
Transmit power	43dBm/antenna	23dBm

symbols especially when a large cell range expansion of small cells is used in order to prompt traffic offloading. In order to cope with this issue, a blank subframe with no signal transmission at all is effective as in Fig. 6.3 (d).

In the network-based coordinated interference control system, the interference between small cells also needs to be solved. This interference can also be controlled by eICIC because the interference between small cells can also be reduced by applying ABSs. On top of this interference control, various techniques based on network coordination such as Coordinated Multi-Point transmission (CoMP) and coordinated beamforming can also be applied [6.7-6.9].

6.2.2 Prototype system

We developed a prototype of the proposed network-based coordinated interference control system. The major parameters of the prototype system are summarized in Table 6.1. We developed the prototype system based on LTE-Advanced system. The downlink and uplink carrier frequencies are 3385MHz and 3315MHz, respectively. The system bandwidth is 10MHz. The downlink wireless access system is OFDMA and the number of sub-carriers is 600; the sub-carrier spacing is 15 kHz and the symbol length is 66.67 μs. Extended cyclic prefix is used, the length of which is 16.67 μs. The downlink antenna configuration is two transmit and two receive antennas, which enables 2x2 MIMO; the uplink antenna configuration is one transmit

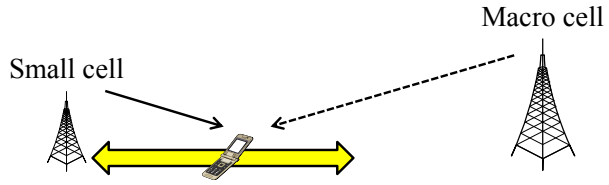

Figure 6. 4: Evaluation model

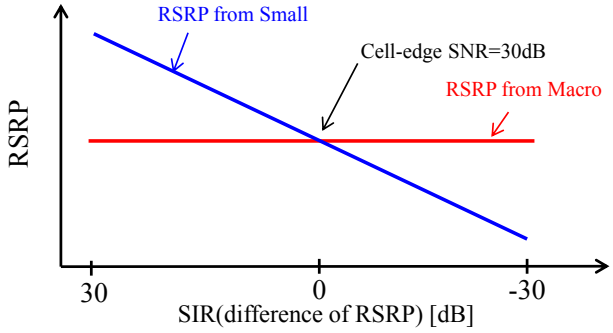

Figure 6. 5: Received power

and two receive antennas, which enables receive diversity. The transmit power of eNB is 20W (43dBm) per transmit antenna and that of UE is 200mW (23dBm).

For the downlink, Adaptive Modulation and channel Coding (AMC) is used; QPSK, 16QAM and 64QAM are implemented and the maximum Modulation and Coding Scheme (MCS) is limited up to 21, so that the maximum throughput is around 42Mbps. Channel Quality Indicator (CQI) is fed back from UE every 1 ms to report its received signal quality; eNB decides MCS based on the fed-back CQI and Outer Loop Link Adaptation (OLLA), with which MCS is controlled to make BLock Error Rate (BLER) at 10%. Retransmission uses Hybrid Automatic Repeat reQuest (HARQ) in Medium Access Control (MAC) layer and Automatic Repeat request (ARQ) in Radio Link Control (RLC) layer. Each eNB in the system is connected to centralized control equipment via an IP backhaul network and the amount and the position of ABSs are controlled from the centralized control equipment. The timing synchronization between macro-cell and small-cell eNBs is ideally established in the following experiments, although it can be achieved by GPS-based, packet-based or network-listening based timing synchronization [5, 10].

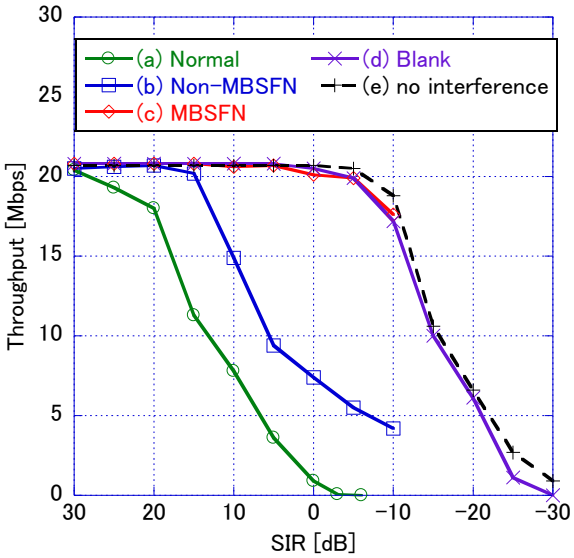

Figure 6. 6: Throughput performance of eICIC

6.2.3 Laboratory experiments

We first conducted laboratory experiments. We assumed the two-cell model shown in Fig. 6.4. We evaluated the throughput of the UE connected to the small cell moving between the neighborhood of the small-cell eNB and the cell edge. The received power from the macro-cell and small-cell eNBs is shown in Fig. 6.5. The x-axis is the Signal-to-Interference Ratio (SIR) of the UE, which is denoted as the ratio of Reference Signal Received Power (RSRP) from the small-cell eNB to that from the macro-cell eNB. We assumed RSRP from the macro-cell eNB was the same everywhere in the small cell since the small cell was quite small compared to the macro cell. The Signal-to-Noise Ratio (SNR) at the cell edge was set at 30dB. We assumed the Additive White Gaussian Noise (AWGN) channel model; MIMO channels were assumed to be uncorrelated.

Fig. 6.6 shows the throughput performance of the coordinated interference control with four different subframe formats shown in Fig. 6.3: (a) Normal subframe, (b) Non-MBSFN ABS, (c) MBSFN ABS and (d) Blank subframe. We also evaluated the performance with (e) no interference from the macro-cell eNB as a reference. In this evaluation, we set the maximum MCS at 13, so the maximum throughput was around 21Mbps. We assumed the UE were

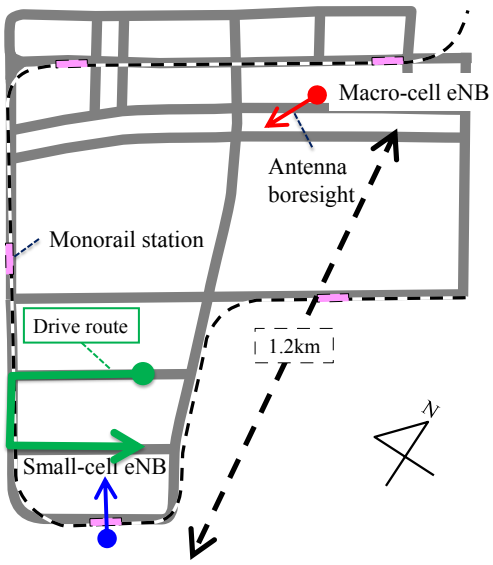

Figure 6. 7: Field trial area and drive route

allocated all the subframes from the small-cell eNB, and all the subframes of the macro-cell eNB were set as ABS or blank subframe to simplify the evaluation, although all the subframes cannot be set as ABS in actual operation in order to serve the UEs in macro cell.

In Fig. 6.6, the x-axis is SIR and the y-axis shows throughput. With (a) Normal subframe, the throughput degraded as the UE moved towards the cell edge because of the increased interference from the macro-cell eNB. With (b) Non-MBSFN ABS, the throughput performance was improved since the data-signal transmission of the macro-cell eNB was muted. Although the transmission of CRS was not stopped, the throughput was improved by around 9dB compared to Normal subframe because the data signal accounted for around 87.5% of the total interference power, which corresponded to 9dB improvement. The reason why the UE was disconnected when SIR became less than -10dB was that it could not receive the control channel (PDCCH) by the interference from CRS in the 0-th OFDM symbol. With (c) MBSFN ABS, the throughput performance became much higher because the CRS transmission in PDSCH region was also stopped. Therefore, there was no interference to PDSCH and the performance matching that of (e) no interference could be achieved. However, PDCCH still received interference because the CRS in PDCCH region was still being transmitted. Therefore, the communication was terminated at the SIR of -10dB as was true in the case of Non-MBSFN

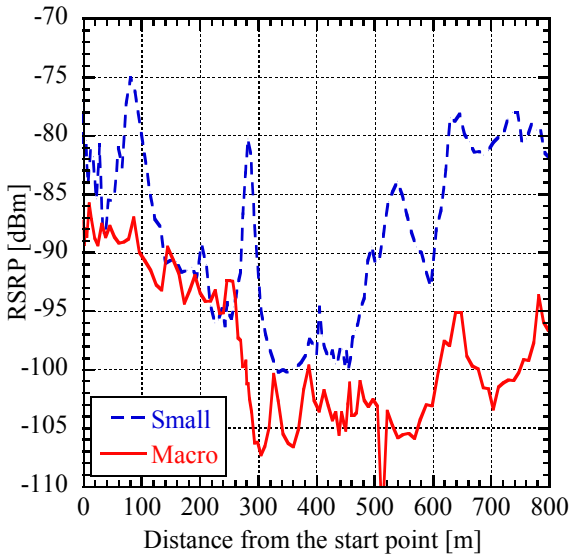

Figure 6. 8: Received power

ABS. Finally, with (d) Blank subframe, there is no interference at all in either PDCCH or PDSCH region, so that the throughput performance well matched that without interference. Although MBSFN ABS is enough as long as the cell-range expansion of the small cell is limited to less than 10dB (corresponding to SIR of -10dB), another approach such as blank subframe can be useful when further cell-range expansion is needed in order to offload the macro-cell traffic more. It is noteworthy that the introduction of CRS interference canceller at UE may lower the importance of MBSFN ABS or blank subframe because Non-MBSFN ABS is enough as long as CRS can be cancelled sufficiently at UE [11].

6.2.4 Field experiments

6.2.4.1 Field experiment environment

We conducted field experiments in an urban area in Tokyo, Japan. The area map is shown in Fig. 6.7. The transmit power of the macro-cell eNB is 20W per transmit antenna and +45/-45 degree dual-polarized sector antennas are used; the gain is 16dBi and the half-value angle is 90 degrees. Denoting magnetic north as 0 degrees, the antenna boresight is 210 degrees in a clockwise fashion. The small-cell eNB is placed within the macro-cell coverage area and the

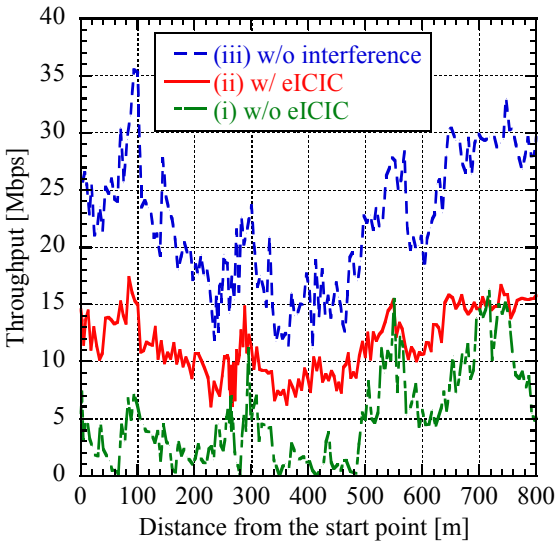

Figure 6. 9: Throughput performance of eICIC

distance from the macro-cell eNB is 1.2km. Although the same sector antenna is used as the macro-cell eNB, the transmit power is set lower than the macro-cell eNB to limit the coverage area; the antenna boresight is 330 degrees. The centralized control equipment is placed in a building in the area and connected to each eNB via an IP backhaul network; the amount and the position of ABSs are controlled from this equipment.

We conducted measurements on a driving course in the small-cell area shown in Fig. 6.7. The total length is around 800 m. RSRP from both eNBs are plotted in Fig. 8. The x-axis shows the distance from the start point of the driving course. The driving course is almost Non-Line Of Sight (NLOS) for the macro-cell eNB; the first 100m and the last 200m is LOS and the remaining part is NLOS for the small-cell eNB. The delay spread of the propagation channel is from 0.2 μs to 1.0 μs for both eNBs. UE movement speed was around 20 km/h (the maximum Doppler frequency was about 60 Hz). In the field experiments, the maximum MCS was set at 21; the maximum throughput was around 40Mbps.

6.2.4.2 Field experiment results

The throughput performance is shown in Fig. 6.9. We compared the following cases: (i) without eICIC, (ii) with eICIC and (iii) without interference. Without eICIC, the UE received

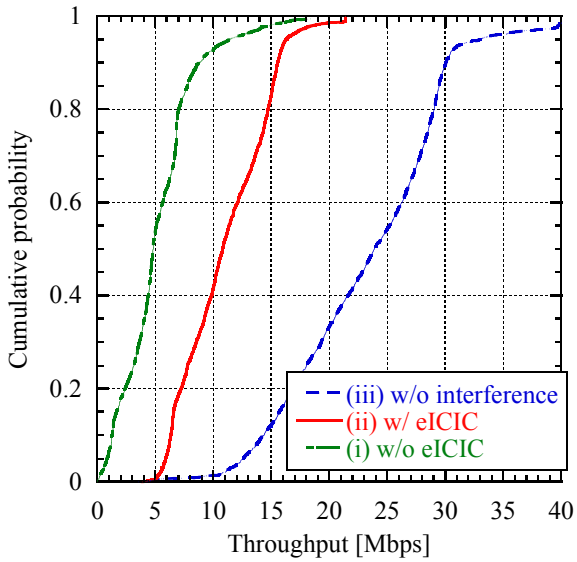

Figure 6. 10: CDF of throughput

the interference from the macro-cell eNB in all the subframes. Therefore, the throughput became low especially when the UE approached the cell edge toward the macro cell area. When the RSRP difference between the small and macro cells was less than 5dB such as 150m to 250m or 350m to 450m as in Fig. 6.8, the throughput dropped to as low as a few Mbps. It is noteworthy that this evaluation environment is interference limited and the impact of thermal noise is slight.

On the other hand, the throughput improved drastically with eICIC. In the field experiments, we used MBSFN ABS for the interference avoidance. We assumed only one half of subframes were allocated to the UE in the small cell, which was different from the case in the laboratory experiments. The corresponding subframes in the macro cell were set as MBSFN ABS in order to reduce interference, and the remaining other half of subframes were allocated to a UE in the macro cell. Therefore, with eICIC, only one half of subframes were used by the small-cell UE compared to the case without eICIC. However, the spectral efficiency was more than doubled in each subframe by the interference avoidance with MBSFN ABS, so that the total throughput also outperformed the case without eICIC. Although there was no interference from the macro-cell eNB and SNR was higher than 20dB throughout the drive route, the throughput was less than the maximum throughput of 21Mbps for the one half of subframes.

This is because the throughput was affected by delay spread, maximum Doppler frequency and antenna correlation. For example, the reason why the throughput did not reach the maximum value from 600m to 800m where SNR was sufficiently high and the delay spread was as low as 0.3 μs was high antenna correlation caused by the LOS environment. It is noteworthy that the throughput with eICIC was half that without interference as expected; all the subframes were allocated in this case without interference.

Fig. 6.10 shows the CDF of the throughput. The 50-percentile throughput of (i), (ii) and (iii) was 5Mbps, 11Mbps and 24Mbps, respectively. The throughput with eICIC was more than doubled compared to the case without eICIC; it was half the throughput without interference as expected. At 5 percent, the throughput with eICIC was 6Mbps while that without eICIC was as low as 1Mbps because the UE received strong interference from the macro-cell eNB especially when it approached the cell edge.

6.3 Adaptive Scheduling Priority Control

6.3.1 Adaptive Scheduling Priority Control

6.3.1.1 Overview of General Scheduling Algorithm

In mobile communications systems, base stations (hereafter, BSs) have their own packet scheduler and control the allocation of radio resources to the MSs. The efficiency of the control algorithm of the packet scheduler (hereafter, scheduling algorithm) is very important in order to improve the cell overall average user throughput (spectral efficiency) and cell-edge user throughput. The scheduling algorithm can be classified as either with or without MS feedback. The former is represented by the Round Robin (RR) algorithm, a channel-unaware scheduling algorithm. The fair throughput algorithm is also known as a channel-unaware scheduling algorithm that enables fair throughput among MSs [6.23] .

These algorithms are quite simple but fail to handle instantaneous changes in received signal quality caused by fast fading because the MSs do not feed back the received signal quality to the BSs. In order to resolve this issue, channel-aware scheduling algorithms are widely used recently; the BS receives the MS feedback (received signal quality) and makes a

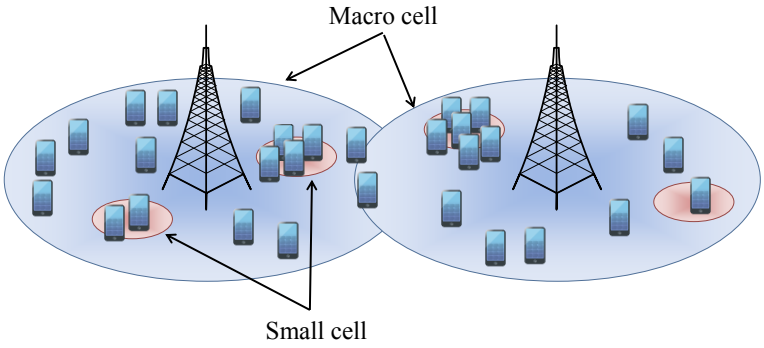

Figure 6. 11: Layered cell configuration

decision on the resource allocation. Maximum Carrier-to-Interference Ratio (Max-CIR) algorithm is a widely known simple channel-aware scheduling algorithm. In allocating radio resources to the MSs, it attempts to maximize the spectral efficiency. However, the Max-CIR algorithm does not allocate any radio resources to cell-edge MSs with low received signal quality, which results in quite low or zero cell-edge user throughput.

PF, which is widely used recently, addresses this problem, as it seeks both high spectral efficiency and fairness among MSs. PF not only takes into account the instantaneous received signal quality like the Max-CIR algorithm but also secures fairness by considering the average received signal quality of the MSs. When the expected throughput of MS u at time t is defined as $R_u(t)$ and the average throughput of MS u up to the time is defined as $\overline{T}_u(t)$, the scheduling metric $m_u(t)$, which is a decision criteria for resource allocation, can be written as

$$m_u(t) = \frac{R_u(t)}{\overline{T}_u(t)} \tag{6.1}$$

PF allocates radio resources to the MS with the highest scheduling metric, so the MS that is to receive resources, $\hat{u}(t)$, is given by

$$\hat{u}(t) = \arg\max_u \left(m_u(t)\right) \tag{6.2}$$

GPF was proposed as an extension of PF and is able to realize flexible scheduling priority control [6.25] . GPF adds weight coefficients α and β to PF scheduling metric $m_u(t)$ in order to realize flexible priority control. The scheduling metric of GPF, $m'_u(t)$, is expressed as

$$m'_u(t) = \frac{R_u(t)^{\alpha}}{\overline{T}_u(t)^{\beta}} \tag{6.3}$$

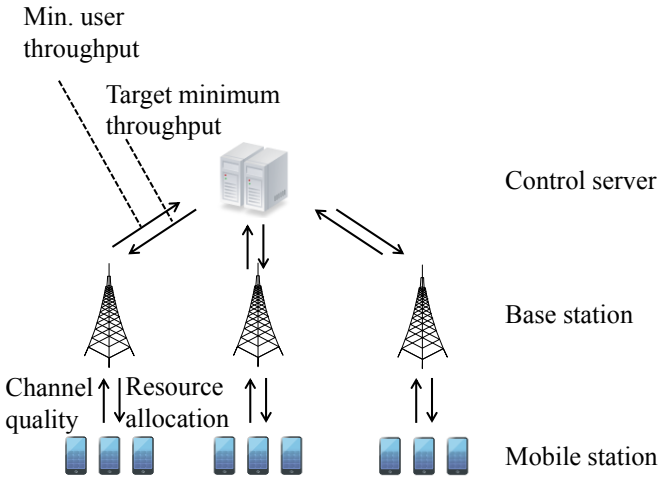

Figure 6. 12: Control system structure

When we increase β, the scheduling metrics of the MSs with low average throughput become relatively higher, so that cell-edge MSs with low Signal-to-Interference plus Noise Ratio (SINR) can be allocated radio resources with high priority. This means that cell-edge MSs are allocated more radio resources (and thus better performance) even though the received SINR is the same. On the other hand, by decreasing β, the scheduling metrics of the MSs with high average throughput become relatively high, which improves spectral efficiency of the system.

In this paper, we fix α at 1 in order to simplify the control and control only β to adjust scheduling priority. It is noteworthy that the scheduling metric becomes the same as that of Max-CIR when β is set at 0 because the denominator becomes 1; it becomes the same as that of PF when β is set at 1.

6.3.1.2 Proposed Adaptive Scheduling Priority Control Algorithm

Fig. 6.11 shows a conceptual diagram of the layered cell configuration. In this cell configuration, the throughput performance in each cell varies greatly depending on MS number and traffic distribution. Considering this variance in throughput among the cells, our proposed method uses GPF to control the scheduling priority and takes into account of the congestion of each cell. In the proposed method, we prioritize cell-edge MSs in radio resource allocation when the cell is congested with a large number of MSs in order to ensure that no MS has extremely

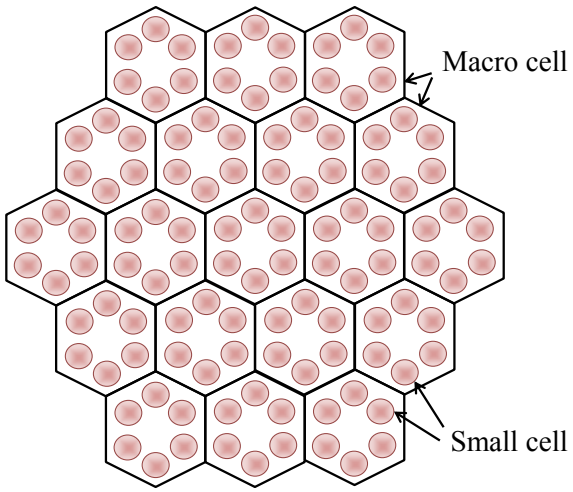

Figure 6. 13: Cell layout

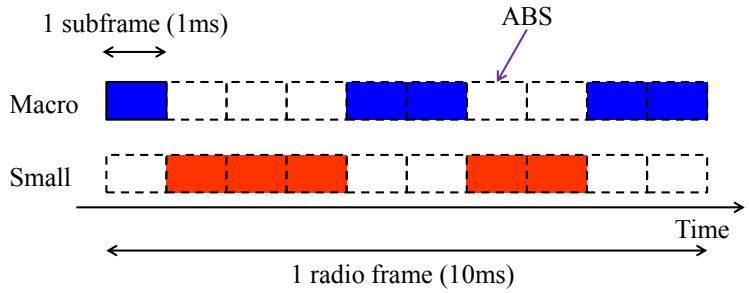

Figure 6. 14: Radio resource allocation by eICIC

low throughput; this can be simply achieved by increasing the weight coefficient β of GPF in the cell.

In the proposed method, setting the weight coefficient of GPF, β, is important because the above scheduling priority control is conducted by adjusting only this weight coefficient. We first define the target minimum throughput, T_{target}, which is the minimum throughput all MSs in the system should satisfy, in order to avoid the generation of MSs with extremely low throughput. Each BS monitors the minimum user throughput in its cell and prioritizes the cell-edge MSs to ensure all MSs have at least T_{target} by increasing β.

How to determine T_{target} is also important. One approach is to use the required data rates for major applications. For example, it can be 10kbps for voice call or a few hundred kbps for web browsing. However, when a cell is congested, many MSs will be unable to receive T_{target}. In this case, GPF tends to allocate excessive radio resources to the MSs with low received signal

Table 6. 2: Major parameters of adaptive scheduling priority control

Parameter	Value
Cell layout	Macro: 19 cells (hexagonal grid) Small: 6 cells per macro cell
Inter-eNB distance (Macro) (Cell radius)	500[m] (r=288[m])
Macro-Small distance	0.5r
Number of UEs	1, 2, 5, 10 (for each Macro and Small)
Transmit power	Macro: 46[dBm] Small: 30[dBm]
Antenna configuration	Tx: 1, Rx: 1
Tx antenna gain	Macro: 5[dBi] Small: 5[dBi]
Penetration loss	20[dB]
Path loss	Macro: L=128.1+37.6*log10(d) Small: L=140.7+36.7*log10(d)
Shadowing standard deviation	8[dB]
Shadowing correlation	0.5
Noise power	-174 [dBm/Hz]
Bandwidth	10 [MHz]

quality in order to near the target minimum throughput, which results in low cell average throughput.

In order to solve the issue, we propose a method to decide the target minimum throughput by taking the congestion of the area. Fig. 6.12 shows the control system structure in order to realize the proposed method. Each BS reports the minimum user throughput of the cell to the control server. The control server determines the minimum user throughput of the area, which the server covers, and notifies each BSs of the minimum throughput as the target minimum throughput, T_{target}. Then, each BS controls its scheduling priority based on the target minimum throughput by GPF. When a BS has the MS with the minimum throughput of the area, the weight coefficient of GPF of the cell, β, is increased in order to improve the worst throughput of the area. The increment is conducted by a step size at regular intervals, and the target minimum throughput is updated accordingly. On the other hand, when the minimum throughput of a cell is

larger than T_{target}, the GPF weight coefficient, β, is decreased by a step at regular intervals as long as the cell's minimum throughput is higher than T_{target}.

6.3.2 Evaluation Conditions

We evaluate the effect of the proposed method by computer simulations. Table 6.2 summarizes the major parameters of the evaluation, which is mostly based on an evaluation model of the 3GPP LTE system [6.26] . The cell layout is shown in Fig. 6.13. As shown in the figure, the macro cells consist of 19 cells placed on hexagonal grid; the inter-BS distance is set at 500m where the cell radius is 288m. We also assume the layered cell configuration and place 6 small cells in each macro cell; the small cells occupy at 60 degree intervals and the distance from the nearest macro BS is one half the cell radius, which means 144m. To simplify the evaluation, we set both macro and small cells as omni cells. Also for simplicity, we assume that the small cells are placed on traffic hot spot and the numbers of MSs in each macro and small cell are the same; the MSs are uniformly distributed in each cell. It is noteworthy that the user throughput distribution varies per cell even with the same number of MSs in all cells; the effect of the proposed method is expected to be stronger when the number of MSs per cell is also distributed.

The transmit powers of macro-cell and small-cell BSs are set at 46dBm and 30dBm, respectively. The antenna configuration is assumed as 1 transmit and receive antenna for evaluation simplicity; the antenna gain of the transmit antenna is set at 5dBi for both macro and small-cell BSs. The penetration loss is set at 20dB and the path loss exponents for each macro and small cells are set at 3.76 and 3.67, respectively where d km means the distance between BS and MS. The standard deviation of log-normal shadowing is set at 8dB and the correlation among BSs is set at 0.5. The thermal noise power is defined as -174dBm/Hz and the system bandwidth is set at 10MHz. We evaluate throughput based on Shannon capacity.

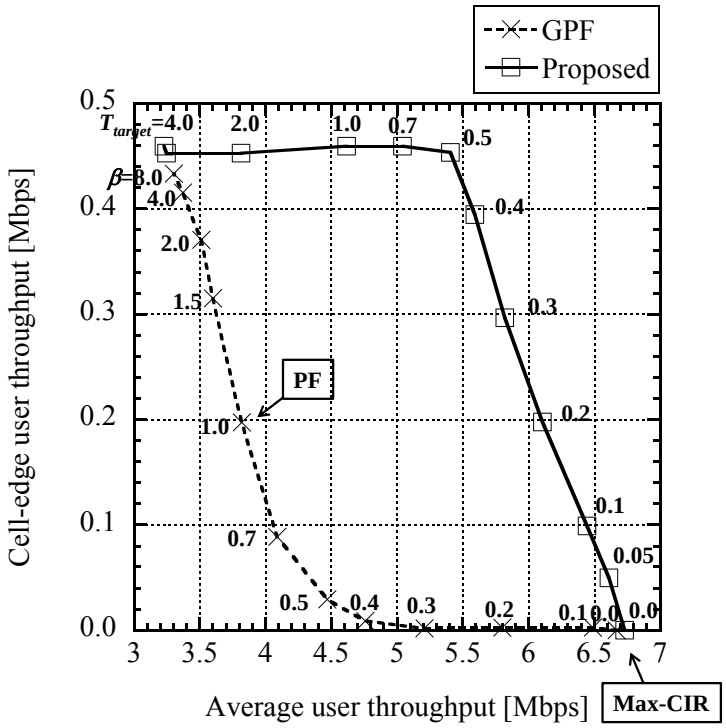

Figure 6. 15: Throughput performance

We use enhanced Inter-Cell Interference Coordination (eICIC) in order to avoid the co-channel mutual interference between macro and small cells. Fig. 6.14 shows the subframe allocation for each macro and small cell. We assume that the radio resource allocation is repeated at 1ms interval like LTE. 1 radio frame consists of 10 subframes, and the half subframes are allocated to macro cells and the other half subframes are allocated to small cells. The subframes not allocated to the MSs are set as Almost Blank Subframe (ABS) where no data signal transmission is conducted. Although Cell-specific Reference Signal (CRS) is still transmitted even in ABS, we assume that the residual CRS interference can be ideally cancelled by using CRS interference cancellation [6.27, 6.28].

6.3.3 Evaluation results

6.3.3.1 Basic Evaluation Results

We evaluated the proposed method from the view point of average user throughput

(spectral efficiency) and cell-edge user throughput. We first evaluated the proposed method with a fixed target minimum throughput and compared with conventional GPF with a fixed weight coefficient. In the proposed method, GPF weight coefficient, β, was controlled individually per cell based on the target minimum throughput, T_{target}. The step size of β was 0.1 and updated every 1ms, the minimum scheduling interval; the feedback of the minimum throughput per cell and the notification of the target minimum throughput in Fig. 6.14 were assumed to be conducted without latency. The evaluation results are shown in Fig. 6.15. In this evaluation, we assumed that the number of MSs was set at 10. User drop was conducted 1000 times and the average user throughput was evaluated. We defined the cell-edge throughput as the minimum throughput of all cells in the 1000 trials. The x-axis and y-axis show the average and cell-edge user throughput, respectively. The target minimum throughput, T_{target}, of the proposed method was changed from 0.0Mbps to 4.0Mbps; the target minimum throughput of 0.0Mbps means that there is no lower limit, i.e. similar to Max-CIR. For comparison, we also show the evaluation results when the same weight coefficient of GPF was used in all cells. We changed β from 0.0 to 8.0. It is noteworthy that the scheduling algorithm is the same as PF when β is set at 1; it becomes the same as Max-CIR when β is set at 0.

When we used PF (β=1), the average user throughput was 3.8Mbps and the cell-edge throughput was 0.2Mbps. With Max-CIR (β=0), the average user throughput improved by 80% and became 6.7Mbps, while the cell-edge throughput was 0Mbps. In this case, the cell-edge MSs were not allocated any radio resource because of their low SINR. On the other hand, GPF can adjust the priority of radio resource allocation by changing weight coefficient, β. When we increase β, the cell-edge throughput improves, while the average user throughput deteriorates because more radio resources are allocated to the users with low SINR. When β=2, the cell-edge user throughput became 0.38Mps, which is twice that of PF. However, the average user throughput became 3.5Mbps, which was lower than that of PF by 10%. On the other hand, when we decrease β, the MSs with high SINR are prioritized and the average user throughput can be improved, while the cell-edge user throughput degrades. For example, when β=0.5, the average user throughput exceeded that of PF by 30% and became 4.5Mbps. However, the cell-edge user throughput fell to as low as 0.03Mbps, which is 85% lower than that of PF.

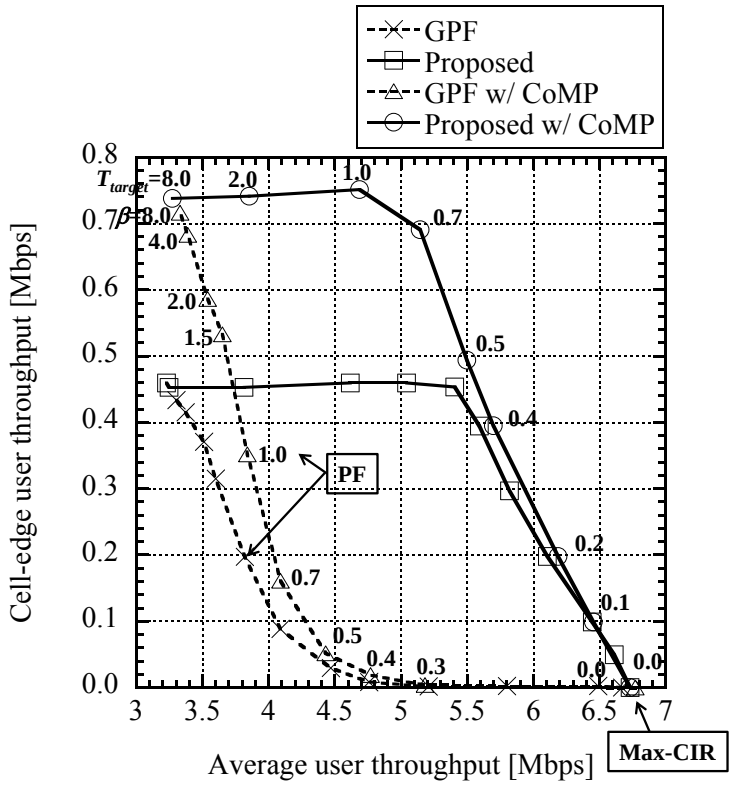

Figure 6. 16: Throughput performance with CoMP

On the other hand, our proposed method can improve cell-edge user throughput without decreasing average user throughput by adjusting GPF weight coefficient individually per cell as long as the target minimum throughput, T_{target}, is satisfied. When we set T_{target} to 0.2Mbps, the average user throughput was improved 1.5 times compared to that of PF and became 6.0Mbps, while the cell-edge user throughput was the same as that of PF. When we set T_{target} at 0.4Mbps, the cell-edge throughput doubled and became 0.4Mbps; the average user throughput was also improved, by 50% from 3.8Mbps to 5.6Mbps, compared with PF. When we set T_{target} higher, the cell-edge user throughput did not improve any more, while the average user throughput decreased. This can be explained as follows. As we increase T_{target}, β tends to be high in order to allocate more radio resources to the cell-edge MSs, which results in fair throughput scheduling in low-throughput cells but the minimum throughput saturates, and no further improvement can be achieved.

6.3.3.2 Evaluation Results with CoMP

We also evaluated the performance of the proposed method in combination with CoMP. The results are shown in Fig. 6.16. In this paper, we assume that the distance between small cells was sufficiently large, so that the effect of CoMP could not be expected between small cells. Therefore, we applied CoMP only for macro cells. We used a simple CoMP, in which the phases of the signals transmitted from both neighboring BSs were adjusted so that the signals are received at MS in phase. When we denote the received power at an MS from desired BS as P_S, the interference power from its neighboring BSs as P_I, the sum of interference power from other BSs and thermal noise as P_{I0+N0}, the received SINR of the cell-edge MS without CoMP can be written as

$$\gamma = \frac{P_S}{P_I + P_{I_0+N_0}} \tag{6.4}$$

On the other hand, when CoMP is applied, the signals from both neighboring BSs are received in phase, so that the received SINR of the MS, γ_{CoMP}, is expressed as

$$\gamma_{CoMP} = \frac{\left(\sqrt{P_S} + \sqrt{P_I}\right)^2}{P_{I_0+N_0}} \tag{6.5}$$

Although the cell-edge user throughput can be improved by the application of CoMP, it should be noted that the cell-edge MS uses the radio resources of both BSs. Therefore, in order not to decrease system throughput, we apply CoMP only when the throughput of the cell-edge MS can be more than doubled [6.29] . Moreover, in order to secure fairness in resource allocation among the BSs, when a BS applies CoMP for its MS, the same amount of radio resource for the CoMP is provided to the cooperating neighbor BS. That is, if the Shannon capacity of a MS with CoMP, $\log_2(1+\gamma_{CoMP})$, is more than doubled compared with the capacity without CoMP, $\log_2(1+\gamma)$, CoMP is applied. However, as mentioned above, one half of the radio resource is provided to the neighbor BS, thus the effective throughput improvement of the cell-edge MS becomes twice when its spectral efficiency, $\log_2(1+\gamma_{CoMP})$, becomes four times higher than that without CoMP.

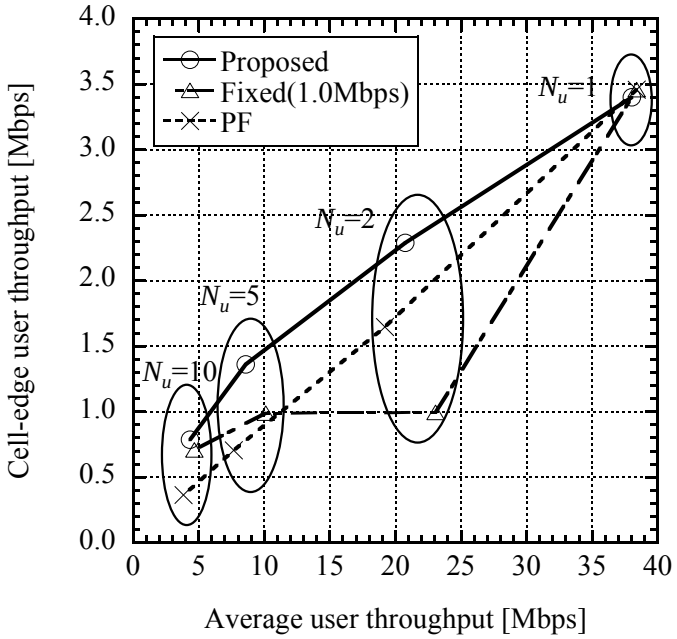

Figure 6. 17: Throughput performance with target throughput control

When CoMP is applied, the received SINR of the cell-edge MSs can be improved, so that the target minimum throughput, T_{target}, can be satisfied with less radio resources. For example, when T_{target} is set at 0.7Mbps, the cell-edge user throughput improved 1.5 times and became 0.7Mbps, while the average user throughput is the same as that without CoMP, which is 5.2Mbps. Also, when CoMP is not applied, the cell-edge user throughput converged at 0.5Mbps regardless of the target minimum throughput because of the low spectral efficiency of the cell-edge MSs. On the other hand, when our proposed method is combined with CoMP, the converged throughput is improved to 0.75Mbps, which is 1.5 times higher than the case without CoMP.

6.3.3.3 Evaluation results with Target minimum throughput Control

Fig. 6.17 shows the evaluation results of the proposed target minimum throughput control method. The proposed method decides the target minimum throughput based on the minimum throughput of the area by collecting throughput information from each cell. Therefore, the target minimum throughput can be decided based on user distribution and receiver environment

without any prior assumption. We set the number of MSs in each cell, N_u, at 1, 2, 5 and 10. We compared the throughput performance of PF, the proposed method (fixed target minimum throughput) and the proposed method (with target minimum throughput control). When N_u is 1, scheduling priority control is not conducted because all the radio resources are allocated to the sole MS. Accordingly, all the methods have the same throughput performance. When the number of MSs is more than 1, the proposed method can improve both average and cell-edge user throughput compared with PF by applying adaptive scheduling priority control per cell. For example, when N_u is 5, the average and cell-edge user throughput is improved by 12% and 93%, respectively. When the target minimum throughput is fixed at 1.0Mbps, the cell-edge user throughput cannot be improved even with fewer MSs. On the other hand, the proposed method with adaptive target minimum throughput control can improve both average and cell-edge throughput compared with PF by adaptively changing target minimum throughput depending on situation.

6.4 Summary

In this chapter, we first proposed the network-based coordinated interference control system based on a centralized approach for the co-channel overlaid cell structure. We also developed a prototype of the proposed system with different three types of ABS subframe formats. The performance characteristics of the different formats were clarified through the laboratory experiments. Although MBSFN ABS achieved the same performance as the case with no interference, another format such as blank subframe is required if the cell range expansion over 10dB is used. We also conducted field experiments with the prototype and clarified that the throughput could be more than doubled with half radio resources by applying the coordinated interference control.

We also proposed a simple scheduling priority control method for the cell configurations that have wide variations in the number and the distribution of the MSs in each cell, such as heterogeneous networks consisting of various cell sizes from macro to small. In the proposed method, the scheduling priority of each cell is controlled based on the target minimum throughput, with consideration of the congestion in the area. We evaluated both average and

cell-edge user throughput of the proposed method by computer simulations and clarified that it can, compared with PF, drastically improve the cell-edge user throughput without degrading the average user throughput; the performance is also much better than GPF with fixed priority control. We also clarified that the proposed method offers useful performance gains when used in combination with conventional cell-edge throughput improvement methods such as CoMP transmission. We also showed that the target minimum throughput could be properly controlled depending on the congestion of the area.

Chapter 7

Conclusion

Cellular mobile communications systems have played an essential role in increasing network capacity to keep up with the rapid growth of mobile data traffic. As mobile data traffic grows, we can gradually increase network capacity by placing more BSs and reusing finite and precious frequency resources in the BSs. However, the communication quality at cell edge has been considered to be an issue because it tends to be low by lower received signal power from connecting BS and higher interference power from neighbor BSs compared to other locations in a service area. In this thesis, I investigated Multi-BS cooperative transmission control, Multi-link signal transmission, channel estimation, handover, and layered cell configuration for cell-edge communication quality improvement. In the following, I first describe the position of each technology for the goal of this thesis and then summarize my contribution in each technology.

Cell-edge user throughput is mainly affected by the interference from neighbor cells, so the control of the interference is the most important part of the countermeasures to increase cell-edge user throughput. This is achieved by Multi-BS cooperative transmission control shown in Chapter 2, in which two or more multiple BSs cooperate in the signal transmission to a cell-edge MS and mitigate the interference from neighbor cells. Multi-link signal transmission shown in Chapter 3 is a form of Multi-BS cooperative signal transmission and effective in the service area with large cells where not only the interference from neighbor cells but also noise affect cell edge user throughput because of the low received signal power. The evolution in radio transmission technologies such as modulation, error correction coding, and channel estimation also contribute to the improvement in cell-edge throughput. Although they are not cell-edge specific technologies, they surely increase the performance at cell edge, and they can be used in combination with above Multi-BS cooperation technologies. I focused on channel estimation in the radio transmission technologies and clarified its performance gain in Chapter 4. When there is no limitation in wired channel resources, we can focus on the communication

quality of wireless channels. That is, Multi-BS cooperative transmission control can be applied as long as it generates throughput gain in wireless channels. However, in the environment with the limitation in wired channel capacity, it should be also taken into account when deciding the application of Multi-BS cooperative transmission control. The impact of the limitation in wired channel is investigated in Chapter 5. Layered cell configuration is a cell configuration, in which a large number of small cells are placed in a macro-cell coverage area. It achieves flexible increase in network capacity by increasing small cells without degrading handover performance because macro-cell coverage area is unchanged. This cell configuration generates new cell edge between macro and small cells, and the technologies to avoid the interference are investigated in Chapter 6. It should be noted that the interference among macro cells or among small cells remains, so the technologies described above such as Multi-BS cooperative transmission control continue to be important even after Layered cell configuration is introduced.

In Chapter 2, I studied on Multi-BS cooperative transmission control. It is further categorized into two technologies: (i) Multi-BS cooperative muting control and (ii) Multi-BS cooperative signal transmission. Multi-BS cooperative muting control improves the cell-edge user throughput of a MS by stopping the signal transmission of one or more neighbor BSs. The stop of signal transmission in a BS is beneficial not only for the MS but also for other MSs in other surrounding cells. We had evaluated the cell-edge user throughput gain by computer simulations and clarified that around 40% gain is obtained without sacrificing overall network capacity in a typical urban cellular network environment. However, in most of real mobile communications systems such as LTE, a BS continues to transmit the signals common to all MSs such as reference signal even in a stopped radio resource. Accordingly, the residual reference signal interference interrupts the throughput improvement at cell edge. In order to solve this issue, I proposed a reference signal interference canceller in Chapter 2. By utilizing the fact that reference signal is a known signal at MSs, MSs estimate channel and make the replica of reference signal by multiplying the channel estimate and the known transmitted reference signal. Then, the residual reference signal interference is mitigated by subtracting the generated replica. I evaluated the proposed method by computer simulations and clarified that the throughput at cell edge with the proposed canceller was almost identical with the ideal case without reference signal interference. I also developed a prototype system of the proposed

canceller and demonstrated that the similar throughput performance is obtained even with real equipment through laboratory and field experiments.

Multi-BS cooperative signal transmission is another approach to improve cell-edge user throughput. It has been reported that almost the same cell-edge user throughput gain is achieved as Multi-BS cooperative muting control in a congested service area. However, certain performance gain is observed when the traffic in a service area is not so busy in exchange for the increase in signal processing cost in MS and traffic volume in backhaul network, which is caused by the nature of the joint transmission from both neighboring BSs. Therefore it is the best strategy to use both Multi-BS cooperative muting control and signal transmission depending on the congestion degree of the traffic in a service area and backhaul network. In order to realize this multi-BS cooperative signal transmission, both neighboring BSs need to share transmit data and simultaneously transmit signal, so the realization in a real equipment has been considered as an issue especially in distributed BS configuration. In the latter half of Chapter 2, I developed a prototype system of multi-BS cooperative signal transmission and demonstrated that the same throughput can be achieved as the case with ideal synchronization.

In Chapter 3, I studied on Multi-link signal transmission for the environment such as rural area where the received signal power of cell-edge MSs is weak, so the influence of thermal noise as well as interference from neighbor BS is severe. In multi-link signal transmission, each BS first concentrate transmit power in a part of its system bandwidth in order to improve the tolerance to thermal noise. On top of this power concentration, neighboring BSs transmit their signal in different frequency to cell-edge MSs in a coordinated fashion, which increases the throughput at cell edge. The signal reception at cell-edge MSs can be achieved simpler compared to multi-BS cooperative signal transmission because the signal from both neighboring BSs are received in a simple frequency-division fashion. However, when neighboring BSs have different frequency offset, the signals from both BSs interfere with each other in the frequency domain, which results in lower communication quality. When the difference in frequency offset is 50% of subcarrier spacing, BER is increased twice; this can be translated into around 3dB loss in QPSK modulation and means 1bps/Hz loss in spectral efficiency. In order to resolve this issue, I propose an interference canceller, which cancels the interference in the frequency domain. I evaluated the proposed method by mathematical analysis and computer simulations

and clarified that the same communication quality as that without frequency offset is achieved.

In Chapter 4, channel estimation methods are studied to further improve channel estimation accuracy In this thesis, I proposed a channel estimation method, in which the averaging of channel estimate is conducted in both time and frequency domains by taking into account the fading fluctuation in both domains. I also combined a channel estimation method based on impulse response. I evaluated the proposed method by computer simulations and clarified that the channel estimation accuracy could be improved by 0.6dB in order to achieve the same BER compared with conventional methods. This means that the spectral efficiency improvement of 0.2bps/Hz, in other words 2Mbps improvement of throughput in 10MHz system.

In Chapter 5, handover performance improvement was studied. Communication quality improvement is important factor to improve handover performance because handover happens at cell edge. The communication quality at cell edge can be improved by transmitting signal from both neighboring BSs like soft handover in CDMA, while the excessive use of soft handover consumes radio and network resources in both neighboring BSs; this may cause poor handover performance. In order to resolve this issue, I studied on the optimization of soft handover region by taking into account both radio and network resources. The effect was confirmed by mathematical analysis.

In Chapter 6, I studied on newly-emerged cell-edge issue caused by the introduction of layered cell configuration, which is attracting much attention in recent years. The layered cell configuration puts a large number of small cells in a macro-cell coverage area; capacity is drastically improved by the small cells while mobility and coverage is secured by macro cell. However, when the layered cell configuration is realized within the same frequency, there exists interference between macro and small cells, which generates new cell edge. Inter-cell interference coordination based on muting is effective in order to solve the interference. In this interference coordination, it is important to optimize the interference control by taking into account user distribution to improve spectral efficiency. In this thesis, I developed a prototype to realize the interference control based on network coordination among macro and small cells and clarified the performance through field experiment. I also studied on radio resource allocation control for the layered cell configuration. Even with the layered cell configuration, because of the distribution of users, there may be some congested cells, in which MS throughput becomes

quite low especially at cell edge. In order to resolve this issue, I proposed a resource allocation priority control method, which is conducted individually per cell. It was clarified that the cell edge performance was improved without degrading cell overall throughput by computer simulations.

In this thesis, I overviewed the technologies effective to increase cell-edge communication quality and proposed new technologies to solve the major issues in this field. Cellular mobile communications systems will continue to play an essential role in increasing network capacity, and cell edge will continue to exist even in the coming 5th generation mobile communications (5G) era. I believe the discussions in this thesis have useful implications for future research in this field, and I will also continue to tackle this issue in order to realize mobile communication networks satisfying the expectations of all users regardless of their locations.

Bibliography

[1.1] S. Uebayashi, et. al., "Mobile communications systems," IEICE Knowledge Base, S4-3-3, Sep. 2011. Available: http://www.ieice-hbkb.org/files/04/04gun_03hen_03.pdf (in Japanese)

[1.2] Ministry of Internal Affairs and Communications, "White paper information and c ommunications in Japan," 2014. Available: http://www.soumu.go.jp/johotsusintokei/ whitepaper/eng/WP2014/2014-index.html

[1.3] A. GoldSmith, “Wireless Communications,” Cambridge Univ Pr, 2005.

[1.4] M. Sawahashi, Y. Kishiyama, A. Morimoto, D. Nishikawa, and M. Tanno, “Coordinated multipoint transmission/reception techniques for LTE-Advanced,” IEEE Trans. Wireless Commun., vol. 17, no. 3, pp. 26-34, June 2010.

[1.5] D. Ogata, A. Nagate, and T. Fujii, “Multi-BS cooperative interference control for LTE systems,” IEEE VTC2012 Spring, May 2012.

[1.6] A. Nagate, D. Ogata, and T. Fujii, "Cell edge throughput improvement by base station cooperative transmission control with reference signal interference canceller in LTE system," IEEE VTC2012 Spring, May 2012.

[1.7] A. Nagate, D. Ogata, and T. Fujii, "Experimental evaluation of reference signal interference canceller for multi-BS cooperative transmission control in LTE," IEEE VTC2012 Fall, Sep. 2012.

[1.8] A. Nagate, K. Hoshino, M. Mikami, and T. Fujii, "A field trial of multi-cell cooperative transmission over LTE system," IEEE ICC2011, June 2011.

[1.9] A. Nagate, S. Nabatame, D. Ogata, K. Hoshino, and T. Fujii, "Field experiment of CoMP Joint Transmission over X2 interface for LTE-Advanced," IEEE VTC2013 Spring, June 2013.

[1.10] F. H. P. Fitzek, P. Popovski, J. Theeuwes, C. Wijting, R. Prasad, and M. Katz, “Sub-carrier assignment for OFDM based wireless networks using multiple base stations,” IEEE ICC, 2005.

[1.11] T. Fujii, N. Izuka, H. Masui, and A. Nagate, "A proposal of sub-carrier selecting

MC-CDMA system for 4G systems," IEEE VTC2005 Fall, Sep. 2005.

[1.12] A. Nagate, K. Hoshino, and Teruya Fujii, "A Study on Frequency Offset Interference Canceller for Multi-Link Transmission in OFDM Systems," IEEE VTC2008 Spring, May 2008.

[1.13] A. Nagate, K. Hoshino, and T. Fujii, "Frequency Offset Interference Canceller for Multi-Link Transmission in OFDM Systems," IEICE Transactions on Communications, vol. E93-B, no. 3, pp. 620-628, March 2010.

[1.14] T. S. Rappaport, “Wireless Communications,” Pearson Education, 1996.

[1.15] Y. Saito, "Digital Modulation Techniques for Wireless Communications," IEICE, 1996.

[1.16] H. Andoh, M. Sawahashi, and F. Adachi, “Channel Estimation Filter Using Time-Multiplexed Pilot Channel for Coherent RAKE Combining in DS-CDMA Mobile Radio,” IEICE Trans. Commun., vol. E81-B, No. 7, pp. 1517-1526, 1998.

[1.17] T. Onizawa, M. Mizoguchi, and M. Morikura, “A Novel Channel Estimation Scheme Employing Adaptive Selection of Frequency-Domain Filters for OFDM Systems,” IEICE Trans. Commun., vol. E82-B, No. 12, pp. 1923-1931, 1999.

[1.18] J. J. van de Beek, O. Edfors, M. Sandell, S. K. Wilson, and P. O. Börjesson, “On Channel Estimation in OFDM Systems,” IEEE VTC'95, Sep. 1995.

[1.19] A. Nagate, H. Masui, and T. Fujii, "A Study on Channel Estimation Methods for MC-CDMA Systems," IEEE VTC2003 Spring, Apr. 2003.

[1.20] A. Nagate and T. Fujii, "A Study on Channel Estimation Methods for Time-Domain Spreading MC-CDMA Systems," IEEE Transactions on Wireless Communications, vol. 7, no. 12, pp. 5233-5237, Dec. 2008.

[1.21] A. Nagate and T. Fujii, "A Study on Channel Estimation Methods for Time-Domain Spreading MC-CDMA Systems," IEICE Transactions on Communications, vol. E92-B, no. 3, pp. 980-991, Mar. 2009.

[1.22] C. Paik and G. Jin, "Soft Handoff Call Controls in the CDMA Mobile Communication Systems," 11th ITC Specialist Seminar, pp. 118–126, Oct. 1998.

[1.23] A. Nagate, M. Murata, H. Miyahara, and M. Sugano, "An Integrated Approach for Performance Modeling and Evaluation of Soft Handoff in CDMA Mobile Cellular Systems," IEEE VTC2000 Fall, Sep. 2000.

[1.24] A. Nagate, M. Sugano, M. Murata, and H. Miyahara, "Impact of Limited Number of Wired Channels on Soft Handoff in CDMA Cellular Systems," IEICE Transactions on Communications, vol. E84-B, no. 3, pp. 520-526, Mar. 2001.

[1.25] A. Damnjanovic, J. Montojo, Y. Wei, T. Ji, T. Luo, M. Vajapeyam, T Yoo, O. Song, and D. Malladi, "A survey on 3GPP heterogeneous networks," IEEE Wireless Communications, vol. 18, pp. 10-21, June 2011.

[1.26] D. Lopez-Perez, I. Guvenc, and X. Chu, "Mobility management challenges in 3GPP heterogeneous networks," IEEE Communications Magazine, vol. 50, no. 12, pp. 70-78, Dec. 2012.

[1.27] D. Lopez-Perez, I. Guvenc, G. de la Roche, M. Kountouris, T. Q. S. Quek, and J. Zhang, "Enhanced intercell interference coordination challenges in heterogeneous networks," IEEE Wireless Communications, vol. 18, no. 3, pp. 22-30, June, 2011.

[1.28] A. Nagate, S. Nabatame, K. Hoshino, and T. Fujii, "Experimental evaluations of coordinated interference control for co-channel overlaid cell structure," IEEE VTC2015 Spring, May 2015.

[1.29] A. Nagate, T. Fujii, and M. Murata, "A study on adaptive scheduling priority control for layered cell configuration," submitted to IEICE Transactions on Communications.

[2.1] S. Sesia, I. Toufik and M. Baker, "LTE The UMTS Long Term Evolution," WILEY, 2011.

[2.2] M. Sawahashi, Y. Kishiyama, A. Morimoto, D. Nishikawa, and M. Tanno, “Coordinated Multipoint Transmission/Reception Techniques for LTE-Advanced,” IEEE Trans. Wireless Commun., vol. 17, no. 3, pp. 26-34, June 2010.

[2.3] M. C. Necker, “A Graph-Based Scheme for Distributed Interference Coordination in Cellular OFDMA Networks,” IEEE VTC’08 Spring, May 2008.

[2.4] M. C. Necker, “Towards frequency reuse 1 cellular FDM/TDM systems,” ACM/IEEE MSWiM 2006, Oct. 2006.

[2.5] S. G. Kiani, G. E. Oien, and D. Gesbert, “Maximizing multicell capacity using distributed power allocation and scheduling,” IEEE WCNC 2007, Mar. 2007.

[2.6] A. Nagate, K. Hoshino, M. Mikami, and T. Fujii, “Throughput Improvement by Power

Reallocation in Multi-cell Coordinated Power Control", IEEE VTC 2009 Spring, May 2009.

[2.7] H. Shirani-Mehr, H. Papadopoulos, S. A. Ramprashad, G. Caire, "Joint Scheduling and Hybrid-ARQ for MU-MIMO Downlink in the Presence of Inter-Cell Interference", IEEE ICC 2010, May 2010.

[2.8] A. Tölli, H. Pennanen and P. Komulainen, "On the Value of Coherent and Coordinated Multi-cell Transmission", IEEE ICC Workshop 2009, Jun. 2009.

[2.9] A. Tölli, M. Codreanu, and M. Juntti, "Cooperative MIMO-OFDM cellular system with soft handover between distributed base station antennas," IEEE Trans. Wireless Commun., vol. 7, no. 4, pp. 1428-1440, Apr. 2008.

[2.10] A. Osseiran, E. Hardouin, A. Gouraud, M. Boldi, I. Cosovic, K. Gosse, J. Luo, S. Redana, W. Mohr, J. F. Monserrat, T. Svensson, A. Tölli, A. Mihovska, and M. Werner, "The Road to IMT-Advanced Communication Systems: State-of-the-Art and Innovation Areas Addressed by the WINNER+ Project", IEEE Communications Magazine, Jun. 2009.

[2.11] Softbank Mobile, "DL CoMP configuration," 3GPP TSG RAN WG1 Meeting #60, R1-101617, Oct. 2009.

[2.12] A. Nagate, K. Hoshino, M. Mikami, and T. Fujii, "A Field Trial of Multi-cell Cooperative Transmission over LTE System," IEEE ICC 2011, June 2011.

[2.13] D. Ogata, A. Nagate, and T. Fujii, "A Study on Multi-BS Cooperative Interference Control," IEICE Technical Report RCS2011-16, Apr. 2011 (in Japanese).

[2.14] J. J. van de Beek, O. Edfors, M. Sandell, S. K. Wilson, and P. O. Börjesson, "On Channel Estimation in OFDM Systems," IEEE VTC'95, Jul. 1995.

[2.15] Softbank Mobile, "DL CoMP configuration," 3GPP TSG RAN WG1 Meeting #60, R1-101617, Oct. 2009.

[2.16] 3GPP TS 36.211, "Physical Channels and Modulation," 3GPP, Sep. 2008.

[2.17] T. Okamawari, L. Zhang, A. Nagate, H. Hayashi, and T. Fujii, "Design of Control Architecture for Downlink CoMP Joint Transmission with Inter-eNB Coordination in Next Generation Cellular Systems," IEEE VTC 2011 Fall, Sep. 2011.

[2.18] T. Okamawari, H. Hayashi, and T. Fujii, "A Proposal on Network Control Architecture

for CoMP JT with IP Network between eNBs," IEEE VTC 2012 Spring, May. 2012.

[2.19] M. Mikami, M. Miyashita, H. Miyajima, K. Hoshino, H. Yoshino, and T. Fujii, "Field Evaluations on a Prototype System of Cooperative Multi-Cell MIMO Transmission for Asynchronous Inter-Site Base Station Networks," IEEE VTC 2012 Spring, May 2012.

[2.20] L. Zhang, Y. Nagai, T Okamawari, and T. Fujii, "Field Experiment of Network Control Architecture for CoMP JT in LTE-Advanced using Asynchronous X2 interface," submitted to IEEE VTC 2013 Spring, June 2013.

[2.21] D. Ogata, A. Nagate, and T. Fujii, "Multi-BS cooperative interference control for LTE systems," IEEE VTC2012 Spring, May 2012.

[3.1] T. S. Rappaport, "Wireless Communications," Prentice Hall, 2001.

[3.2] Nortel, "Adaptive Fractional Frequency Reuse," 3GPP R1-060905, 2006.

[3.3] S. W. Halpern, "Reuse Partitioning in Cellular Systems", IEEE VTC, 1983.

[3.4] G. Fodor, "Performance Analysis of a Reuse Partitioning Technique for OFDM Based Evolved UTRA," IEEE IWQoS, 2006.

[3.5] S. Faruque, "High Capacity Cell Planning Based on Fractional Frequency Reuse With Optimum Trunking Efficiency," IEEE VTC, 1998.

[3.6] B. Jabbari, E. H. Dinan, and W. Fuhrmann, "Performance Analysis of a Multilink Packet Access for Next Generation Wireless Cellular Systems," IEEE PIMRC, 1998.

[3.7] W. Fuhrmann, B. Jabbari, "Multiple Link Packet Access for Wireless Cellular Networks," IEEE ICUPC, 1998.

[3.8] B. Jabbari, E. Dinan, "Modeling and Performance of a Multilink Packet Access for Wireless Cellular Systems," IEEE MILCOM, 2001.

[3.9] F. H. P. Fitzek, P. Popovski, J. Theeuwes, C. Wijting, R. Prasad, and M. Katz, "Sub-carrier Assignment for OFDM Based Wireless Networks Using Multiple Base Stations," IEEE ICC, 2005.

[3.10] A. Nagate, K. Hoshino, and T. Fujii, "A Study on Frequency Offset Interference Canceller for Multi-link Transmission in OFDM Systems," IEEE VTC'08 Spring, 2008.

[3.11] A. Nagate, K. Hoshino, and T. Fujii, "Frequency Offset Interference Canceller for Multi-Link Transmission in OFDM Systems," IEICE Transactions on Communications,

vol.E93-B, no.3, pp.620-628, March, 2010.

[3.12] J. J. van de Beek, O. Edfors, M. Sandell, S. K. Wilson, P. O. Borjesson, “On Channel Estimation in OFDM Systems,” IEEE VTC’95, Jul. 1995.

[4.1] N. Yee, J-P. Linnartz and G.Fettweis, “Multicarrier CDMA in Indoor Wireless Radio Networks,” in Proc. IEEE PIMRC’93, Sept. 1993, pp. 109-113.

[4.2] K. Fazel, and L. Papke, “On the performance of convolutionally-coded CDMA/OFDM for mobile communication system,” in Proc. IEEE PIMRC’93, Sept. 1993, pp. 468-472.

[4.3] A. Chouly, A. Brajal, and S. Jourdan, “Orthogonal multicarrier techniques applied to direct sequence spread spectrum CDMA systems,” in Proc. IEEE GLOBECOM'93, Nov. 1993, pp. 1723-1728.

[4.4] S. Hara and R. Prasad, “Design and Performance of Multicarrier CDMA System in Frequency-Selective Rayleigh Fading Channels,” IEEE Trans. Veh. Technol., Vol.48, No.9, pp.1584-1595, Sept. 1999.

[4.5] A. Matsumoto, K. Miyoshi, M. Uesugi, and O. Kato, “A Study on Time Domain Spreading for OFCDM,” in Proc. WPMC’02, pp. 725-728, Oct. 2002.

[4.6] A. Nagate, H. Masui, and T. Fujii, “A Study on Channel Estimation Methods for MC-CDMA Systems,” in Proc. VTC’03 spring, pp. 2101-2105, Apr. 2003.

[4.7] H. Andoh, M. Sawahashi, F Adachi, “Channel Estimation Filter Using Time-Multiplexed Pilot Channel for Coherent RAKE Combining in DS-CDMA Mobile Radio,” IEICE Trans. Commun., vol. E81-B, No. 7, pp. 1517-1526, 1998.

[4.8] S. Abeta, M. Sawahashi, F. Adachi, “Adaptive Channel Estimation for Coherent DS-CDMA Mobile Radio Using Time-Multiplexed Pilot and Parallel Pilot Structures,” IEICE Trans. Commun., vol. E82-B, No. 9, pp. 1505-1513, 1999.

[4.9] J. J. van de Beek, O. Edfors, M. Sandell, S. K. Wilson, P. O. Börjesson, “On Channel Estimation In OFDM Systems,” in Proc. VTC’95, vol. 2, pp. 815-819, Sep. 1995.

[4.10] O. Edfors, M. Sandell, J. J. van de Beek, S. K. Wilson, P. O. Börjesson, “OFDM Channel Estimation by Singular Value Decomposition,” IEEE Trans. Commun., vol. 46 no. 7, pp. 931-939, Jul. 1998.

[4.11] I. Sato and T. Fujii, “A Study on MMSE Combining for MC-CDMA,” IEEE VTC’03

Spring, pp. 383-387.

[4.12] T. Fujii, N. Izuka, H. Masui, and A. Nagate, “Channel Construction in SCS-MC-CDMA System,” IEEE VTC’04 Fall.

[4.13] T. Fujii, N. Izuka, H. Masui, and A. Nagate, “SCS-MC-CDMA System with Best Effort Cell Structure,” IEEE ICC’05.

[4.14] T. S. Rappaport, “Wireless Communications,” Pearson Education, 1996.

[4.15] T. Yücek, R. M. A. Tannious, and H. Arslan, “Doppler spread estimation for wireless OFDM systems,” IEEE Sarnoff Symposium, Apr., 2005.

[4.16] G. H. Park, D. Hong, and C. E. Kang, “A new Doppler spread estimation using FFT,” IEICE Trans. Commun., E86-B, No. 9, Sep., 2003.

[4.17] T. Onizawa, M. Mizoguchi, and M. Morikura, “A Novel Channel Estimation Scheme Employing Adaptive Selection of Frequency-Domain Filters for OFDM Systems,” IEICE Trans. Commun., E82-B, No. 12, Dec., 1999.

[4.18] H. Tomeba, K. Takeda, and F. Adachi, “BER Performance Analysis of MC-CDMA with Overlap-FDE,” IEICE Trans. Commun., E91-B, No. 3, Mar., 2008.

[4.19] C. Zhang, X. Lin, and M. Hatori, “Two Dimensional Combined Complementary Sequence and Its Application in Multi-Carrier CDMA,” IEICE Trans. Commun., E88-B, No. 2, Feb., 2005.

[4.20] J. I.-Z. Chen, “Performance Analysis for an MC-CDMA System over Single- and Multiple-Cell Environments in Correlated-Nakagami-m Fading,” IEICE Trans. Commun., E90-B, No. 7, Jul., 2007.

[4.21] L. Wang, X. Shan, Y. Ren, and Z. Ma, “Scattered Pilot-Aided Channel Estimation and Tracking for MIMO-OFDM Systems,” IEICE Trans. Commun., E86-B, No. 1, Jan., 2003.

[4.22] S. Suyama, M. Ito, K. Fukawa, and H. Suzuki, “A Scattered Pilot OFDM Receiver Employing Turbo ICI Cancellation in Fast Fading Environments,” IEICE Trans. Commun., E88-B, No. 1, Jan., 2005.

[5.1] A. J. Viterbi, A. M. Viterbi, K. S. Gilhousen, and E. Zehavi, "Soft Handoff Extends CDMA Cell Coverage and Increases Reverse Link Capacity," IEEE Journal on Selected

Areas in Communications, 12(8):1281–1288, Oct. 1994.

[5.2] C. Paik and G. Jin, "Soft Handoff Call Controls in the CDMA Mobile Communication Systems," the 11th ITC Specialist Seminar, pp. 118–126, Oct. 1998.

[5.3] M. Chopra, K. Rohani, and D. Reed, "Analysis of CDMA Range Extension due to Soft Handoff," IEEE VTC'95, pp. 917–921, July 1995.

[5.4] P. Se¨ite, "Soft Handoff in a DS-CDMA Microcellular Network," IEEE VTC'94, pp. 530–534, June 1994.

[5.5] R.Prasad, "CDMA for Wireless Personal Communications," Artech House Publishers, 1996.

[5.6] S. Su, J. Chen, and J. Huang, "Performance Analysis of Soft Handoff in CDMA Cellular Networks," IEEE Journal on Selected Areas in Communications, 14(9):1762–1769, Dec. 1996.

[6.1] A. Damnjanovic, J. Montojo, Y. Wei, T. Ji, T. Luo, M. Vajapeyam, T Yoo, O. Song, and D. Malladi, "A survey on 3GPP heterogeneous networks," IEEE Wireless Communications, vol. 18, pp. 10-21, June 2011.

[6.2] D. Lopez-Perez, I. Guvenc, G. de la Roche, M. Kountouris, T. Q. S. Quek, and J. Zhang, "Enhanced intercell interference coordination challenges in heterogeneous networks," IEEE Wireless Communications, vol. 18, no. 3, pp. 22-30, June, 2011.

[6.3] E. Larsson, O. Edfors, F. Tufvesson and T. Marzetta, "Massive MIMO for next generation wireless systems," IEEE Communications Magazine, vol.52, no.2, pp.186-195, Feb. 2014.

[6.4] D. Lopez-Perez, I. Guvenc, and X. Chu, "Mobility management challenges in 3GPP heterogeneous networks," IEEE Communications Magazine, vol. 50, no. 12, pp. 70-78, Dec. 2012.

[6.5] D. Bladsjo, M. Hogan, and S. Ruffini, "Synchronization aspects in LTE small cells," IEEE Communications Magazine, vol.51, no.9, pp.70-77, Sep., 2013.

[6.6] P. Okvist and A. Simonsson, "LTE HetNet Trial - Range Expansion including Micro/Pico Indoor Coverage Survey," IEEE VTC 2012 Fall, Sep. 2012.

[6.7] A. Nagate, S. Nabatame, D. Ogata, K. Hoshino, T. Fujii, " Field Experiment of CoMP

Joint Transmission over X2 Interface for LTE-Advanced," IEEE VTC 2013 Spring, June 2013.

[6.8] A. Nagate, K. Hoshino, M. Mikami, and T. Fujii, “A Field Trial of Multi-cell Cooperative Transmission over LTE System,” IEEE ICC 2011, June 2011.

[6.9] K. Hoshino, S. Nabatame, A. Nagate and T. Fujii, " Network Coordinated Inter-Cell Interference Control using Horizontal-Plane Beamforming on Small Cells in 3D Cell Structure," submitted to IEEE 2015 Spring, May 2015.

[6.10] M. Konishi, D. Ogata, A. Nagate and T. Fujii, "Network-Listening Based Synchronization with Loop-Back Interference Avoidance for Small Cells in LTE-Advanced," submitted to IEEE VTC2015Spring, May, 2015.

[6.11] A. Nagate, D. Ogata and T. Fujii, “Experimental Evaluation of Reference Signal Interference Canceller for Multi-BS Cooperative Transmission Control in LTE,” IEEE VTC 2012 Fall, Sep. 2012.

[6.12] I. Hwang, B. Song, S. S. Soliman, "A holistic view on hyper-dense heterogeneous and small cell networks," IEEE Communications Magazine, vol. 51, no. 6, pp. 20-27, June 2013.

[6.13] C. X. Wang, F. Haider, X. Gao, X. H. You, Y. Yang, D. Yuan, H. M. Aggoune, H. Haas, S. Fletcher, E. Hepsaydir, "Cellular architecture and key technologies for 5G wireless communication networks," IEEE Communications Magazine, vol. 52, no. 2, pp. 122-130, Feb. 2014.

[6.14] A. Lobinger, S. Stefanski, T. Jansen, I. Balan, "Coordinating Handover Parameter Optimization and Load Balancing in LTE Self-Optimizing Networks," IEEE VTC2011 Spring, May 2011.

[6.15] N. Miki, Y. Saito, M. Shirakabe, A. Morimoto and T. Abe, "Investigation on Interference Coordination Employing Almost Blank Subframes in Heterogeneous Networks for LTE-Advanced Downlink," IEICE Trans. Commun. Vol E95-B, No. 4, Apr. 2012.

[6.16] Y. Wang and K. I. Pedersen, "Performance Analysis of Enhanced Inter-cell Interference Coordination in LTE-Advanced Heterogeneous Networks," IEEE VTC2012 Spring, May 2012.

[6.17] J. Pang, J. Wang, D Wang, G. Shen, Q. Jiang and J. Lju, "Optimized Time-Domain

Resource Partitioning for Enhanced Inter-Cell Interference Coordination in Heterogeneous Networks," IEEE WCNC2012, Apr. 2012.

[6.18] S. Deb, P. Monogioudis, J. Miernik and J. P. Seymour, "Algorithms for Enhanced Inter-Cell Interference Coordination (eICIC) in LTE HetNets," IEEE/ACM Trans. Networking, Vol. 22, No. 1, Feb. 2014.

[6.19] M. Sawahashi, Y. Kishiyama, A. Morimoto, D. Nishikawa, and M. Tanno, "Coordinated Multipoint Transmission/Reception Techniques for LTEAdvanced," IEEE Wireless Commun., vol. 17, no. 3, pp. 26-34, June 2010.

[6.20] A. Nagate, K. Hoshino, M. Mikami, and T. Fujii, "A Field Trial of Multicell Cooperative Transmission over LTE System," IEEE ICC 2011, June 2011.

[6.21] A. Nagate, S. Nabatame, D. Ogata, K. Hoshino, T. Fujii, "Field Experiment of CoMP Joint Transmission over X2 Interface for LTE-Advanced," IEEE VTC Spring 2013, June 2013.

[6.22] 3GPP TR 36.819 V11.0.0, "Coordinated multi-point operation for LTE physical layer aspects (Release 11)," Sep., 2011.

[6.23] F. Capozzi, G. Piro, L.A. Grieco, G. Boggia, P. Camarda, "Downlink Packet Scheduling in LTE Cellular Networks: Key Design Issues and a Survey," IEEE Communications Surveys & Tutorials, vol. 15, no. 2, pp. 678-700, May 2013.

[6.24] A. Jalali, R. Padovani and R. Pankaj, "Data throughput of CDMA-HDR a high efficiency-high data rate personal communication wireless system," IEEE VTC2000 Spring, May 2000.

[6.25] C. Wengerter, J. Ohlhorst and A. G. E. von Elbwart, "Fairness and throughput analysis for generalized proportional fair frequency scheduling in OFDMA," IEEE VTC2005 Spring, June 2005.

[6.26] 3GPP TR 36.872 V12.1.0, "Small cell enhancements for E-UTRA and E-UTRAN - Physical layer aspects(Release 12)," Dec., 2013.

[6.27] A. Nagate, D. Ogata, T. Fujii, "Cell Edge Throughput Improvement by Base Station Cooperative Transmission Control with Reference Signal Interference Canceller in LTE System," IEEE VTC2012 Spring, May 2012.

[6.28] A. Nagate, D. Ogata, T. Fujii, "Experimental Evaluation of Reference Signal

Interference Canceller for Multi-BS Cooperative Transmission Control in LTE," IEEE VTC2012 Fall, Sep. 2012.

[6.29] D. Ogata, A. Nagate, T. Fujii, "Multi-BS Cooperative Interference Control for LTE Systems," IEEE VTC2012 Spring, May 2012.